University of Zurich[UZH]

Long-term evolution of different permafrost landforms on the northern slope of Piz Corvatsch, Engadin.

GEO 511 Master's Thesis

Author
Flurina Durisch
19-100-650

Supervised by
Dr. Isabelle Gärtner-Roer

Faculty representative
Prof. Dr. Andreas Vieli

06.12.2023
Department of Geography, University of Zurich

University of Zurich[UZH]

Long-term evolution of different permafrost landforms on the northern slope of Piz Corvatsch, Engadin

GEO511 Master's Thesis

Author

Flurina Durisch

19-100-650

Supervisor

Dr. Isabelle Gärtner-Roer

Faculty representative

Prof. Dr. Andreas Vieli

December 2023

Department of Geography, University of Zurich

SUMMARY

This study investigates the complex dynamics of rockglacier and solifluction movements in the Engadine (Swiss Alps), a high alpine geosystem, with focus on the Murtèl cirque north of the Piz Corvatsch. Seven active periglacial landforms are focused on, including four rockglaciers and three solifluction lobes, all of which are subject to the same climatic influences. The study area includes the Murtèl rockglacier, which contains the oldest rockglacier borehole and the longest series of temperature measurements on rockglaciers worldwide. The surface movement of the periglacial landforms is observed using aerial images over a period of 66 years (1955 – 2021), covering nine time steps. Horizontal and vertical changes are quantified by several methods, which all reveal similar to consistent results.

This work identifies spatio-temporal variations in both horizontal and vertical movements within the seven landforms, requiring a comprehensive analysis of the underlying controls, including climatic and topographic factors. The famous Murtèl rockglacier shows small rates of movement (about 0.15 m/a), while the Gupf, a small, developing rockglacier, shows the highest values inside the study area of up to 1.7 m/a. Vertical thinning is observed, especially on the Marmugnun rockglacier, suggesting potential internal melting. No relation is found between air temperature and horizontal movements. However, it cannot be ruled out that the movements will respond to climate change-induced warming with a long time lag and are still pending.

Capturing and quantifying the complex processes within periglacial landforms that are influenced by multiple parameters remains a challenge. The continuation of long measurement series is therefore very valuable and, especially in the context of climate change, essential for the future.

Cover page: The Murtèl cirque below the Piz Corvatsch.

ZUSAMMENFASSUNG

Diese Studie untersucht die komplexen Dynamiken der Bewegungen von Blockgletschern und Solifluktion im Engadin (Schweizer Alpen), einem hochalpinen Geosystem, mit dem Schwerpunkt auf dem Gebiet nördlich des Piz Corvatsch. Sie konzentriert sich auf sieben aktive periglaziale Landformen, darunter vier Blockgletscher und drei Solifluktionsloben, die alle denselben klimatischen Einflüssen ausgesetzt sind. Das Untersuchungsgebiet beinhaltet den Murtèl Blockgletscher, der das älteste Blockgletscherbohrloch und die längste Serie von Temperaturmessungen auf Blockgletschern weltweit enthält. Die Oberflächenbewegung der periglazialen Landformen wird über einen Zeitraum von 66 Jahren (1955 - 2021) in neun Zeitschritten anhand von Luftbildern erfasst. Horizontale und vertikale Veränderungen werden mithilfe mehrerer Methoden quantifiziert, die alle ähnliche oder übereinstimmende Ergebnisse liefern.

Diese Arbeit zeigt räumlich-zeitliche Variationen sowohl in horizontalen als auch in vertikalen Veränderungen innerhalb der sieben Landformen auf, was eine umfassende Analyse der zugrunde liegenden Kontrollfaktoren, einschließlich klimatischer und topografischer Faktoren, erfordert. Der berühmte Murtèl Blockgletscher zeigt geringe Bewegungsraten (ca. 0,15 m/Jahr), während der Gupf, ein kleiner, sich entwickelnder Blockgletscher, die höchsten Werte innerhalb des Untersuchungsgebiets von bis zu 1,7 m/Jahr aufweist. Insbesondere am Marmugnun Blockgletscher wird eine vertikale Ausdünnung beobachtet, was auf mögliche innere Eisschmelze hinweist. Zwischen der Lufttemperatur und den horizontalen Bewegungen besteht kein Zusammenhang. Es ist jedoch nicht auszuschließen, dass die Bewegungen auf die durch den Klimawandel verursachte Erwärmung zeitverzögert reagieren und noch ausstehen.

Das Erfassen und Quantifizieren der komplexen Prozesse innerhalb periglazialer Landformen, die von mehreren Parametern beeinflusst werden, bleibt eine Herausforderung. Die Fortsetzung langer Messreihen ist daher sehr wertvoll und, insbesondere im Kontext des Klimawandels, für die Zukunft unerlässlich.

CONTENT

LIST OF FIGURES

Chapter 2

Chapter 3

Chapter 4

Chapter 5

Chapter 6

LIST OF TABLES

Chapter 3

Chapter 4

Chapter 5

Chapter 6

LIST OF ACRONYMS

ALT	active layer thickness
a.s.l.	above sea level
BP	before present
BTS	Bottom temperature of the winter snow cover
DEM	Digital elevation model
GST	Ground surface temperature
MAAT	Mean annual air temperature
MAGST	Mean annual ground surface temperature
PERMOS	Permafrost Monitoring Network Switzerland
RB	Reference block in CIAS
SA	Search area (test area) in CIAS
TLS	Terrestrial laser scanning
ZAA	Zero annual amplitude

1. INTRODUCTION

1.1 Relevance

Monitoring of rockglaciers and solifluction in a high mountain environment is becoming increasingly important, particularly in the light of climate change. High mountain permafrost is highly heterogeneous due to individual influencing factors and microclimates, which implies a high spatial variability. Consequently, comparing different permafrost regions can be challenging or even infeasible. Thus, the development of large-scale permafrost models is subject to great challenges and uncertainties. Permafrost landforms are highly sensitive to environmental changes and act as effective climate change indicators. Long-term monitoring data series provide valuable insights into the evolution of landforms and their relationship with climatic warming. Long-term data series are ideal for capturing slow or delayed responses, which are often observed in permafrost landforms (Haeberli et al., 2010; Schneider et al., 2012).

1.2 Research context

1.2.1 History of rockglacier monitoring

Rockglaciers play an essential role in comprehending permafrost creep processes in periglacial mountain regions. Their monitoring has gained increasing importance, especially in the context of climate change. It is estimated that Switzerland is home to approximately 2000 active landforms, although there is currently no complete inventory (Delaloye et al., 2010; Kääb et al., 2003). The history of rockglacier monitoring dates back about a century. Early methods involved simple techniques, such as the repeated measurement of painted lines on rockglaciers (e.g. Chaix, 1923). These measurements were later supplemented and replaced by geodetic techniques (e.g. Wahrhaftig & Cox, 1959) and remote sensing methods, including air- and space-borne approaches (e.g. Barsch & Hell, 1975; Kääb, 2005; Kääb & Vollmer, 2000). Space-borne methods involve the retrieval of remote sensing data using satellites, while air-borne methods include the use of aircraft, drones, or even hot air balloons to collect remote sensing data at altitudes typically ranging from 10 to 40 km. The increasing temporal and spatial resolution of remote sensing data has substantially increased their application in rockglacier studies. Such data are particularly valuable in terrain which is difficult to access or that complement field observations (Kääb, 2005; Kääb et al., 2003). The first scientific borehole drilling on an active rockglacier was carried out in 1987 on the Murtèl rockglac-

ier. Since then, it has been possible to make measurements inside the rockglacier, providing previously unknown information about the internal structure. These measurements now represent the longest series of internal rockglacier measurements worldwide (Haeberli et al., 1988). The software CIAS (Correlation Image Analysis System) was developed to capture the surface movement of permafrost creep. It enables the examination of spatio-temporal variations on rockglacier surfaces. Automatic monitoring of surface movements of permafrost creep through block matching from repeated orthophotos is applied. By comparing orthophotos from different years, displacement vectors are derived, providing insights into the three-dimensional deformation of rockglacier surfaces over time (Kääb & Vollmer, 2000, 2001). On a regional scale in the Canton of Valais (Swiss Alps), Roer (2005) quantified rockglacier movements over a 26-year period (1975 – 2001). Different methods were applied to measure horizontal velocities, vertical variations and changes in rockglacier geometry. The state of activity for 45 rockglaciers was analyzed through digital photogrammetry and geomorphologic mapping. Digital photogrammetry was combined with high resolution imagery for the first time in rockglacier research. On a local scale, dendrogeomorphological methods were implemented to assess permafrost creep (Roer, 2005). Using digital photogrammetry and geomorphological mapping, the activity states of several rockglaciers could be determined on a regional scale in the Swiss Alps by Roer and Nyenhuis (2007). The combination of digital photogrammetry and geomorphological mapping provided the most accurate results for the assessment of the former and present permafrost distribution (Roer & Nyenhuis, 2007). The monitoring of the active rockglacier Laurichard in France over two decades showed an increase in surface movements during the 1990s, followed by a decrease after 2004. This decrease is attributed to a lack of snow and cold air temperatures resulting in decreasing ground surface temperatures (GST) (Bodin et al., 2009). A similar trend of rockglacier slowing has also been observed on other rockglaciers in the Alps (e.g. Schneider et al., 2012). Brunner (2020) and Gärtner-Roer et al. (2022) monitored periglacial processes and landforms over 50 years at the Gruben site in the Swiss Alps (1970 – 2016). The evolution of rockglaciers resulting from past and present climatic dynamics was observed by photogrammetric analysis. Rates of movement and changes in rockglaciers thickness were analyzed over both long- and short-term periods. Kääb et al. (1997) provided a detailed rockglacier kinematic monitoring series between 1970 and 1995 at the Gruben site. The strong time lag in rockglacier dynamics in response to climatic influence was demonstrated, requiring decades to centuries. Climatic influences have only a minor effect on thawing of perennially frozen soils, leading to a few centimeters of change per year (Brunner, 2020; Gärtner-Roer et al., 2022; Kääb et al., 1997).

Several rockglacier monitoring studies have established a clear relation between surface velocities and GST changes over the past few decades (e.g. Bodin et al., 2009; Delaloye et al., 2010; Roer et al., 2005). Current rates of change in subsurface and surface ice display rates of movement without historical precedent. This has required rapid development of research and will continue to be a crucial focus in the future (Cicoira, 2020; Cicoira et al., 2021; Kääb, 2005).

1.2.2 History of solifluction monitoring

The observation of past and current solifluction rates in the Swiss Alps has a rich research history (e.g. Furrer, 1965; Krummenacher et al., 1998; Matsuoka, 2011; Matsuoka et al., 1997). To control environmental factors, laboratory simulation experiments were conducted for the first time by Higashi and Corte in 1971. In addition, boundary conditions of solifluction processes have been defined to simplify the studies of process variables. They conducted the experiments with cooled air from a refrigerator and were able to observe the growth and deformation of needle ice. The slope inclination was identified to be the controlling factor of surface displacement rates (Higashi & Corte, 1971). Harris et al. (1997) conducted physical modelling of solifluction processes and demonstrated the relevance of thaw settlement to downslope soil displacements. Periglacial slope processes were simulated on a slope, constructed in the laboratory. Many years of soil displacement were modeled in a few months by reducing the duration of the annual cycle of freezing and thawing to a few weeks. The strong relation between total downslope movement and frost heave found in previous work was confirmed (Harris et al., 1993, 1997). Ridefelt et al. (2010) used statistical modelling to demonstrate the importance of vegetation patterns for the presence of solifluction processes on a local scale in Northern Sweden. Combining field measurements with logistic regression models represents a promising method for assessing the occurrence and level of activity of solifluction processes (Ridefelt et al., 2010). To observe changes in movement of solifluction lobes, specific field monitoring methods have been applied (Kellerer-Pirklbauer, 2018; Matsuoka, 2011). During field measurements, several studies observed the temporal variation of soil movement (Matsuoka et al., 1997). During eight years, Benedict (1970) monitored soil movement processes above the treeline at a study site in the Colorado Front Range. The origins, rates and former rates of the moving soil were observed. Differences in moisture availability and slope gradient strongly influenced the displacement rates. In wet sites, solifluction processes were most effective. Any differences in temperature and soil texture did not show strong influences on the movement rates (Benedict, 1970). Soil movement mechanisms as a function of environmental control factors were studied by Åkerman (1993). Using a 20-year

data set from Spitsbergen, complex interactions between solifluction rates and climatic parameters were detected. A significant influence was observed by the non-climatic factors soil granulometry and soil moisture content (Åkerman, 1993). Kellerer-Pirklbauer (2018) used near-surface markers and painted lines to quantify annual rates of surface velocity and depths of movement in central Austria. Site-specific factors mostly resulted in individual solifluction rates (Kellerer-Pirklbauer, 2018). Continuous field measurements to quantify vertical and horizontal displacements, soil temperatures and soil moisture were conducted by several studies (e.g. Matsuoka, 1994, 1998; Matsuoka et al., 1997). Radiocarbon data from organic layers underlying advancing solifluction lobes is used to quantify long-term changes in solifluction rates (Matthews et al., 2005).

1.3 Objectives

The objective of this Master's Thesis is to analyze the evolution of different permafrost landforms on the northern slope of Piz Corvatsch between 1955 and 2021 and to investigate differences between time periods and processes. This results in the following research questions:

- How do the different permafrost landforms at the Murtèl site develop over a period of over six decades?
- Are there changes across different time periods?
- Are relations between local influences and the movements detectable?

These questions seek to support or reject the corresponding hypotheses:

- Although the landforms are right next to each other and their physical conditions (geology, altitude, climate) are similar, they have different rates of horizontal movement.
- External conditions influence the changes, which can therefore vary across the different time periods.
- Local influences lead to individual evolution of the different landforms.

To answer the research questions, the geomorphological characteristics of the periglacial landforms and their development over time will be mapped. The horizontal surface displacements and vertical surface changes will be determined using aerial photogrammetry.

2. THEORETICAL BACKGROUND

2.1 Periglacial and Permafrost

2.1.1 Periglacial framework

The literal translation of the term periglacial is "*surrounding the ice*" (Zepp, 2017: 208). Periglacial environments are typically related to frozen ground (Ballantyne, 2017). Periglacial processes occur in the close vicinity of glaciers, as well as at distances of more than 1000 km from glaciers. No relation of actual or former proximity to glacier ice is made in the modern use of the term periglacial. Nowadays, cold and non-glacial conditions are described with this term (Ballantyne, 2017). Periglacial formation contains cold-climatic conditions, which are characterized by seasonal and daily frost changes as well as by permafrost, a year-round frozen underground, down to greater depths (Zepp, 2017). Freezing and thawing of the ground strongly impacts the landform development (Ballantyne, 2017). Climatic, topographic and geological conditions are reflected by periglacial landforms (Matsuoka et al., 2005). Alpine periglacial environments are influenced by altitude and shading, which is determined by the slope aspect. The treeline, which lies between 2000 – 4000 m a.s.l. in most alpine mountains, roughly represents the lower limit of alpine periglacial environments (Ballantyne, 2017).

2.1.2 Introduction to permafrost

Permafrost is defined as the thermal state of the subsurface that has at least two winters and an intermediate summer with temperatures below 0° C. This perennially cryotic ground can be rock, sediment or any other earth material. A ground temperature < 0 °C and the presence of ice is described with the term cryotic (Ballantyne, 2017; Romanovsky et al., 2007). The heat balance of the ground surface and the subsurface determines the occurrence as well as the thickness of permafrost. The interaction between atmosphere and soil defines the temperature at the surface. Material properties, water content and the heat flow from the subsurface change the temperature with increasing depth (Zepp, 2017). With depth, the differences in surface temperature between summer and winter are weakened. This attenuation runs exponentially and the seasonal variations are very small from approximately 20 m below the surface and therefore negligible. This depth is referred to as zero annual amplitude (ZAA). Above the depth of the ZAA lies the active layer, the soil layer that reaches temperatures above 0° C. The active layer is defined as the "*seasonally cryotic ground overlying permafrost, or, where water is present, the nearsurface zone where ground freezes in winter and*

thaws in summer" (Ballantyne, 2017: 5a). In Switzerland, active layers typically reach thicknesses of 3 m to 5 m. The permafrost table is below the thaw layer. From this boundary onwards, the permafrost-body with negative temperatures throughout the year occurs. The permafrost body is located between the permafrost table and the permafrost base, which represents the 0° C isotherm. Within permafrost bodies, taliks can occur. A talik is defined as "*a layer of unfrozen ground that occurs in permafrost due to anomalies in thermal, hydrologic or hydrochemical conditions*" (van Everdingen, 2005). Below the permafrost base, temperatures are increasing and the ground is unfrozen (Ballantyne, 2017; Nötzli & Gruber, 2005; Zepp, 2017). A typical temperature profile is shown Figure 2-1. The red curve corresponds to the warmest temperatures in summer and the blue curve to the coldest in winter. The mean annual ground surface temperature is labelled MAGST (after Nötzli & Gruber, 2005).

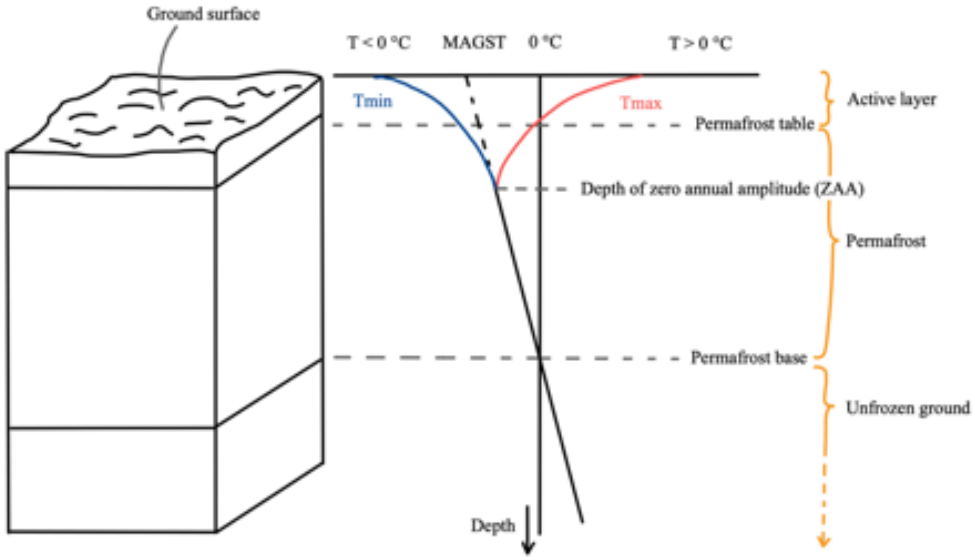

Figure 2-1: Schematic illustration of the most important terms related to permafrost (adapted from Nötzli & Gruber, 2005).

2.1.3 Permafrost-influencing factors

Permafrost occurs, to a first approximation, in conditions where the mean annual air temperature (MAAT) is below -1° C and the annual precipitation is below 1000 mm (Zepp, 2017). In mountainous regions, extreme spatial and temporal variations in weather conditions and surface energy balance can occur within short distances and strongly influence periglacial processes and forms (Noetzli et al., 2007). The distribution of permafrost depends not only on the climate (temperature and precipitation), but also on the altitude, exposition, position relative to the slope, soil properties, geology, surface properties as well as snow occurrence (Gruber &

Haeberli, 2009). Detailed descriptions of these parameters and some of their possible influence on permafrost are given in the following:

Altitude	Permafrost presence correlates positively with increasing altitude and hence decreasing air temperature (Haeberli et al., 2010).
Exposition	Surface energy exchange is different on north- or south-exposed slopes. North-exposed slopes are shadier and receive less energy from solar radiation in the northern hemisphere. The differences of solar radiation can cause MAGST variations up to 15 °C at the same altitude. The height of the lower limit of permafrost on south-exposed slopes is located clearly higher than on north-exposed slopes (Haeberli et al., 2010; Noetzli et al., 2007; Romanovsky et al., 2007).
Position relative to the slope	At the foot of slopes lies loose material that can be mobilized. If this material freezes, rockglaciers can form and permafrost creep occurs (Haeberli et al., 2010).
Soil properties / geology	Rock flanks or bedrock in the summit regions show large areas of permafrost. The composition of the active layer affects the efficiency of energy transport between the atmosphere and the ground, and hence the permafrost. These determining factors are the material, the grain size, the porosity and the water content of the active layer (Nötzli & Gruber, 2005).
Surface properties	Different surface properties, such as vegetation, can impact the surface energy balance, humidity and albedo. Depending on the vegetation, mechanisms of heat addition or heat loss from the soil can occur. Vegetation has a complex and multifaceted impact on permafrost, which additionally varies by region (Brown, 1963).
Snow occurrence	The influence of snow is determined by the thickness and duration of the snow cover, the density as well as the time of snowing in as well as snowing out. An early snowfall in autumn prevents the cooling of the still warm ground. A lack of snow cover or a low snow cover in autumn leads to a stronger cooling of the subsoil, which is favorable for the build-up and preservation of permafrost. If the snow melts early in spring, the heat reaches the permafrost quickly. A long-

lasting snow cover in spring prevents the warming of the subsoil and is beneficial for permafrost due to its insulating effect (Gruber & Haeberli, 2009; Haeberli et al., 2010; Nötzli & Gruber, 2005).

2.1.4 Spatial distribution of permafrost

24 % of the land area on the northern hemisphere consists of permafrost, which represents a covered area of 22.8 million km^2. This area is equivalent to an ice volume of 4.5 million km^3 and, in case of complete melt, to a potential sea level rise of about 7 cm (Lemke et al., 2007).

Permafrost occurs in the zones of continuous, discontinuous and sporadic permafrost. The continuous permafrost zone is characterized by permafrost that lies beneath the entire surface. Only areas below large rivers and deep lakes are excluded (Romanovsky et al., 2007). Continuous permafrost needs MAAT values below -6° C (Zepp, 2017). During and prior to the last ice age, most of the continuous permafrost developed and is therefore older than the beginning of the Holocene, which is set at 11'700 years before present (BP). Permafrost is below 10 – 90 % of the surface in the discontinuous permafrost zone, which has formed during the last few thousand years. Discontinuous permafrost is therefore much younger than continuous permafrost (Haeberli et al., 1988, 1999; Romanovsky et al., 2007). MAAT values ranging from -1 °C to -2 °C are required for discontinuous permafrost. Sporadic permafrost is defined as individual permafrost islands, each a few meters thick. The active layer of the sporadic permafrost is with a depth of up to 3 m thicker than the discontinuous (up to 1.5 m) and the continuous (up to 0.5 m) permafrost (Zepp, 2017).

Temperature ranges for permafrost vary from one or two degrees below 0 °C to -10 °C and colder. The thickness of permafrost varies from a few centimeters to 150 m in the subarctic and 500 m to 1400 m in the Arctic (Romanovsky et al., 2007). In the Alps, thicknesses of a few decimeters to several hundred meters occur (Nötzli & Gruber, 2005). In Switzerland, about 5 % of the area is permafrost. Glaciers cover about half as much area across Switzerland (SLF, 2023).

2.1.5 Permafrost indicators

On the surface, permafrost is invisible and can be detected by distinct phenomena. Such permafrost indicators show where part of the permafrost is located in the subsurface. The most obvious indicators are active rockglaciers, perennial snow patches, ice faces and hanging

glaciers, primarily in shady, north-facing positions in the northern hemisphere. However, the absence of these landforms in the terrain does not mean that permafrost is not present in the subsurface (Gruber & Haeberli, 2009; Nötzli & Gruber, 2005; Romanovsky et al., 2007). These permafrost indicators are characterized in the following:

Active rockglaciers	Active rockglaciers are prominent landforms of permafrost and characterize the high mountainous regions. In active rockglaciers, the ice volume is larger than the pore space of the debris piles. This ice supersaturation allows frozen debris piles to move under the influence of gravity and form rockglaciers (Gruber & Haeberli, 2009; Nötzli & Gruber, 2005) (see Chapter 2.2 for a more detailed description).
Perennial snow patches	Snow can lie at the foot of avalanche slopes all year round if the ground temperature does not exceed the 0° C threshold. Perennial (multi-annual) snow patches are thus indicators of permafrost in the underground (Gruber & Haeberli, 2009; Haeberli, 1975).
Hanging glaciers and ice faces	Ice faces and hanging glaciers require a base below 0° C on steep rockwalls, otherwise these landforms would not be stable. Therefore, they are also clear indicators of permafrost (Gruber & Haeberli, 2009; Nötzli & Gruber, 2005).

2.1.6 Permafrost degradation

The increase in permafrost temperature and the deepening of the active layer are consequential processes of global warming. A variety of serious impacts result from permafrost degradation. Changes in local topographical and hydrological conditions or impacts on vegetation, wildlife and infrastructure are possible consequences (Streletskiy et al., 2015). Degradation of high-mountain permafrost leads to instability of steep slopes and exposure of erodible material that can cause rock avalanches and debris flows. Over the last decades, the frequency and magnitude of rockfalls in the high mountains has already increased significantly. It is very likely that they will further increase in the future. Locations that were not previously affected by rockfalls will become affected as well. Hanging glaciers lose their stability as permafrost is warming, and consequently can no longer be held on the rockwalls (Günzel & Haeberli, 2020; Nötzli & Gruber, 2005). The supply of debris to rockglaciers may increase due to increased rockfall activity (Ballantyne, 2017). Warming and thickening of the active layer results in a

thicker mobile soil and thus an increase in the rate of movement and volume of soil transported through slope processes such as solifluction (Matsuoka, 2001). A small increase in ground temperature can already lead to a significant thawing of the permafrost, as permafrost temperatures are typically only just below freezing. Thin permafrost bodies near the lower limit of permafrost distribution will therefore be most affected by permafrost warming (Haeberli & Beniston, 1998; Harris et al., 2001). Building on permafrost ground requires special measures to overcome instabilities caused by permafrost thawing. This is particularly problematic in high mountain environments for cableway stations or avalanche protection barriers. Pipelines or traffic routes also suffer damage when the ground subsides (Nötzli & Gruber, 2005).

Several projects have been launched for long-term observation and monitoring of changes in permafrost. The PACE project and the following PACE 21 project are active on the European level. For this purpose, eight boreholes were drilled all over the European continent to measure ground temperatures. The boreholes are additionally a part of the Permafrost Monitoring Network Switzerland (PERMOS). Three of the boreholes are located in Switzerland (on the Murtèl rockglacier, Schilthorn and Stockhorn). A further aim of the PACE 21 project is to predict the evolution of permafrost and the impact of permafrost degradation on different parts of the environment (Harris et al., 2001, 2009; Nötzli & Gruber, 2005).

2.2 Rockglaciers

2.2.1 Rockglacier definition

As a key landform of the periglacial, active rockglaciers are distinctive indicators for permafrost. Centering on the process, Haeberli (1985) defined the phenomenon as "*active rockglaciers are the visible expression of steady-state creep of supersaturated mountain permafrost bodies in unconsolidated materials*" (from Barsch, 1992: 176). The creep of high-mountain permafrost is supersaturated with ice and its deformation results in the formation of rockglaciers. Unconsolidated but frozen rock components, coming from talus slopes or moraine deposits, form active rockglaciers (Barsch, 1996). Another definition of rockglaciers is "*steadily creeping perennially frozen and ice-rich debris on non-glacierised mountain slopes*" (Haeberli et al., 2006: 190).

2.2.2 Rockglacier distribution

Rockglaciers consist of an ice-core or ice-debris mixture and coarse debris on the surface. Regions with high rates of talus accumulation in predominantly continental dry climates are

often characterized by rockglacier occurrences (Haeberli, 1985; Janke et al., 2013). Rockglaciers often develop in regions, where there is not enough snowfall to form or preserve glacier ice. The presence of rockglaciers is positively correlated with increasing altitude and thus decreasing temperature, and negatively in correlation with precipitation (Ballantyne, 2017). MAAT below -1 °C to -2 °C and an annual precipitation lower than 2500 mm are the large-scale climatological boundary conditions, at which active rockglaciers occur. On the local scale, the individual rockglacier is influenced by two boundary conditions. First, the type of debris source, which is crucial for forming the rockglacier and is controlled through the lithological and structural characteristics. Rockglaciers often exist at the foot of rockwalls with a high joint density. Second, the thermal conditions, which influence the build-up and occurrence of ice. Occurrence of permafrost and debris and the right inclination are factors that determine the development of rockglaciers. For rockglacier creep a slope between 5° and 30° is required, which limits the occurrence of rockglaciers to mountainous regions (Ballantyne, 2017; Haeberli, 1985). The movement of rockglaciers (permafrost creep) results from creep of frozen mass deeper than the permafrost table. Rockglaciers can show length or width dimensions of several hundred meters and reach heights of several decameters (Janke et al., 2013; Matsuoka et al., 2005). Different relative and absolute age determination methods indicate a general age of rockglaciers in the order of some to many millennia. The dating methods applied include surface dating, dating of borehole contents, ^{14}C dating of organic matter or cosmogenic nuclide exposure dating (Barrows, 2004; Frauenfelder & Kääb, 2000; Haeberli et al., 1999; Steinemann et al., 2020).

2.2.3 Rockglacier classification

Rockglaciers can be classified according to different criteria. The three classifications based on activity, morphology and location are differentiated in this work. Figure 2-2 provides an overview of the classifications distinguished with the respective rockglacier terminology.

2.2.3.1 Rockglacier activity

Rockglaciers can be divided into three classes, based on their degree of activity: active, inactive and relict / fossil rockglaciers. The transition between these three theoretical classes is gradual (Barsch, 1992; Haeberli, 1985; Kääb, 2007).

Active rockglaciers

Active rockglaciers are presently moving downslope with typical movement rates of 0.1 - 1 m/a. Active rockglaciers show MAGST at around 0 °C and bottom temperature of the winter snow cover (BTS) of < -3 °C. Rockglaciers in an active state are reliable indicators of permafrost (Barsch, 1992; Ikeda & Matsuoka, 2002). According to Frauenfelder & Kääb (2000), active rockglaciers are typically located in altitudes between 2439 and 2878 m a.s.l. in the Swiss Alps. Additional information about active rockglacier morphology is given in Chapter 2.2.4.1.

Inactive rockglaciers

In an inactive state, rockglaciers still contain some frozen material, but show no movement anymore. The front has an inclination of about 35°. MAGST of > 0 °C and BTS of about -2 °C are typical values for inactive rockglaciers. A division into climatic and dynamic inactive rockglaciers can be made. Rockglaciers become climatic inactive when the frozen core melts. Climatic inactive rockglaciers are located at the lower boundary of the discontinuous permafrost belt. When debris production on the headwalls above the rockglacier and ice input decrease, rockglaciers can become dynamically inactive. Inactive rockglaciers can be covered with vegetation (Barsch, 1992; Haeberli, 1985; Ikeda & Matsuoka, 2002).

Relict / fossil rockglaciers

Formerly active rockglaciers are called relict or fossil rockglaciers and they are not moving anymore today. They are characterized by a less steep front (< 30°) and by sunk or collapse structures, as all ice has melted out. The furrows and ridges on the surface can still be observable. MAGST of > 0 °C and BTS of > -2 °C characterize relict rockglaciers. Often they are already more densely vegetated. Fossil rockglaciers are useful for paleoclimatic reconstructions, as they are clear indicators of past permafrost distribution and show the permafrost limit by the moment of their collapse. Relict rockglaciers generally occur below 2556 m a.s.l. in the Swiss Alps (Barsch, 1992; Frauenfelder & Kääb, 2000; Haeberli, 1985; Ikeda & Matsuoka, 2002; Steinemann et al., 2020).

In addition to the distinction made by morphological characteristics, the state of activity can, for example, be derived through photogrammetric methods or geodetic surveys. Active and inactive rockglaciers are, based on their ice content, summarized as intact rockglaciers (Haeberli, 1985).

2.2.3.2 Rockglacier location

Rockglaciers mainly occur at geomorphological sites where loose material frequently accumulates. The most common sites are below talus slopes and below the end or side moraines of glaciers. This distinction leads to the definition of the two main rockglacier types, namely talus and debris rockglaciers. Their incorporated material is different, but their type of flow is the same (Barsch, 1992).

Talus rockglaciers — Talus rockglaciers are situated at the foot of free rockwalls, below mountain talus slopes and transport frost-shattered rock fragments. This rockglacier type occurs in discontinuous mountain permafrost environments (Barsch, 1992).

Debris rockglaciers — This other main rockglacier type occurs below the end or side moraines of mostly small glaciers. Debris rockglaciers consist of mainly morainic or glacial debris and are located in a mountain permafrost environment (Barsch, 1992).

2.2.3.3 Rockglacier form type

Another classification can be made based on the form types of rockglaciers: tongue-shaped, lobate and complex rockglaciers. The distinction between tongue-shaped and lobate rockglaciers is defined, using pure geometric terms, by the ratio between the length and width (l:w) (Barsch, 1996).

Tongue-shaped rockglaciers — Rockglaciers with a greater length than width are described as tongue-shaped ($l > w$). These rockglaciers are sometimes seen as more developed lobate ones (Barsch, 1996). Tongue-shaped rockglaciers can be divided into ice-cored and ice-cemented rockglaciers, based on their ice content. In ice-cemented rockglaciers, the ice mass consists of a mixture of debris and ice. The pore space between the rock fragments is often filled by the ice. Retreating debris-covered cirque glaciers often develop into rockglaciers with pure ice cores. Rockglaciers with pure ice cores are characterized by depressions

between the rockwall and rockglacier, where former glaciers melted. In most cases, these are large rockglaciers whose core consists of pure, coarse-grained glacial ice (Barsch, 1996; Krainer, 2015; White, 1976).

Lobate rockglaciers — If the rockglacier length is smaller than the width, rockglaciers are lobate (l < w). They are mainly located at sites with a small talus production, for example below rockwalls or small cliffs or beneath small glaciers (Barsch, 1996).

Complex rockglaciers — Complex rockglaciers are aggregated of several overlying rockglaciers, which may show different states of activity, material sources and ages. They can contain several lobes or tongues (Barsch, 1996).

In addition to the length and width, there are other geometric features that describe the shape of rockglaciers. The thickness and the gradient of the front slope, the maximum thickness or the area of the rockglacier in relation to the source area are commonly measured characteristics. Aspect, slope, altitude or surface relief description are other morphometric features (Barsch, 1996).

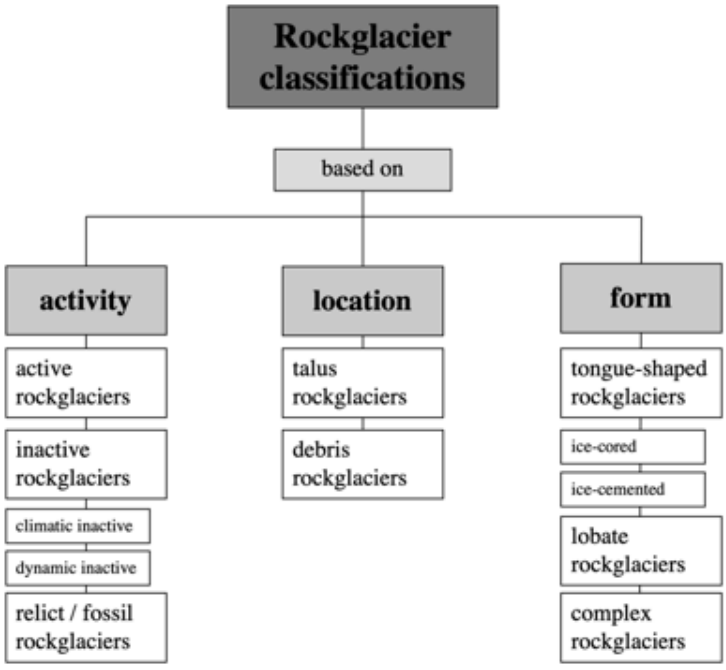

Figure 2-2: The three main rockglacier classifications, based on different criteria.

2.2.4 Rockglacier morphology

2.2.4.1 Morphological characteristics

Typical morphological characteristics of an active rockglacier are illustrated in Figure 2-3. The margins of active rockglaciers are typically vegetation-free, as the present movement complicates any growth of vegetation. Active rockglaciers have characteristically steep fronts (> 35°), which generally show heights of at least 10 – 20 m. Rockglacier thicknesses are assumed to be correlated to their surface area. Direct thickness measurements are often complicated and the thickness values at the rockglacier front are therefore usually estimated. The assumed average thickness of active rockglaciers with a small area (< 0.01 km^2) is 20 – 30 m. For larger areas (> 0.1 km^2), the thickness is estimated to be 60 – 80 m (Barsch, 1977, 1996). Active rockglaciers display a distinctive surface morphology in the form of transverse and longitudinal structures. The transverse ridges and furrows result from compressive flow of the active layer and can have height differences of up to several meters. The thickness of the active layer is a useful indicator of the current heat balance on active rockglaciers. The light-colored and unweathered fine material is at the front and side slopes, while the upper surface consists of more exposed and darker boulders. Boulders on rockglacier surfaces can be gravel- to house-sized fragments. There is no preferred rock type for the formation of rockglaciers,

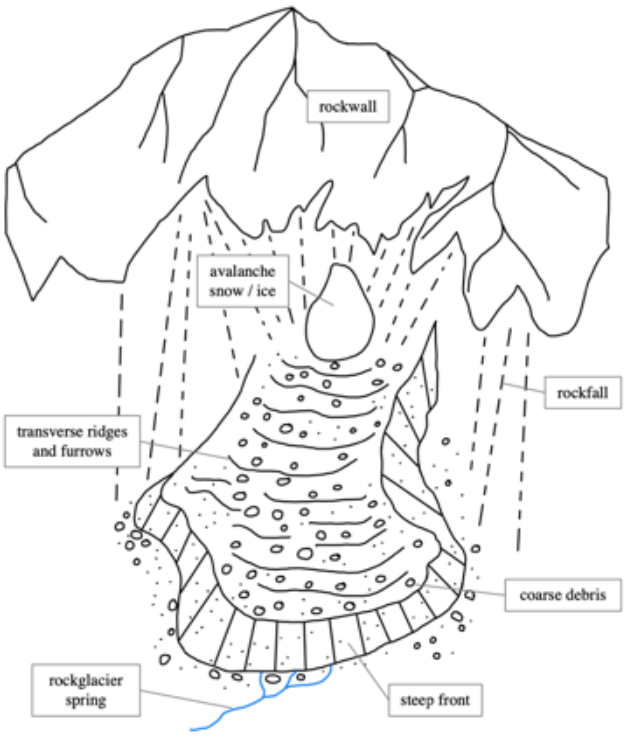

Figure 2-3: Schematic illustration of an active rockglacier with the typical morphological features (adapted from Krainer, 2015).

as they can develop in nearly all rock types that can break down into components of at least a few cm^3. In the Swiss Alps, rockglaciers are mostly situated in crystalline rock. A rockglacier spring usually develops at the rockglacier front (Barsch, 1996; Gruber & Haeberli, 2009; Haeberli, 1985). Rockglaciers represent one of the main storage and archive components in the alpine sediment cascade. Because of their long persistence in the landscape, they are regarded as sediment traps of the coarse debris system (Gärtner-Roer, 2012; Giardino et al., 1989).

2.2.4.2 Rockglacier stratigraphy

Information on the internal structure of rockglaciers was gained from excavations, core drilling, geophysical surveys and studies of natural outcrops. Three main layers form the typical rockglacier stratigraphy. Big boulders form the top layer with thicknesses between 1 - 5 m. Underneath is an ice-rich permafrost core consisting of up to 70 % ice and about 30 % fine-grained material. This second, low-viscous and highly deformable layer is creeping downslope. The lowest unit again contains larger rocks, which are deposited at the rockglacier front and are continuously overrun by the other, overlying two layers. At the front and side slopes of active rockglaciers, this typical stratigraphy is observable (Barsch, 1992, 1996; Haeberli, 1985; Humlum, 2000).

2.2.5 Rockglacier kinematics

The quantification of movement, without consideration of forces, is performed with the help of kinematics. The movement of rockglaciers results from creeping permafrost. The surface velocity (v^s) of rockglaciers is the combination of the internal deformation of permafrost, sliding on shear horizons and the deformation of the underlying sedimentary bed. The basal velocity can be summarized from the sliding on shear horizons and the deformation of the underground. Rockglacier movement can be quantified in terms of horizontal displacement, vertical movement and the front advance (Barsch, 1996; Haeberli, 1985; Kääb, 2006). Roer (2005) has provided a compilation of published data on horizontal velocities, vertical changes, and front advance of rockglaciers.

Horizontal displacement

Active rockglaciers show mean horizontal surface velocities between several centimeters (e.g. 0.03 m/a at Murtèl rockglacier or 0.05 m/a at Albana rockglacier) to about two meters per year (e.g. 1.45 m/a at Büz North rockglacier or 1.6 m/a at Suvretta rockglaci-

er) (Barsch, 1996; Barsch & Hell, 1975; Frauenfelder et al., 2003; Ikeda et al., 2003). Extremely large movement rates of > 100 m/a were measured at the Grabengufer rockglacier (Valais) (Delaloye et al., 2013; Geomorphology Research Group, 2022a). At the Tsarmine rockglacier (Valais), speeds of up to 18 m/a were observed (Geomorphology Research Group, 2022b; Kummert et al., 2021). As a characteristic average value for the horizontal surface movement of active rockglaciers, a few decimeters per year can be assumed (e.g. 0.21 m/a at Muragl rockglacier or 0.5 m/a at Furggentälti rockglacier) (Barsch, 1996; Barsch & Hell, 1975; Krummenacher et al., 1998). The permafrost creep of active rockglaciers is individual and displays internal variations. The maximum horizontal velocities are concentrated in the central flowline and decrease towards the rockglacier margins (Barsch, 1996).

Vertical change

The vertical movement of rockglaciers is composed of three components: change in elevation resulting from local topography, subsidence due to internal melt and mass gain due to freezing of internal water. Vertical changes are observable on the surface or by thinning or thickening of the rockglacier. However, vertical movements are usually much smaller than the horizonal displacements. On Murtèl rockglacier, Kääb et al. (1997) observed a typical vertical movement of -0.04 m/a. Local vertical heave can be explained by the structure of furrow and ridges (Barsch, 1996; Frehner et al., 2015; Kääb et al., 1997).

Front advance

The front advance of rockglaciers is around 0.05 m/a (measured by Kääb et al. (1997) at Muragl rockglacier) and typically amounts for approximately 10 % of its respective horizontal movement (Kääb et al., 1997; Roer, 2005).

Most alpine glaciers move one to two orders of magnitude faster than rockglaciers. Polar rockglaciers are rather cold and move slower than alpine rockglaciers, which tend to be warmer. Short-term climate forcing results in varying annual rates of movement (Ballantyne, 2017; Barsch, 1996; Haeberli, 1985). Kääb et al. (2007) illustrated the major influence of air temperature on rockglacier creep on global scale. Apart from mean air temperature, early win-

ter snow coverage, slope and sediment supply are the main external forcing factors for rockglacier deformation velocity. Internal factors are the presence of liquid water, particle size, ice content and thickness of the rockglacier (Haeberli et al., 2010; Kääb et al., 2007).

Different rockglacier advance mechanisms are described in Figure 2-4 (Haeberli, 1985; Wahrhaftig & Cox, 1959). The advance of rockglaciers depends on the behavior of permafrost creep. The advance rate of a rockglacier is composed of the vertical distribution of the horizontal velocity, the change in ice volume due to melting and freezing, the change in air content, and the erosion and removal of debris at the front. In Figure 2-4, the surface velocity (v^s) and the mean velocitiy (v^m) are indicated with thin arrows. On the left side of each illustration, the vertical velocity profile within the rockglacier at the beginning is shown. The dotted line represents the assumed geometry of the front after the advected mass has been added horizontally to the downward facing front. The dashed line represents the shape of the front after the transported mass has been uniformly partitioned across the whole front. The extent of the latter mass redistribution affects the particle vectors (bold arrows) inside the front. Unlike glaciers, the front of rockglaciers moves forward continuously due to limited melting of internal ice and remaining solid materials at the front (Kääb, 2005; Wahrhaftig & Cox, 1959).

The two processes of internal plastic deformation and shear at a sliding horizon dominate the deformation of a rockglacier (Figure 2-5). Subsidence and uplift of the rockglacier surface additionally result from these processes. At the bedrock, the plastic deformation rates are low and increase towards the rockglacier surface. Uplift of the rockglacier surface can occur when debris is added or by a decrease in flow velocity due to compression. The rockglacier surface may be subsiding due to melting of internal ice, which implies a change in mass balance, or due to an increase in rockglacier flow velocity. Due to the accumulation of rockfall material,

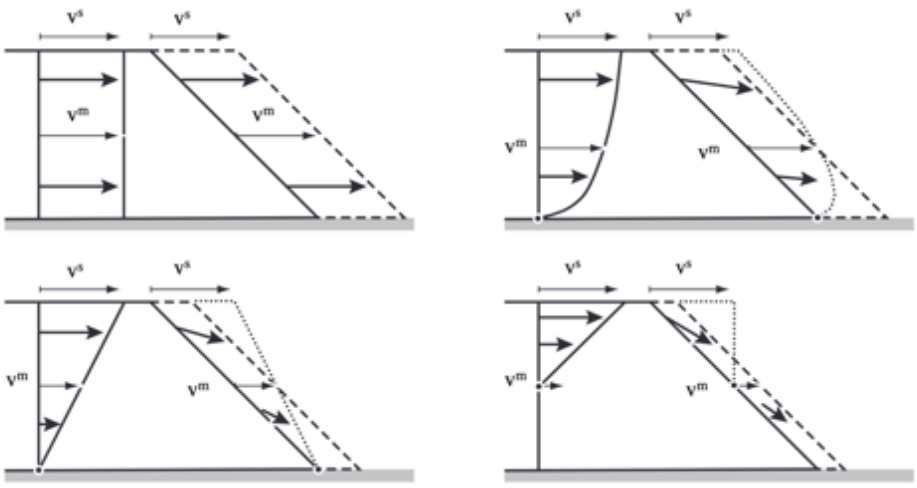

Figure 2-4: Schematic diagrams of the advance mechanisms of rockglaciers as a function of velocity variation at depth (from Kääb, 2005; modified after Wahrhaftig and Cox, 1959).

gravitationally influenced plastic deformation dominates in the root zone. This area of increasing mass – the so-called accumulation area – shows high flow velocities and consequently a subsidence of the rockglacier surface. Below the area of subsidence, a lifting zone occurs at the front of the downslope moving mass. While propagating downwards, the moving layer continuously thins, which leads to decreasing plastic deformation. Further downslope, the dominant deformation process to be observed is basal shearing (Arenson et al., 2002; Kenner et al., 2017).

Temporal rockglacier topography changes are observed using several techniques, for example aerial photogrammetry, air-borne laser scanning, geodetic observations, terrestrial laser scanning or in situ global positioning system (GPS) (e.g. Ballantyne, 2017; Haeberli, 1985; Kääb et al., 1997; Kenner et al., 2017).

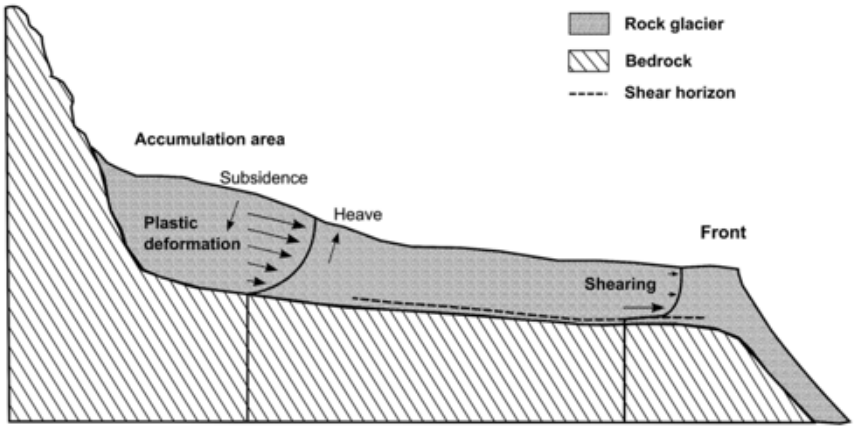

Figure 2-5: Deformation processes of an idealized rockglacier (from Kenner et al., 2017, p. 20).

2.2.6 Response of rockglaciers to climatic changes

Strikingly many alpine rockglaciers show a significant increase in surface velocity in recent years. A growing number of studies measuring surface displacement of rockglaciers have observed increasing velocities in the last decades (e.g. Bodin et al., 2009; Delaloye et al., 2008; Kääb et al., 2007; Roer et al., 2005). Increasing rockglacier temperature results in greater sensitivity to temperature fluctuations, which can lead to an exponential rise in the average surface movement of rockglaciers (Delaloye et al., 2008; Kääb et al., 2007; Roer et al., 2005). Temperature increases can result in changes in the rheological properties and an increase in internal deformation. Basal sliding is affected due to melting of internal ice and increased water supply, resulting in an acceleration of rockglacier displacements (Kenner et al., 2017; Roer et al., 2008). This acceleration is probably attributable to the reduction in vis-

cosity of the underlying permafrost. In addition to the increased movement, melting of the internal ice can result in rockglacier surface lowering. Due to this rockglacier degradation, an active rockglacier can develop into an inactive and ultimately a relict rockglacier (Barsch, 1996). Rockglaciers usually show delays of a few months to years to increasing GST (Arenson et al., 2002; Delaloye et al., 2008; Romanovsky et al., 2007). The response to cooling periods is faster than to warming periods. This is explained by the availability or absence of liquid water in the rockglacier body (Kellerer-Pirklbauer & Kaufmann, 2012). An acceleration of rockglacier velocity in spring often coincides with water infiltration from snow melt water. The onset of surface freezing in autumn results in a deceleration of rockglacier velocity. Between precipitation and rockglacier movement, only weak correlation was observed (Kääb et al., 2007; Kenner et al., 2020).

2.3 Solifluction

2.3.1 Solifluction processes

Solifluction refers to gravitational mass movements that undergo slow deformation (a few cm/a) of the upper soil layer, due to cyclic freezing and thawing of the ground. Minor slopes as steep as 2° are already sufficient (Ballantyne, 2017; Matsuoka, 2001; Matsuoka et al., 2005; Zepp, 2017). The four different solifluction processes are needle ice creep, frost creep, gelifluction and plug-like flow: They frequently occur in combination and are displayed in Figure 2-6 (Matsuoka, 2001).

Needle ice creep — Needle ice creep, the most superficial solifluction process, happens when a thin surface layer is raised on the tips of long, thin ice needles and its deposition is farther downslope, when the ice crystals are thawing (Matsuoka, 2001).

Frost creep — Frost creep occurs in greater depth than needle ice creep. Repeated cycles of frost heave of soil, perpendicular to the slope, due to volumetric expansion during freezing and thawing result in downward movement of the soil (Matsuoka, 2001; Zepp, 2017).

Gelifluction — Gelifluction occurs on impermeable permafrost tables and in fine-grained material. The meltwater is retained during thawing of ice-rich soil. This waterlogging leads to water saturation and the buildup of high porewater pressure. The active layer consequently flows

downslope and represents elastoplastic deformation of the soil. Ice lenses in the uppermost layer are formed by one-sided freezing and lie on a desiccated zone. One-sided (downward) freezing occurs mostly in non-permafrost and warm permafrost ground. Ice lenses can't grow deep, as desiccation related with ice segregation in the upper soil is an obstacle (Matsuoka, 2001; Zepp, 2017).

Plug-like flow

Plug-like flow describes the slow movement of the active layer as a result from thawing of ice-rich soil directly overlying the permafrost table (Ballantyne, 2017). The permafrost undergoes two-sided freezing and ice lenses can form in depth. In cold permafrost, two-sided (up- and downward) freezing occurs, as the upward penetration of frost from the top of permafrost is enabled by a large thermal gradient. Ice lenses next to the bottom of the frozen active layer are produced through the process of upward freezing. In between the two layers of ice lenses there is a desiccated zone. If the ice lenses in shallow depth thaw, the soil layer can move like a plug (Matsuoka, 2001). Plug-like flow usually occurs in late summer (Ballantyne, 2017).

Needle ice creep, frost creep and gelifluction dominate in sites with MAAT of -3 °C. Plug-like flow usually occurs at colder sites with MAAT < -6 °C (Matsuoka, 2001). The rates of movement are depending on the periglacial environment. In regions with continuous permafrost and MAAT of < -6 °C, surface velocities rarely surpass 5 cm/a. Surface velocities over

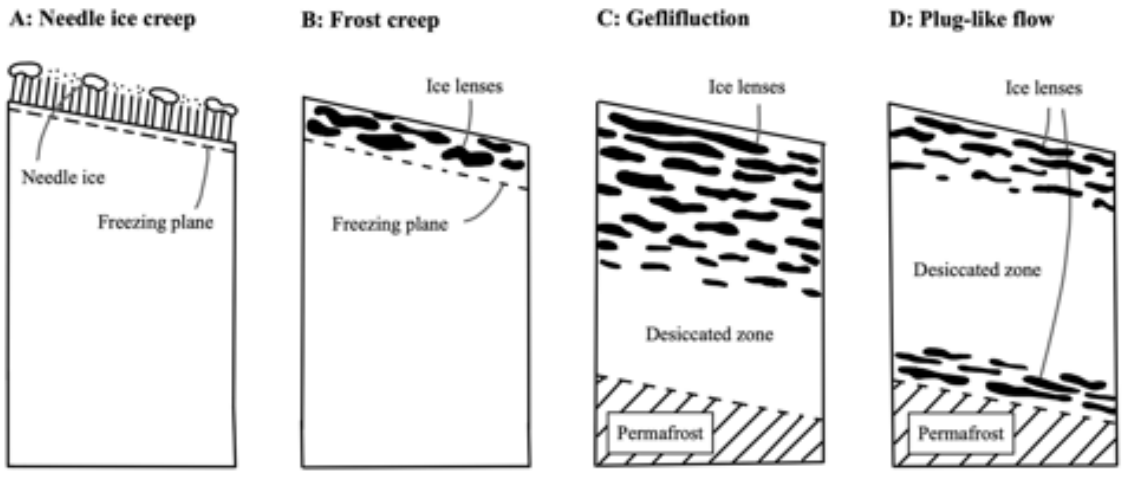

Figure 2-6: Schematic illustration of the four components of solifluction (adapted from Ballantyne, 2017; Matsuoka, 2001)

10 cm/a are measured at sites with MAAT between -3 °C and +5 °C. Sites with rapid but shallow needle ice creep and frost creep, resulting from frequent freezing and thawing cycles, show the highest values for surface velocities. Sites in the continuous permafrost zone show the greatest maximum depths of movement with values of > 0.5 m (Ballantyne, 2017; Kellerer-Pirklbauer, 2018; Matsuoka, 2001).

2.3.2 Solifluction landforms

Resulting landforms of solifluction are solifluction terraces and solifluction lobes (flow tongues). Solifluction terraces spread over the slope for distances of tens to hundreds of meters roughly parallel to the contour. Solifluction lobes often consist of coarse debris on the forehead and finer material inside the lobes. They are lobate and show widths or lengths of 2 to 50 m and heights of up to 1 m. Bounded solifluction occurs when there is a closed vegetation cover that reduces the flow velocity. Free or unbound solifluction occurs when there is no vegetation cover or when the vegetation cover is not closed (Ballantyne, 2017; Matsuoka, 2001; Zepp, 2017). Solifluction sheets are an additional landform, resulting directly from solifluction processes. This term is used to refer to soils, which have moved uniformly downslope with no rise, except on the end. Solifluction sheets have homogenous surface conditions and are horizontal continuous. Solifluction sheets can develop into lobate solifluction sheets, as they move further downslope (Ballantyne & Harris, 1995; Matsuoka, 2001). In Figure 2-7, the resulting landforms of solifluction are displayed. Besides rockglaciers, solifluction lobes are the most prominent and widespread landforms of the periglacial. Rockglacier movements appear in greater depth than the creep of solifluction lobes (Matsuoka et al., 2005).

A further distinction into four basic forms is possible, which is based on the presence or absence of sorting: turf-banked terraces, turf-banked lobes, stone-banked terraces and stone-banked lobes (Benedict, 1970). The classification of Benedict (1970) is applied by most authors.

Turf-banked terraces — As "*bench-like accumulations of moving soil that lack conspicuous sorting*" are turf-banked terraces described (Benedict, 1970: 170). They prefer concave over convex positions on the slope and contain fine, unsorted material and are mostly vegetated (Benedict, 1970).

Turf-banked lobes — Turf-banked lobes are "*lobate accumulations of moving soil*" and show no sorting (Benedict, 1970: 172). These landforms are vulnerable to

wind erosion, as they are limited to snow-free areas in winter. Frost cracks are frequent on turf-banked lobes and occur in the direction of slope. Turf-banked lobes contain, like turf-banked terraces, unsorted soil, are mostly covered with vegetation and usually contain fine material (Ballantyne, 2017; Benedict, 1970).

Stone-banked terraces

Stone-banked terraces are "*terrace- or garland-like accumulations of stones and boulders*" and show sorting of materials (Benedict, 1970: 174). These landforms lie on a stone-free moving subsoil and have lobate, steep and rocky fronts. Stone-banked terraces have often developed from stone-banked lobes. They are often located on higher slopes, covered with coarse debris (Ballantyne, 2017; Benedict, 1970).

Stone-banked lobes

Stone-banked lobes are "*lobate masses of rocky debris underlain by relatively stone-free, fine-textured, moving soil*" (Benedict, 1970: 176). Stone-banked lobes have front-heights of less than one meter and they often occur together with stone-banked terraces on higher slopes (Benedict, 1970).

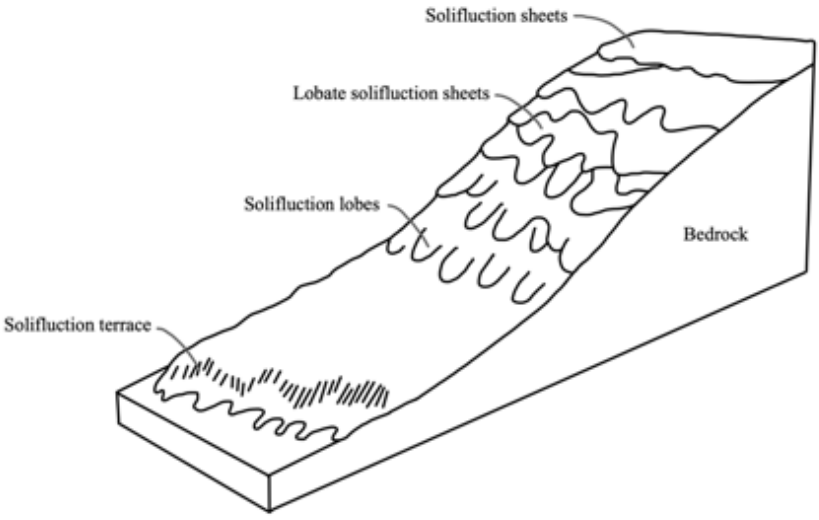

Figure 2-7: Schematic illustration of the typical landforms resulting from solifluction (adapted from Ballantyne & Harris, 1995).

3. STUDY SITE

3.1 General characteristics

The Murtèl site is located in the Upper Engadine in the Canton of Grisons in the south-eastern part of Switzerland (Figure 3-1). In the European Alps, the Engadine represents one of the hotspots for rockglaciers (Gärtner-Roer & Hoelzle, 2021). A typical periglacial mountain slope with the characteristic landforms of headwall, talus slopes and rockglaciers is found at the northern slope of Piz Corvatsch. Above the timber line, which lies at about 2100 m a.s.l., active periglacial landforms such as solifluction lobes or rockglaciers are present (Matsuoka, 2008; Müller et al., 2014). The site, located at 46° 25' N / 9° 49' E, lies below the northern slope of Piz Corvatsch, which reaches an altitude of more than 3300 m a.s.l. (Swisstopo, 2015). On the rockwalls, the physical weathering is highly active. In combination with rock-falls and avalanches, large quantities of fine and coarse debris are transported into the talus slopes below (Hanson & Hoelzle, 2005). Within the proximal zone of the active rockglaciers, multiple fossil rockglaciers can be observed, exhibiting former local periglacial extensions.

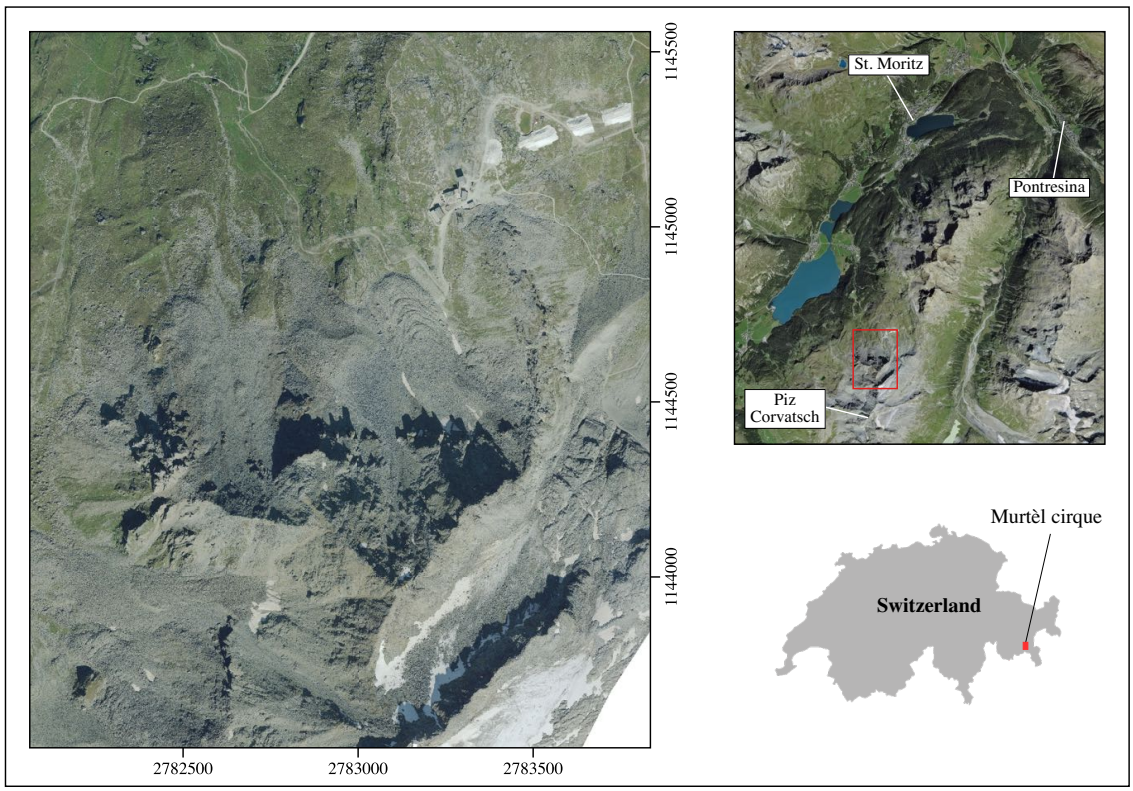

Figure 3-1: The location of the study site, the Murtèl cirque, in Switzerland (Swisstopo, 2021).

During the late 19th century, the Murtèl cirque was covered by ice, as depicted in Figure 3-2. However, the precise timeframe of the glacier retreat remains uncertain due to the absence of historical map material specific to this region during the turn of the century (Swisstopo, 1860, 1879). Figure 3-3 illustrates the slope and Figure 3-4 shows the aspect of 2021 in the study area.

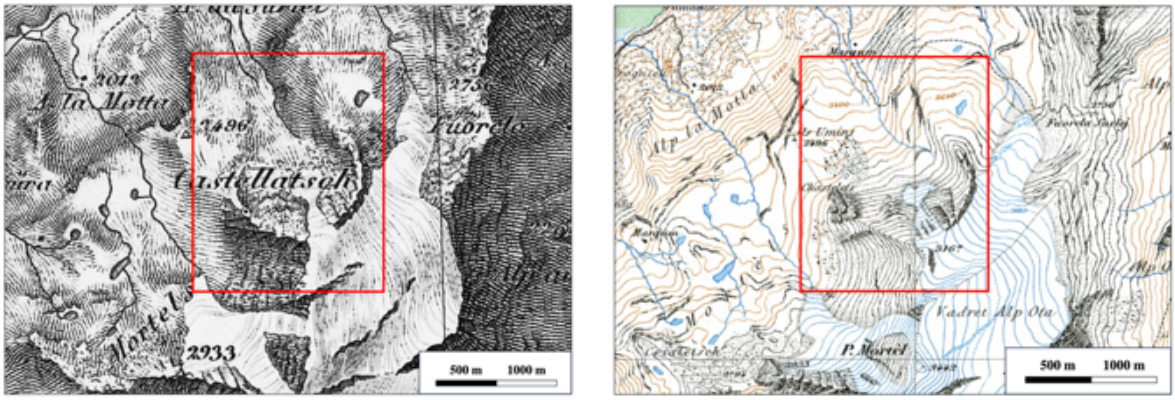

1860 **1879**

Figure 3-2: The glaciated Murtèl cirque in 1860 and 1879 on the Dufour map of Swisstopo (Swisstopo, 2023).

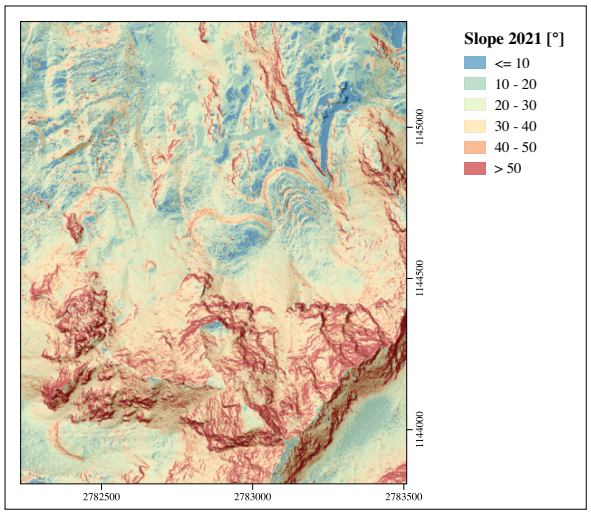

Figure 3-3: Slope of 2021 (Swisstopo, 2021).

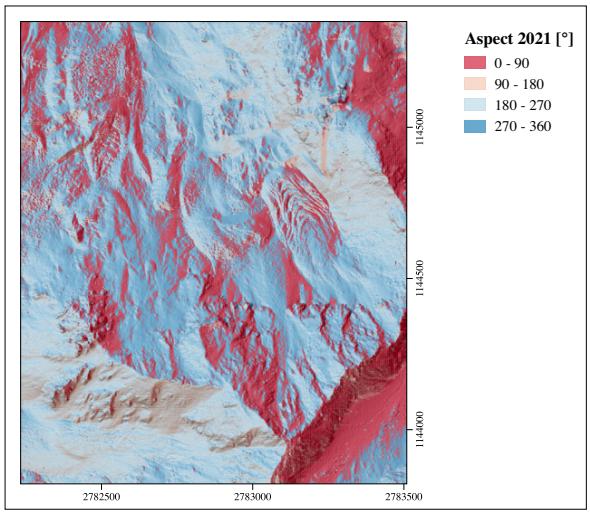

Figure 3-4: Aspect of 2021 (Swisstopo, 2021).

3.2 Climate

The Murtèl cirque is impacted by air masses from the south-west and dominated by a continental climate. The valley floors are rather dry and receive about 800 mm of annual precipitation. At higher altitudes and in periglacial areas, annual precipitation values range from 1000 mm to 1500 mm. The climate is generally continental (Schwarb et al., 2000). The mean

annual zero-degree isotherm is located at about 2200 m a.sl. and during winter, a snow cover of about 1.5 – 2 m covers the area (Hanson & Hoelzle, 2004). The closest weather station to the Murtèl cirque is at 3297 m a.s.l. on top of Piz Corvatsch and is maintained by MeteoSwiss (station code: COV). The station has been providing data since 1979 and currently measures temperature, precipitation, wind, sunshine, humidity, global radiation, dew point and pressure (MeteoSwiss, 2023a).

3.3 Periglacial landforms at Murtèl cirque

The study site includes several periglacial landforms, such as active, inactive, and fossil rock-glaciers, as well as solifluction lobes. The four active rockglaciers (Murtèl, Marmugnun, Chastelets and Gupf) and the three solifluction lobes in the talus slope above the Chastelets rockglacier are subject of this study. They are all located right next to each other at a similar altitude in the Murtèl cirque. Accordingly, these landforms are influenced by comparable weather conditions, such as the same amount of precipitation and similar temperatures. Each landform is characterized and described in the following Chapters 3.3.1 until 3.3.5.

3.3.1 Murtèl rockglacier

The Murtèl rockglacier is located near several other rockglaciers, glaciers and glacier fore-fields in the Corvatsch area (Hoelzle et al., 2002). With a surface area of about 0.05 km^2 in 2019 (active rockglacier without talus slope), the rockglacier faces NNW and is located between approximately 2630 and 2730 m a.s.l. (Swisstopo, 2019). It has developed in a small cirque at the foot of the Murtèl rockwall below the northern slope of Piz Corvatsch. The crystalline rockwall mainly consists of gneiss (upper part) and carbonatic mica-schist (lower part), which often form coarse boulders (Matsuoka, 2008; Spillmann & Trommsdorff, 2007; Springman et al., 2012). The Murtèl rockwall has an average inclination of 41° and highest slopes of up to 80° (Müller et al., 2014; Swisstopo, 2019). The mean slope of the Murtèl rockglacier is around 10° - 12° (Kenner et al., 2020; Müller et al., 2014; PERMOS, 2016). With an average crack width of 2 mm, Matsuoka (2008) detected intense shattering of the Murtèl rockwall (Matsuoka, 2008). Talus slopes are characterized as abrupt hillslope changes without any bedrock. The talus slope between the Murtèl rockwall and rockglacier consists of heterogenous loose material coming from the rock face. It acts as a successive sedimentary body below the rockwall (Müller et al., 2014). Underground ice, which includes segregation

ice and the embedment of avalanche snow and perennial snowbanks, has accumulated in the talus slope. This caused the mass to behave in a fluid manner and creep downslope (Humlum et al., 2007; Müller et al., 2014). Consequently, the Murtèl rockglacier was described as a talus derived rockglacier (Haeberli et al., 2006). By permafrost creep, the talus slope provides sediment and as a secondary transport, avalanches and debris flow carry sediment to the Murtèl rockglacier (Müller et al., 2014). In the talus slope, Kääb et al. (1998) define an upper part of longitudinal extension, where the Murtèl rockglacier originates. In the lower part, where the rockglacier propagates over flatter ground, longitudinal compression results in an ogive-like pattern of well-developed transverse furrows and ridges (Barsch, 1996; Kääb et al., 1998; D. Vonder Mühll & Haeberli, 1990). The following figures illustrate the Murtèl rock-glacier system, highlighting its characteristic features (Figure 3-5 until Figure 3-9).

Figure 3-5: The entire system of the Murtèl rockglacier with its rockwall, the talus slope and the rockglacier body with its characteristic furrow and ridge structure.

Figure 3-6: The front part of the tongue of the Murtèl rockglacier with its steep front.

Figure 3-7: Boreholes and measuring devices on the tongue of the Murtèl rockglacier. For an overview of the installations on the rockglacier, see Table 3-3 and Figure 3-20.

Figure 3-8: The lateral margin of the Murtèl rockglacier's tongue on the eastern part.

Figure 3-9: The upper part of the rockglacier tongue with large boulders on top, with the view uphill to the talus slope and the rockwall above the Murtèl rockglacier.

3.3.1.1 Research history at Murtèl rockglacier

As this site is located in the middle of the Corvatsch / Furtschellas ski area and a cable car leads near it, the Murtèl rockglacier is easily accessible. It is one of the most researched permafrost landform and has the world's longest data record in mountain permafrost (Hoelzle et al., 2002). The Murtèl rockglacier was accurately mapped for the first time in 1851 by Johann Coaz (Ribi, 1975) and has been analyzed and studied in particular detail in many projects (e.g. Barsch & Hell, 1975; Haeberli et al., 1988; D. Vonder Mühll, 1993; D. S. Vonder Mühll & Klingelé, 1994). Barsch (1973) measured several refraction seismic profiles to determine the upper boundary of the frozen layer. Values of thaw depth between 2.5 - 4.5 m were measured, depending on the position of the measurement on the rockglacier. A total thickness of 60 m was identified (Barsch, 1973). Barsch and Hell (1975) conducted measurements of rockglacier movement using photogrammetrical methods. Horizontal velocities of 7.1 cm/a (1931 - 1955) and 3.2 cm/a (1955 - 1971) were observed (Barsch & Hell, 1975). In 1977, a sediment transfer rate of 0.15 Mt/a was calculated using an average velocity of 6 cm/a for the Murtèl rockglacier (Barsch, 1977). Using geoelectric and radio-echo soundings, King et al. (1987) found the thickness of the permafrost layer to be between 20 and 50 m, which is consistent with the results of other studies (e.g. Barsch & Hell, 1975; Haeberli et al., 1988). In 1987, the first scientific core drilling on an active rockglacier was conducted on the Murtèl rockglacier. Boreholes of 21.7 m (labeled 1/1987) and 62.5 m (labeled 2/1987) depths were drilled in April 1987 in the scope of a project funded by the ETH Zurich. The main objectives of this

research project were (1) to study the thermal conditions and their evolution regarding atmospheric warming, (2) to analyze the creep processes and the influence of material properties and (3) to document the characteristics of the perennially frozen material as an environmental archive (Haeberli et al., 1988, 1998). Since 1987, temperatures are measured in the 2/1987 borehole of 62.5 m depth. To search for remaining organic matter to directly date the rock-glacier ice was one major objective of the borehole drilling project (Barsch, 1996; Haeberli et al., 1999). In 1989, Geotest AG carried out a major project of seismic measurements on the Murtèl rockglacier with geophones placed in the boreholes of 1987. In addition, an explosive loading was initiated in a furrow to achieve a transversal sonication of the ice-rich permafrost body (D. Vonder Mühll, 1993). In April 1990, georadar measurements were taken on the Murtèl rockglacier for the first time, during which longitudinal and transverse profiles could be established. Gravimetric measurements were performed in August 1991 to determine the regional gravity field (D. Vonder Mühll, 1993). Changes in elevation between 1987 and 1996 reveal a pattern, where the surface lowered up to 0.1 m/a on the back of transverse ridges, while on the front of the ridges, unchanged elevation was observed (Arenson et al., 2002; Frauenfelder & Kääb, 2000; Kenner et al., 2020). Two additional boreholes were drilled in 2000, up-slope from the 2/1987 borehole. Water was first reached near the permafrost table, implying that meltwater flows over the permafrost. Giant blocks and air voids were reached at a depth of 49 m, where the bedrock was estimated to be (Arenson et al., 2002). Using a combination of digital terrain model analysis, digital photogrammetry and geodetic surveys, supplemented by geomorphological mapping, Gärtner-Roer (2012) was able to determine sediment transfer rates on Murtèl rockglacier. With average horizontal velocities around 10 cm/a, mean sediment transfer rates between 0.24 – 0.51 Mt/a were determined. Maximal values for sediment transfer rates of 0.67 Mt/a during the measurement period 2002 - 2007 were estimated (Gärtner-Roer, 2012). Compared to the study by Barsch (1977), higher horizontal velocities were assumed, resulting in greater sediment transfer rates. Barsch (1977) assumed smaller values for the rockglacier length, width and thickness, while Gärtner-Roer (2012) used the thickness values determined during the borehole drilling by Haeberli et al. (1998). The different sediment transfer rates can be explained by the dependence on the rockglacier geometries, especially the thickness, and on the horizontal velocities (Barsch, 1977; Gärtner-Roer, 2012; Haeberli et al., 1998). Utilizing an eight-year (2002 - 2009) data set of borehole temperatures from the Murtèl rockglacier, Schneider et al. (2012) investigated the influence of rockglacier material on its thermal regime. Climate-driven temperature trends were smaller than material-specific temperature changes during this period. For the occurrence and mainte-

nance of alpine permafrost, the results validate that the existence and growth of ice, combined with subsurface air circulation, are essential drivers (Schneider et al., 2012). Müller et al. (2014) conducted the first study involving an analysis of geomorphologic work, using vertically differentiated sediment production as well as transport processes for the Murtèl rockglacier. They allow a comparison of the sediment budgets by describing the sedimentation pathways and quantifying the geomorphological work, which is defined as potential energy. These investigations on mass and energy transfers are carried out at the Murtèl rockglacier as well as at the directly adjacent Marmugnun rockglacier. In this study, a combination of terrestrial surveys and air-borne photogrammetry was applied. To monitor geometry changes on steep areas such as talus slopes or rockwalls, terrestrial laser scanning (TLS) has been used. Only 29 % (35.3 GJ) of the geomorphic work generated by the entire system is effectively transferred from the headwall to the Murtèl and Marmugnun rockglaciers and the rest is temporarily stored along the way. The rockglaciers themselves contribute only 4 % (1.44 GJ) to the geomorphic work of this effective transport, as they represent long-lasting sediment storages (Müller et al., 2014). In 2015, a replacement borehole was drilled by PERMOS on the Murtèl rockglacier to ensure the continuing data measurement series. Borehole instruments show limited lifetimes and permafrost creep leads to shearing at the measurement sites. Incomplete data series could therefore result at old boreholes. The new borehole on the Murtèl rockglacier (COR_0315) is drilled in the proximity of the old one (2/1987 or COR_0287) (Figure 3-20). In Figure 3-10 the measured ground temperature time series in the old (COR_0287) and new (COR_0315) borehole at Murtèl rockglacier are compared. The measurements in the new borehole started in January 2016. The high accuracy between the old and new borehole is evident (Noetzli et al., 2021; PERMOS, 2019). The locations of the boreholes are indicated in Figure 3-20.

Figure 3-10: Ground temperatures in the old (COR_0287) and new (COR_0315) boreholes at Murtèl rockglacier. The temperatures measured in the new borehole are displayed with lighter colors (PERMOS, 2019, p. 25).

3.3.1.2 Internal structure and age

The deep borehole at the Murtèl rockglacier (2/1987) reveals the complex internal structure of active talus rockglaciers (Barsch, 1996). Haeberli et al. (1988) observed a structure with six layers, displayed in Table 3-1 and Figure 3-11. Between 2003 and 2010, a constant active layer depth of 3.5 m was measured (Schneider et al., 2012). In the Murtèl rockglacier, the shear zone has evolved in the sandy layer (layer 4) in the middle of the permafrost body. The shear zone is located between 28.4 m and 31.4 m depth and shows velocities of about 4 cm/a (Arenson et al., 2002; Haeberli et al., 1988; Wagner, 1992). Between 52 m and 58 m depth, a thin seasonal talik with temperature variations around the melting point are observed. However, even with temperatures around 0 °C at this depth, a total permafrost thickness of about 100 m is assumed and extends into the underlying bedrock (Arenson et al., 2002; Haeberli et al., 1998). The layer labels in Table 3-1 refer to the same numbers in Figure 3-11. Within the PERMOS network, the active layer thickness (ALT) of the Murtèl rockglacier is determined. In alpine regions, ALT is estimated with linear interpolation between adjacent thermistors in boreholes. Due to latent heat effects, the processes of freezing and thawing are not linear. Figure 3-12 shows ALT observations for the PERMOS borehole on Murtèl rockglacier (2/1987) from 1987 to 2018. At Murtèl rockglacier, new record ALT were measured during the reporting period of 2014/2015 to 2017/2018. In 2018, a record ATL thickness of 4.5 m was observed at Murtèl rockglacier. Within all selected PERMOS boreholes with ALT observations, no significant ALT decrease was measured during this measurement period (PERMOS, 2019).

Table 3-1: Internal structure of the Murtèl rockglacier (borehole 2/1987) (Haeberli et al., 1988).

Layer label	Depth	Properties
1	0 – 3 m	Active layer, blocks, temperatures are above 0 °C
2	3 – 15 m	Permafrost body, high ice content (90 - 100 %), seasonally variable temperatures, average temperature is between -2 to -3 °C, density is around 1 Mg/m^3
3	15 – 28 m	Frozen and highly supersaturated silt, sand and gravel, ice lenses, average temperature is between -1 and -2 °C, density is between 1 - 1.5 Mg/m^3
4	28 – 32 m	Frozen and highly supersaturated silt, sand and gravel, density is nearly 2 Mg/m^3, shear zone

5	32 – 50 m	Coarse and saturated frozen rock debris with layers of frozen sand, temperature is around the melting point, high density of 2 - 2.5 Mg/m^3
6	> 50 m	Fissured, highly weathered and permeable bedrock, thin, seasonal talik (52 - 58 m), total permafrost thickness of 100 m

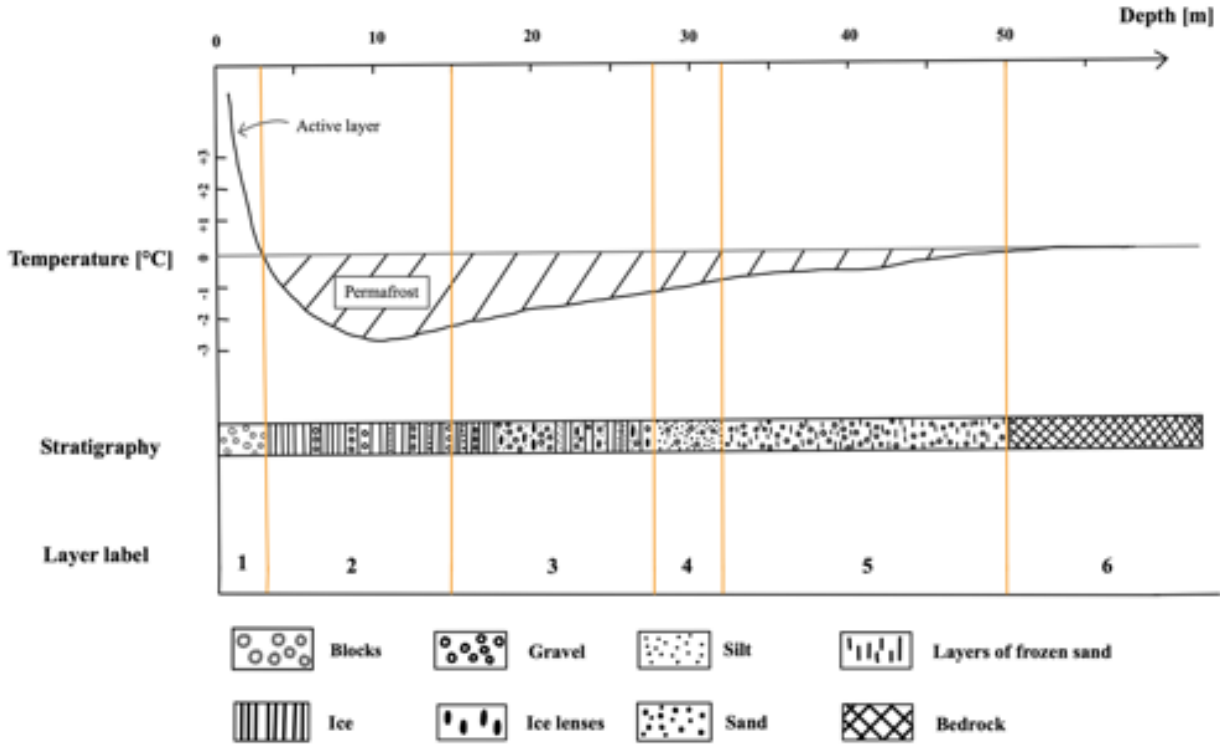

Figure 3-11: Temperature profile and stratigraphy of Murtèl rockglacier (borehole 2/1987) (after Haeberli et al., 1988).

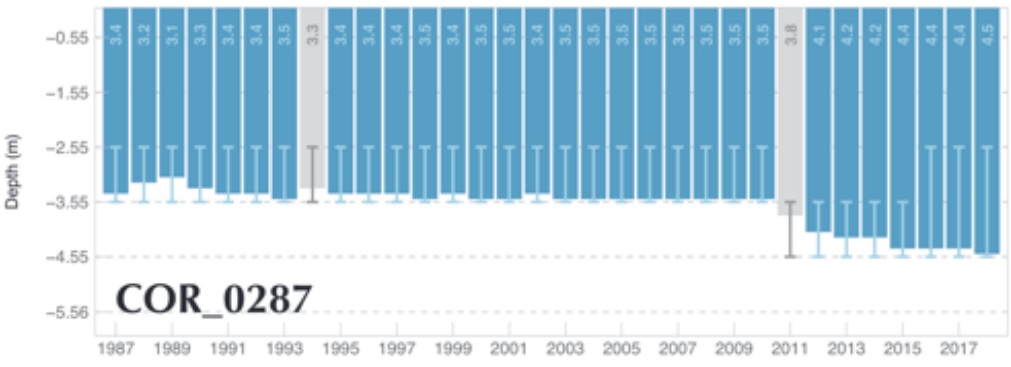

Figure 3-12: Active layer thickness (ALT) of Murtèl rockglacier from 1987 to 2018 (borehole COR_0287). Grey bars represent years with reduced data quality. The depth of the thermistors used for the interpretation is indicated with the error bars (PERMOS, 2019, p. 20).

The age determination of the Murtèl rockglacier was conducted utilizing different methods. By analyzing different moss fragments found in the permafrost of the Murtèl rockglacier, with ^{14}C dating and botanical analysis, Haeberli et al. (1999) determined its age to be 2250 ± 100 years. Most probably around the final stages of the last ice age or with the onset of the Holocene (11'700 years BP), when the area of the current rockglacier became deglaciated, the evolution of the Murtèl rockglacier began. Frauenfelder and Kääb (2000) used streamlines interpolated from the rockglacier velocity field to determine the age structure. They concluded that the surface age of the Murtèl rockglacier dates back at least 4000 years. According to these findings, the current creeping ice-rock mixture is probably several thousand years old (Frauenfelder & Kääb, 2000; Haeberli et al., 1999).

3.3.2 Marmugnun rockglacier

The Marmugnun rockglacier is another active talus rockglacier in the Murtèl cirque, adjacent to the Murtèl rockglacier to the west. With a surface area of about 0.04 km2 in 2019, the rockglaci-er is located between approximately 2620 and 2950 m a.s.l. and it faces NW (Swisstopo, 2019). The average slope is 18° and an ice volume of 40 % was assumed (Gärtner-Roer & Nyenhuis, 2009; Müller et al., 2014). The horizontal velocities of the Marmugnun rockglacier are on average 15 cm/a and therefore higher than those of the Murtèl rockglacier. Unlike the Murtèl rockglacier, there is no borehole on the Marmugnun rockglacier (Müller et al., 2014). Figure 3-13 until Figure 3-16 show the Marmugnun rockglacier system.

Figure 3-13: The Marmugnun rockglacier with the steep front, its rockwall and talus slope.

Figure 3-14: A close-up view of the steep front of the Marmugnun rockglacier.

Figure 3-15: The rockwall above the Marmugnun rock-glacier.

Figure 3-16: The border between the Murtèl (right) and Marmugnun (left) rockglaciers.

3.3.3 Chastelets rockglacier

Besides the Murtèl and Marmugnun rockglaciers, there is a third active rockglacier in the Murtèl cirque. The Chastelets rockglacier is located on the western side of the Marmugnun rockglacier and it faces NNW. In 2019, the rockglacier covered an area of approximately 0.04 km^2 (Swisstopo, 2019). In 2002, two boreholes were drilled on the Chastelets rockglacier (Figure 3-20). One borehole is located in coarse material, while the other is in fine material (Hanson & Hoelzle, 2005). The active layer thickness in the coarse underground was measured to be at a constant depth of 3 m between 2003 and 2010. In fine material, the active layer depth was at 6 m in 2003, became smaller until 2005 (4 m depth) and grew again to a depth of 6 m until 2010. The Chastelets rockglacier is illustrated in Figure 3-19.

3.3.4 Gupf

The Gupf is situated within the talus slope of the Chastelets rockglacier, representing a permafrost landform that has undergone relatively recent development compared to other periglacial landforms within the study area. Referred to as "baby-rockglacier", the Gupf is characterized by its small size and isolated occurrence of permafrost creep. The Gupf is recognized as a small-scale rockglacier that undergoes continuous development (Gärtner-Roer, 2023, unpublished). Close up views of the Gupf are shown in Figure 3-17 and Figure 3-18. The entire talus slope with the Gupf is visible in Figure 3-19.

Figure 3-17: The front of the Gupf from below.

Figure 3-18: View at the lateral right side of the Gupf.

3.3.5 Solifluction lobes

Located within the talus slope above the Chastelets rockglacier, three solifluction lobes can be observed. Solifluction, a process involving the downslope movement of soil under the influence of gravity, is not exclusively associated with permafrost (Matsuoka et al., 2005). However, considering the presence of active rockglaciers in close proximity and the associated occurrence of permafrost, it is hypothesized that the solifluction lobes in this particular case also contain permafrost. The solifluction lobes are shown in Figure 3-19.

Figure 3-19: In the talus slope situated behind the Marmugnun rockglacier, the Gupf (violet dashed) and solifluction lobes (blue dashed) are observable. Below this talus slope lies the Chastelets rockglacier (red dashed).

3.3.6 Monitoring at Murtèl cirque

Several studies performed monitoring measurements at the Murtèl cirque. The resulting values for horizontal velocities, vertical changes and the front advance are listed in Table 3-2.

Table 3-2: Monitoring measurements in previous studies at the Murtèl cirque.

Horizontal Velocities				
Landform	**Mean value (m/a)**	**Measurement period**	**Method**	**Reference**
Murtèl rockglacier	0.07	1932-1955	Photogrammetry	(Barsch & Hell, 1975)
	0.03	1955-1971	Photogrammetry	(Barsch & Hell, 1975)
	0.04	1971-1973	Terrestrial geodetic survey	(Barsch & Hell, 1975)
	0.15 (max)	1987, 1988, 1991, 1995, 1996	Photogrammetry	(Kääb, 1997; Kääb et al., 1998)
	0.05-0.15	1987-1996	Digital photogrammetry	(Kääb et al., 1998)
	0.07	1987-1995	Borehole deformation	(Arenson et al., 2002)
	0.05-0.12	2009-2010	Terrestrial geodetic surveys	(Müller et al., 2014)
	0.06-0.11	2009-2015	Terrestrial geodetic surveys	(PERMOS, 2016)
	0.06-0.12	2010-2011	Terrestrial geodetic surveys	(Müller et al., 2014)
	0.02-0.11	2011-2012	Terrestrial geodetic surveys	(Müller et al., 2014)
	0.07-0.15	2009-2023	Geodetic survey	(Gärtner-Roer, 2023, unpublished)
	0.08-0.1	2012-2021	Terrestrial geodetic surveys	(PERMOS, 2021)
Marmugnun rockglacier	0.1-0.3	2009-2010	Terrestrial geodetic surveys	(Müller et al., 2014)
	0.08-0.27	2010-2011	Terrestrial geodetic surveys	(Müller et al., 2014)
	0.1-0.3	2011-2012	Terrestrial geodetic surveys	(Müller et al., 2014)
	0.02-2.1	2009-2023	Geodetic survey	(Gärtner-Roer, 2023, unpublished)
Chastelets rockglacier	0.4-0.8	2009-2019	Geodetic survey	(Gärtner-Roer, 2023, unpublished)

Gupf	0.5-1.1	2009-2023	Geodetic survey	(Gärtner-Roer, 2023, unpublished)

Vertical changes				
Landform	**Mean value (m/a)**	**Measurement period**	**Method**	**Reference**
Murtèl rockglacier	-0.06	1932-1955	Photogrammetry	(Barsch & Hell, 1975)
	+0.02	1955-1971	Photogrammetry	(Barsch & Hell, 1975)
	-0.02	1971-1973	Terrestrial geo-detic survey	(Barsch & Hell, 1975)
	-0.04	1987-1996	Photogrammetry	(Kääb, 1997)

Front advance				
Landform	**Mean value (m/a)**	**Measurement period**	**Method**	**Reference**
Murtèl rockglacier	0.01	1987-1996	Photogrammetry	(Kääb, 1997)

Table 3-3 illustrates the boreholes and other installations (Global navigation satellite system (GNSS) and the meteorological station) in the Murtèl cirque. The labels in Table 3-3 correspond to the labels in Figure 3-20.

Table 3-3: Boreholes and installations at Murtèl cirque, which are displayed in Figure 3-20.

Number	**Year**	**Label**	**Location and Properties**	**Reference**
1	1987	2/1987, COR_0287	Murtèl rockglacier, 62.5 m deep	(Haeberli et al., 1988)
2	2000	1/2000	Murtèl rockglacier	(Arenson et al., 2002)
3	2000	2/2000	Murtèl rockglacier	(Arenson et al., 2002)
4	2002	BH31	Vegetated bedrock, boulders, 6 m deep	(Hanson & Hoelzle, 2005; Schneider et al., 2012)
5	2002	BH32	Talus slope, coarse blocky, 6 m deep	(Hanson & Hoelzle, 2005; Schneider et al., 2012)
6	2002	BH30	Bare bedrock, outcrop, 6 m deep	(Hanson & Hoelzle, 2005; Schneider et al., 2012)

7	2002	BH34	Chastelets rockglacier, fine-grained loose material, vegetated, smear layer in 4.8 m depth, 6 m deep	(Schneider et al., 2012)
8	2002	BH33	Chastelets rockglacier, coarse blocky boulders, running water in 3.5 m and 4.5 m depth, smear layer in 4.7 m depth, 6 m deep	(Schneider et al., 2012)
9	2015	COR_0315	Murtèl rockglacier, replacement borehole, 60.5 m deep	(PERMOS, 2019)
10	1997		Meteorological station (air temperature, air humidity, radiation, surface temperature, snow depth, wind speed, wind direction)	(Hoelzle et al., 2022a; Noetzli et al., 2021)
11			Permanent GNSS device with a solar panel	(Noetzli et al., 2021)

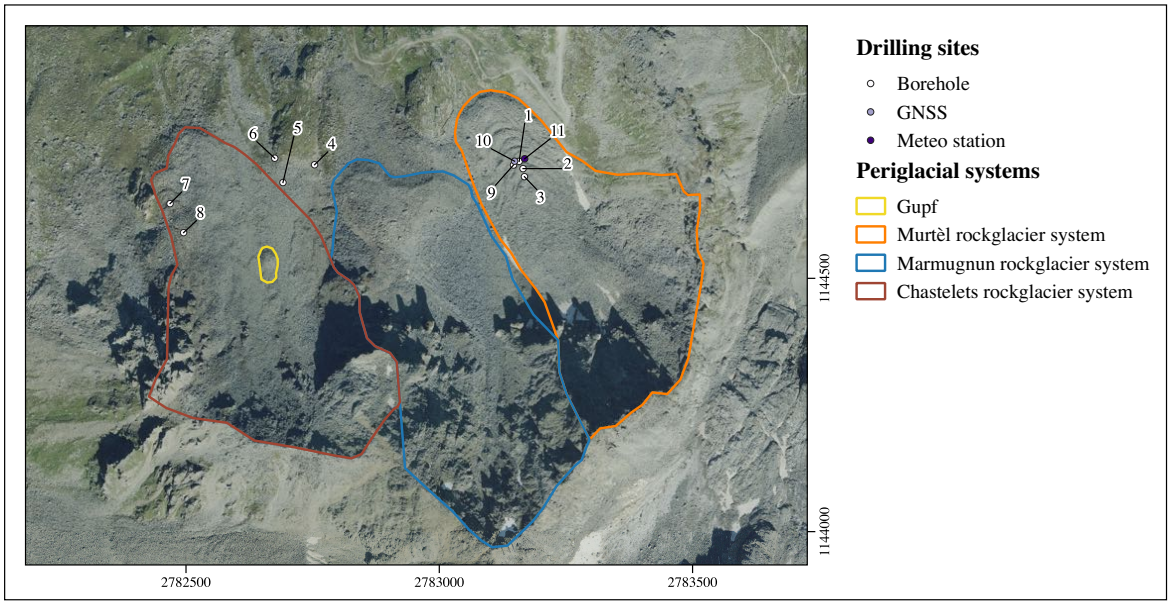

Figure 3-20: Boreholes (labelled with 1 – 9) and other installations at the Murtèl cirque. The labels are corresponding to Table 3-3 (Swisstopo, 2021).

4. DATA AND METHODS

4.1 Geomorphological Mapping

Geomorphological maps contribute to the understanding of the physical characteristics of the earth's surface. They include objective descriptions of landforms, their status of activity and spatial properties. Geomorphological mapping often serves as fundamental basis for following analysis. The purpose of investigation defines the scale of the collected geomorphic data. Usually, geomorphological mapping is executed directly in the field. In addition, aerial images and digital elevation models (DEM's) are evaluated to map inaccessible sites and large areas (Dramis et al., 2011). This classical method to create a rockglacier inventory is referred to as the geomorphological approach. Subsequently, the geomorphological map is complemented by the kinematic approach, in which moving surfaces are detected to quantify permafrost creep (Delaloye & Echelard, 2022). In this study, these two approaches are used complementarily. Geomorphological mapping provides an essential foundation for all subsequent research and interpretations. The focus of this work lies in the mapping of geomorphologic features within the periglacial environment of the Murtèl cirque. Therefore, rockglaciers and other periglacial landforms are focused on. In addition, the environments that shape and influence the periglacial features are mapped. The mapping was carried out by means of an analysis of aerial images and DEM's, which enabled the quantification of temporal changes. This allowed detailed observation and investigation of sections that are difficult to access. The geomorphological mapping was complemented by inspection directly in the field. Previous studies, conducted in the Murtèl cirque, were also taken into account (e.g. Burga et al., 2004; Müller et al., 2014; Schneider et al., 2012). The geomorphological mapping of the periglacial landforms is completed with the parameters of size, position, slope and vegetation cover and, in the case of rockglaciers, with the state of activity (active, inactive, relict). The determination of rockglacier activity is based on evaluation criteria according to Roer & Nyenhuis (2007), such as e.g. the slope angle of the rockglacier front, the vegetation cover or the geomorphological appearance of the rockglacier front. These characteristics are shown in the geomorphological map and presented in an inventory list, according to Nyenhuis (2005). The concepts given by the IPA Action Group Rockglacier inventories and kinematics were taken as a guideline. This inventory strategy follows the following steps: locating rockglaciers and relevant landforms, locating and georeferencing the rockglacier, describing and characterizing the rockglacier, and finally, delineating the rockglacier system (Delaloye et al., 2022; Delaloye & Echelard, 2022).

4.2 Photogrammetry

4.2.1 Basic principles

Photogrammetry is broadly divided into two types: aerial, using an airborne camera, and terrestrial, where the camera is either hand-held or fixed on a tripod. Aerial photogrammetry, a technique used to derive precise measurements and three-dimensional information from aerial imagery, is influenced by several key parameters that collectively determine the accuracy and quality of the results. The bundle block adjustment represents a mathematical approach (triangulation) used to determine the precise position and orientation of multiple images taken from different viewpoints. Therefore, this technique is an essential process in reconstructing three-dimensional information from two-dimensional images (Aber et al., 2010; Heisig & Simmen, 2021; Kääb, 2005; Konecny & Lehmann, 1984; Luhmann, 2018). The flight altitude at which the camera operates above the ground directly impacts the scale of the captured images and the level of detail they reveal. Adequate overlap and sidelap between consecutive images are crucial to compute the three-dimensional terrain topography, ensuring stereoscoping vision (stereo coverage). Overlap refers to the coverage shared between images, both along the flight direction (forward overlap) and perpendicular to it (side overlap). This requirement, as highlighted in Kääb (2005), is crucial for establishing points in space through the convergence of directed rays from overlapping photography. Sufficient overlap is indispensable to reconstruct the three-dimensional information from aerial imagery (Kääb, 2005). The camera's focal length, the distance between its lens and image sensor, significantly influences the field of view and scale. Additionally, the size of the image sensor plays a role; larger sensors tend to capture more detail and produce higher-quality imagery. The film format has changed over time, as it increased from 15 x 15 cm to 23 x 23 cm. Therefore, older images are often smaller and often more degraded due to longer storage. Furthermore, older images were taken on less technically advanced systems. Proper camera calibration informations allow for correction of camera-intrinsic distortions and ensure accurate measurements. The interior orientation defines the internal geometry of a camera or sensor by establishing transformation parameters between the camera coordinate system and the image pixel coordinate system. The spatial placement and angular alignment of a photograph in relation to the ground coordinate system define its exterior orientation (Egels & Kasser, 2001; Quarter, 2005). Ground control points (GCPs), known sets of reference points on the ground with precisely surveyed coordinates, are crucial for georeferencing and scaling the aerial imagery (Kääb, 2005). Other factors include image resolution, defined by the level of detail in each image,

and the Ground Sampling Distance (GSD), which relates pixel size to ground dimensions. Image acquisition timing is also important, impacting lighting conditions, shadows, and potential obstructions in the imagery (Egels & Kasser, 2001; Kääb, 2005).

4.2.2 Processing steps

In this work, the following processing steps and the generation of DEM's and orthophotos were carried out by the Federal Office of Topography Swisstopo. The processing steps and resulting outputs associated with both analogue and digital aerial imagery are examined. In this study, the years between 1955 and 2007 are covered by analogue images, while the images of 2012 and 2021 are represented by digital images. These procedures and outcomes shed light on the evolution of aerial imaging techniques and their applicability across different time periods. In the context of analogue aerial photography, the initial processing involves the conversion of physical photographs to digital format through scanning. Subsequent procedures take place at the photogrammetric workstation, where the basic elements of interior and exterior orientation are established. This involves the precise determination of spatial position and angular orientation of the camera's projection center for each acquisition. In addition, a key aspect of this process is the computation of a DEM, which provides a representation of the underlying terrain. A further processing step consists in the generation of orthophotos, rectified images that alleviate distortions and offer accurate representations of the observed area. The primary outputs from this sequence of operations are, therefore, the orthophotos and the derived DEM data (Heisig & Simmen, 2021). In the digital aerial imagery from 2012 and 2021 in this study, a technological shift is evident as the data is already digitally captured and no longer needs to be scanned. To ensure high accuracy, manual reference points must still be measured to determine orientations through iterative bundle block adjustment. Additionally, the DEM computation process continues, contributing to the spatial understanding of terrain morphology. The automated process, like its analogue counterpart, leads to the creation of orthophotos and DEM data. These outcomes resonate in diverse applications (Baltsavias, 1996; Jiménez-Jiménez et al., 2021; Kääb, 2005). In this study, the orthophotos are used within the Correlation Image Analysis Software (CIAS), enabling the generation of two-dimensional flow vectors and providing the analysis of movement patterns. In contrast, DEM data play a central role in Geographic Information Systems (GIS), serving as the basic elevation source for investigating topographic variations such as changes in elevation.

4.3 Data sets

4.3.1 Aerial images

Aerial images and aerial image strips represent the data basis of this work. The selected products, provided by Swisstopo, are listed in Table 4-1. In selecting the data for this study, particular attention was given to obtaining a consistent and regular time interval. The time intervals ranged from 4 years (2003-2007) to 16 years (1955-1971), with an average interval of 7.3 years. The choice of specific years was constrained by the availability of stereo coverage in the study area. It was essential to ensure that the entire study area was adequately covered by at least three images from the same flight date. In cases where this requirement was not met, the respective year could not be included in the analysis. This stereo coverage was necessary for subsequent processing steps, including the generation of orthophotos. Furthermore, careful consideration was given to select aerial imagery that minimized the presence of large shadows and excessive snow cover. These characteristics, if present, could introduce complications or distort the information extracted from the images. Therefore, efforts were made to minimize the impact of shadows and snow in order to ensure the accuracy and reliability of the derived information (Joerg et al., 2012; Kääb, 2005). The steps of the selection process of the aerial images are displayed in Figure 4-1.

Table 4-1: Aerial images and image strips from Swisstopo used as a basis for DEM and orthophoto generation.

Year	Flight date	Product	Picture number	Flying height [m]	Dimensions of original image [cm]
1955	02.09.55	Aerial Images swisstopo b / w	19551440030865 19551440030866 19551440030867	5400	18 x 18
1971	02.09.71	Aerial Images swisstopo b / w	19719990194170 19719990194171 19719990194172	5700	23 x 23
1979	17.09.79	Aerial Images swisstopo b / w	19799990268666 19799990278883 19799990278884	5800 6000	23 x 23
1985	30.08.85	Aerial Images swisstopo b / w	19851440035070 19851440035071 19851440035072	5800	23 x 23
1991	30.08.91	Aerial Images swisstopo b / w	19910441555350 19910441555351 19910441555352 19910441555353 19910441555354	3400	23 x 23
1998	11.08.98	Aerial Images swisstopo b / w	19981440054696 19981440077642 19981440077643	7000	23 x 23
2003	17.09.03	Aerial Images swisstopo color	20031451023915 20031451023916 20031421023980 20031421023981	6400	23 x 23
2007	24.09.07	Aerial Images swisstopo b / w	20070721554483 20070721554484 20070721554485 20070721554486 20070721554487	3400	23 x 23
2012	20.08.12	Image strip swisstopo color	Flying line: 30030201208200939		
2021	01.09.21	Image strip swisstopo color	Flying line: 12501202109011035		

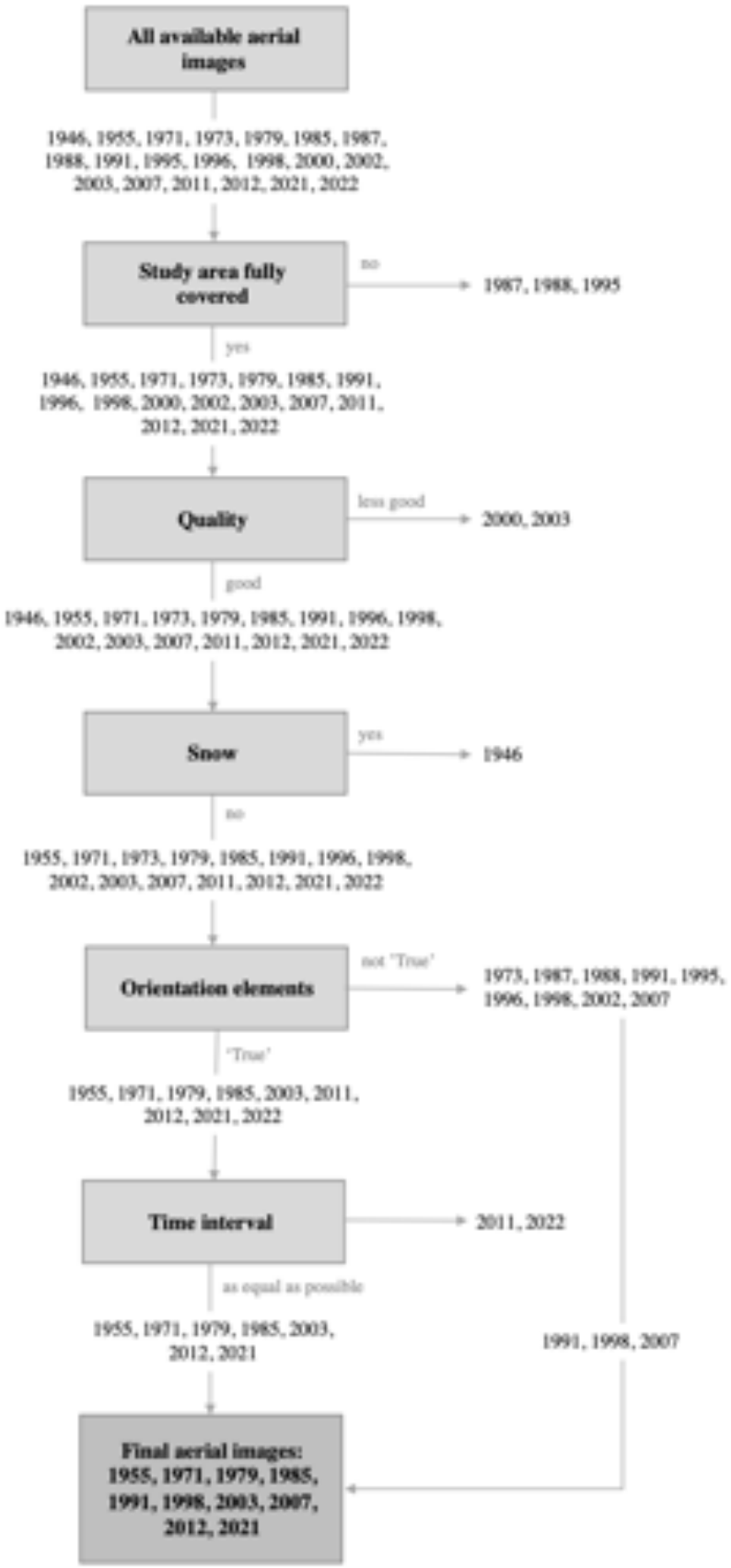

Figure 4-1: The selection process leading to the final ten aerial images, provided by Swisstopo.

4.3.2 Orthophotos and digital elevation models

The aerial images and aerial image strips from the Federal Office of Topography Swisstopo served as the basis for creating the orthophotos and DEM's, which were generated by Swisstopo (Swisstopo, 2021a, 2021b). The details regarding the orthophotos are listed in Table 4-2 (Swisstopo, 2023b). The DEM's as well as the orthophotos were later modified using the values from co-registration from Table 4-3 (Chapter 4.3.2.2). For the analysis and quantification of both horizontal and vertical displacements, the orthophotos serve as the primary data basis. In contrast to aerial images, orthophotos are free from distortions and maintain a uniform scale throughout their entire extent (Egels & Kasser, 2001; Kääb, 2005).

Table 4-2: The utilized orthophotos, which were generated from the aerial images and image strips listed in Table 4-1.

Year	Flight date	Pixel size	Image basis	Color
1955	02.09.55	0.25m x 0.25m	Analogue images	Greyscale
1971	02.09.71	0.25m x 0.25m	Analogue images	Greyscale
1979	17.09.79	0.25m x 0.25m	Analogue images	Greyscale
1985	30.08.85	0.25m x 0.25m	Analogue images	Greyscale
1991	30.08.91	0.25m x 0.25m	Analogue images	Greyscale
1998	11.08.98	0.25m x 0.25m	Analogue images	Greyscale
2003	17.09.03	0.25m x 0.25m	Analogue images	Greyscale
2007	24.09.07	0.25m x 0.25m	Analogue images	Greyscale
2012	20.08.12	0.25m x 0.25m	Image strip Leica ADS80	RBG
2021	01.09.21	0.1m x 0.1m	Image strip Leica ADS100	RBG

4.3.2.1 Qualitative analysis of DEM's

There are several ways to evaluate the accuracy of DEM's, such as the qualitative evaluation of shaded reliefs (Kääb, 2005). In order to qualitatively compare the elevation values of the DEM's at various point locations within the study area, a comparison was conducted using the current topographic map (national map of 2023). This map includes accurately recorded elevation data from the national DEM (swissALTI3D) (Swisstopo, 2023a). The comparison involved calculating the difference between the DEM's and the reference map of 2023 at 15 point locations. These points are positioned outside the examined landforms. This process of qualitatively analyzing the data serves as a preparation for the subsequent quantitative analysis to identify tilting or rotation (Kääb, 2005). In regions characterized by steep slopes or snow cover, reduced levels of accuracies must be expected. The comparison of pixels

(DEM's) to point data introduces imprecision into this analysis (Koblet et al., 2010). The differences between the national map of 2023 and the DEM's are visualized in Figure 4-2. A positive difference indicates that the DEM lies higher than the reference map, while a negative difference signifies that the DEM is located lower at this point location. The differences are listed in Appendix 11.1., where statistical values (mean, root mean square error (RMSE), standard deviation (STDEV) and standard error (SE)) are calculated for further quality assessment. The examination of these differences was used to determine systematic uncertainties in the data (Koblet et al., 2010). Inaccuracies occurred mainly due to steep slopes, shadows, and snow cover. For instance, point number 12, situated on a mountain ridge, shows consistently positive values each year. While this could signify a decrease in elevation caused by gravitational mass movements, it is not necessarily attributed to data inaccuracies. Most of the DEM's are systematically too low. Especially in the year 1985, when the largest snow cover was present, the values of RMSE (16 m) and STDEV (2.4 m) are large. However, the resultant SE of 0.6 m is acceptable. Since the SE's of all years measure 1 m or less, this assessment does not show any clear evidence of tilting or rotation. As a result, further DEM analysis were centred on potential displacements in the x, y and z directions. The method proposed by Nuth & Kääb (2011) was used for this purpose, as it enables the calculation of shifts along these three directions (see Chapter 4.3.2.2).

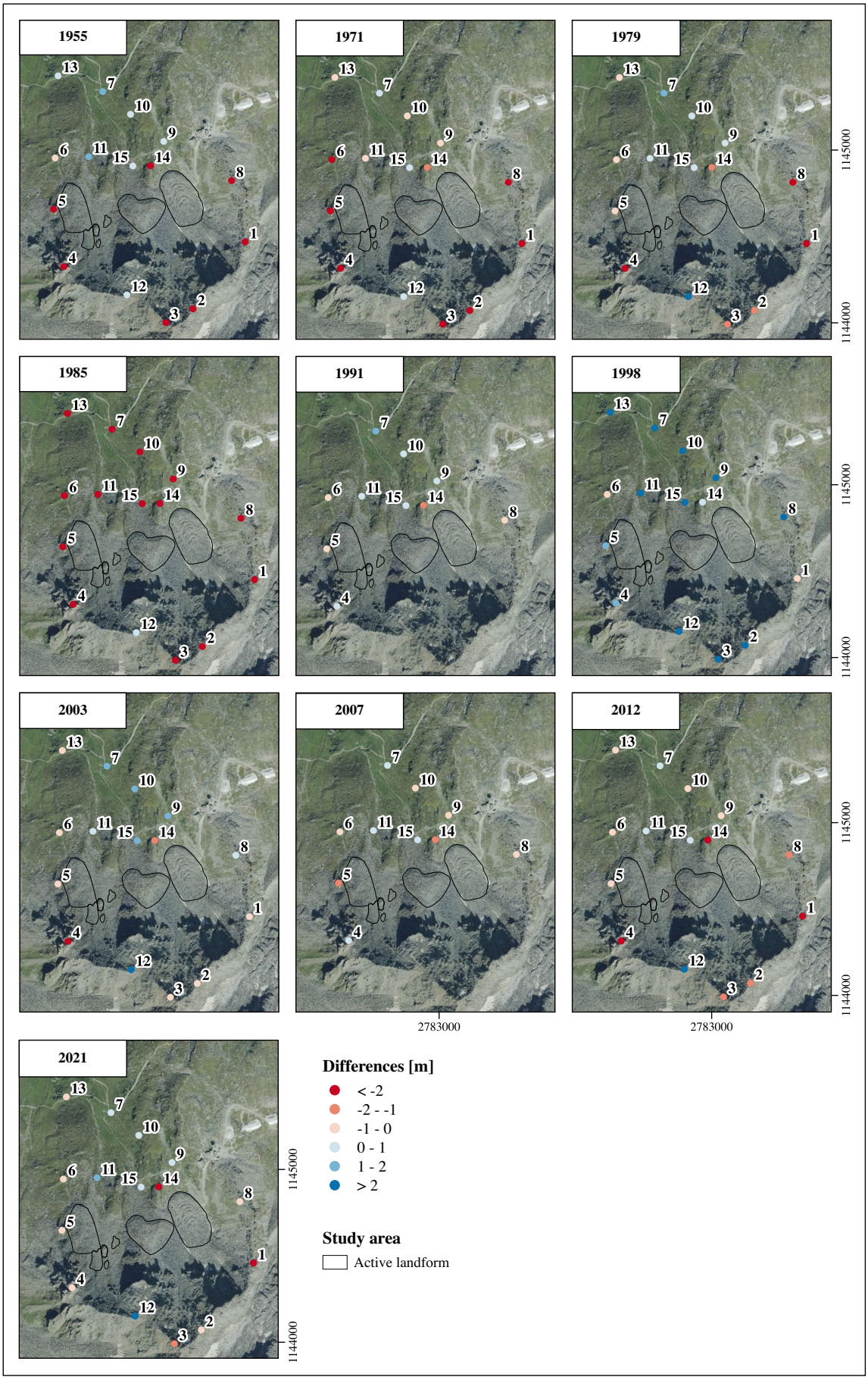

Figure 4-2: Elevation differences between the national map of 2023 and the DEM's of different years. The point labels correspond to the numbers in Appendix 11-1 (Swisstopo, 2021; Swisstopo, 2023a).

4.3.2.2 Co-Registration

The co-registration process and error estimation in this study are conducted using the method proposed by Nuth & Kääb (2011), which is based on statistical error modeling. Therefore, this method is suitable to determine potential corrections to the DEM's and estimating errors. Given that the step of data processing was performed by Swisstopo, the exact procedure of processing is not specified in this study. Following the approach of Nuth & Kääb (2011), the differences between two elevation models are calculated and analyzed for topographic effects. In the case of a topographic effect, the differences between two DEM's within the stable terrain are tested for horizontal and vertical displacements using a function based on exposure and slope. For two shifted DEM's, a correlation between the elevation differences and the slope exposure can be observed. On steep slopes, the elevation differences are larger compared to flatter slopes. The method proposed by Nuth & Kääb (2011) resolves the dependence of the height differences on the slope inclination and consequently determines the displacements in x, y and z directions. The proposed correction values are applied and tested in a subsequent calculation. This iterative process continues until the standard deviation (σ) between two iterations shows minimal changes (below 2 %) (Joerg et al., 2012; Nuth & Kääb, 2011).

In this study, the DEM's from the years 1955, 1971, 1979, 1985, 1991, 1998, 2003, 2007 and 2012 ("secondary DEM's") were tested and examined for displacements using the DEM from 2021 serving as the reference dataset ("primary DEM"). The DEM from 2021 was selected as the reference dataset, as it is the most recent available image and the study area has minimal snow cover and shadow, which could potentially introduce uncertainties during co-registration. Stable terrain was chosen in the vicinity of the rockglaciers. An attempt was made to cover a wide range of exposures and slopes inside the stable terrain, as the method of

Table 4-3: Results from the Excel-Tool from Nuth & Kääb (2011) for the secondary DEM's compared to the primary DEM of 2021 [m].

Years	Original DEM				Correction				Parameters changed	Iteration
	x	y	z	σ	x	y	z	σ		
1955	0.7	-0.1	-0.2	2.36	-0.7	0.1	-	2.35	x and y	1
1971	-0.9	-1.5	-0.6	2.28	0.9	1.8	0.3	2.24	x, y and z	3
1979	-0.9	0.2	0.2	3.14	0.9	-0.2	-	3.07	x and y	1
1985	-0.9	-1.3	-3.7	5.85	-	-	3	3.13	z	2
1991	-0.1	-0.3	0.2	1.08	-	-	-0.1	1.02	z	2
1998	0	-0.7	3.1	4.21	-	-	-2.7	2.11	z	3
2003	-0.4	-1.3	0.5	1.79	0.4	1.3	-0.5	1.76	x, y and z	1
2007	0.6	-0.4	0	0.94	-0.6	0.4	-	0.94	x and y	1
2012	0.9	-0.2	-0.1	1.13	-0.8	0.4	-	1.08	x and y	2

Nuth & Kääb (2011) relies on these two parameters. However, difficulties were encountered due to the talus slopes and steep slopes surrounding the study area. Such unstable areas are avoided within the stable terrain. A generous selection of stable terrain was made in order to account for potential outliers and minimize their impact on the analysis. Regions that have experienced anthropogenic changes since 1955 are not considered part of the stable terrain. To determine exposure in flat terrain introduces potential errors, leading to the exclusion of slopes with inclinations less than 5° from the analysis. Similarly, slopes greater than 45° were not included in the analysis due to increased uncertainty regarding their stability and inaccuracies in the elevation models (Pulighe & Fava, 2013). Within the stable terrain, the elevation differences from the primary DEM of 2021, the slope and exposure were extracted for each secondary DEM. The calculation of horizontal and vertical displacements between two DEM's was then performed using the Excel tool from Nuth & Kääb (2011). The DEM's were horizontally moved in ArcGIS (shift) and vertically adjusted in QGIS (Raster Calculator), based on the calculated values (Joerg et al., 2012; Nuth & Kääb, 2011). This procedure was repeated through multiple iterations. If the standard deviation between two iterations changed by less than 2 %, the calculated values to shift are applied. The remaining standard deviation over the stable terrain serves as a measure of the random error (Zemp et al., 2013). The correction values for the secondary DEM datasets compared to the primary DEM as well as the applied correction values are listed in Table 4-3. A clear improvement in the standard deviation as a result of the co-registration process was achieved in 1985 and 1998. In the other years, it either remained the same or improved, but to a lower magnitude. All the iterations performed are listed in Appendix 11.2. The obtained shifts in x and y directions were applied to the orthophotos as well. The selected stable terrain is illustrated in Figure 4-3.

4.3.2.3 Comparison of the qualitative and quantitative DEM analysis

The comparison of the qualitative point analysis (comparison of the national map and DEM's, Chapter 4.3.2.1) with the quantitative area-based analysis according to Nuth & Kääb (2011) (Chapter 4.3.2.2) results in different values for most years. This discrepancy is attributable to the fact that the qualitative analysis examines individual points (15 manually chosen points), while the quantitative analysis evaluates at least 10'000 points in each iteration. In addition, the area-based quantitative analysis considers the impact of exposure and slope. The limited number of points in the qualitative analysis leads to a greater susceptibility to error and dependence on outliers. Conversely, the quantitative analysis benefits from a higher number of study points, which helps to reduce errors and outliers, and thus carries comparatively less weight in the analysis. In addition, the quantitative analysis excludes extremely flat and steep

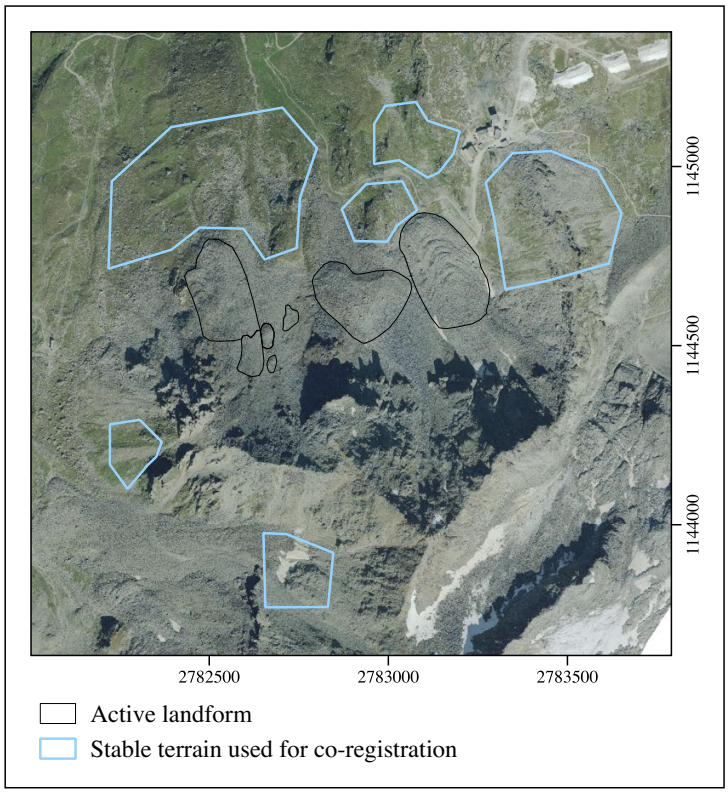

Figure 4-3: Stable terrain used for co-registration. The orthophoto of 2021 is displayed as background (Swisstopo, 2021).

points, which have a higher potential for error. In contrast, some points in the qualitative point analysis were positioned on mountain ridges, where even minor data inaccuracies can result in significant differences. The variability of topography on ridges leads to a higher weighting of elevation differences in the qualitative analysis. Consequently, this study continues using the quantitative method proposed by Nuth & Kääb (2011) for subsequent analysis.

4.3.2.4 Accuracy assessment of DEM's

If the accuracy of each DEM is calculated in relation to the DEM of 2021, the values in Table 4-4 are resulting. This leads to an uncertainty range of 0.04 m/a – 0.12 m/a.

Table 4-4: Accuracies for the DEM's in relation to the DEM of 2021 [cm/a].

	1955	1971	1979	1985	1991	1998	2003	2007	2012
cm/a	3.6	4.5	7.3	8.7	3.4	9.2	9.8	6.7	12

4.3.2.5 Accuracy assessment of orthophotos

The orthophotos are subject to the same accuracy values as the DEM's (0.04 m/a – 0.12 m/a), since they are derived from DEM's and are offset by the same values according to co-registration (Chapter 4.3.2.2). This manual shifting of the orthophotos in x and y direction introduces some inaccuracy, as correctly the orthophotos would be re-calculated after the co-

registration process of the DEM's. However, since this was not possible in this study, the orthophotos were shifted manually. Figure 4-4 provides an overview of all ten orthophotos used, allowing the identification of various features that may influence the subsequent analysis. Above the Marmugnun rockglacier and on both sides of the Murtèl rockglacier, snow can be observed in several orthophotos (e.g., 1955, 1979 or 1991). In some years, small snow patches can be observed on the talus slope of the Chastelets rockglacier. 1979 and 1985 stand out with the most extensive snow cover. In 1985, in addition to the abundant avalanche deposits, there is also a thin layer of fresh snow that covers a wide area. The presence and pattern of shadows in the orthophotos also vary between the orthophotos. Substantial shadows on the Marmugnun talus slope and rockglacier are noticeable in 1979 and 2003, while in particular in 1998 and 2012, the shadows are minimal. These varying features in the orthophotos need to be considered as they can influence the following evaluations.

4.4 Validation data sets

4.4.1 LuBis data

To assess the quality and accuracy of the DEM's in this study, low flown LuBis data sets are used for validation. Such special aerial surveys are conducted in late summer to capture areas as free of snow as possible. Data sets captured in 1996, 2002 and 2007, covering the Murtèl and Marmugnun rockglaciers as well as the Gupf, serve as the basis for comparison. They underwent processing by Isabelle Gärtner-Roer and are available and used at a resolution of 50 cm (provided by Gärtner-Roer, 2023).

4.4.2 Geodetic survey

To validate the results concerning the annual horizontal velocities derived from CIAS, values from the annual geodetic survey, conducted between 2009 and 2023, are utilized. These measurements are conducted in the field using a tachymeter (Leica Smart Station System 1200) and are carried out by Isabelle Gärtner-Roer (Gärtner-Roer, 2023). The values are listed in Table 3-2.

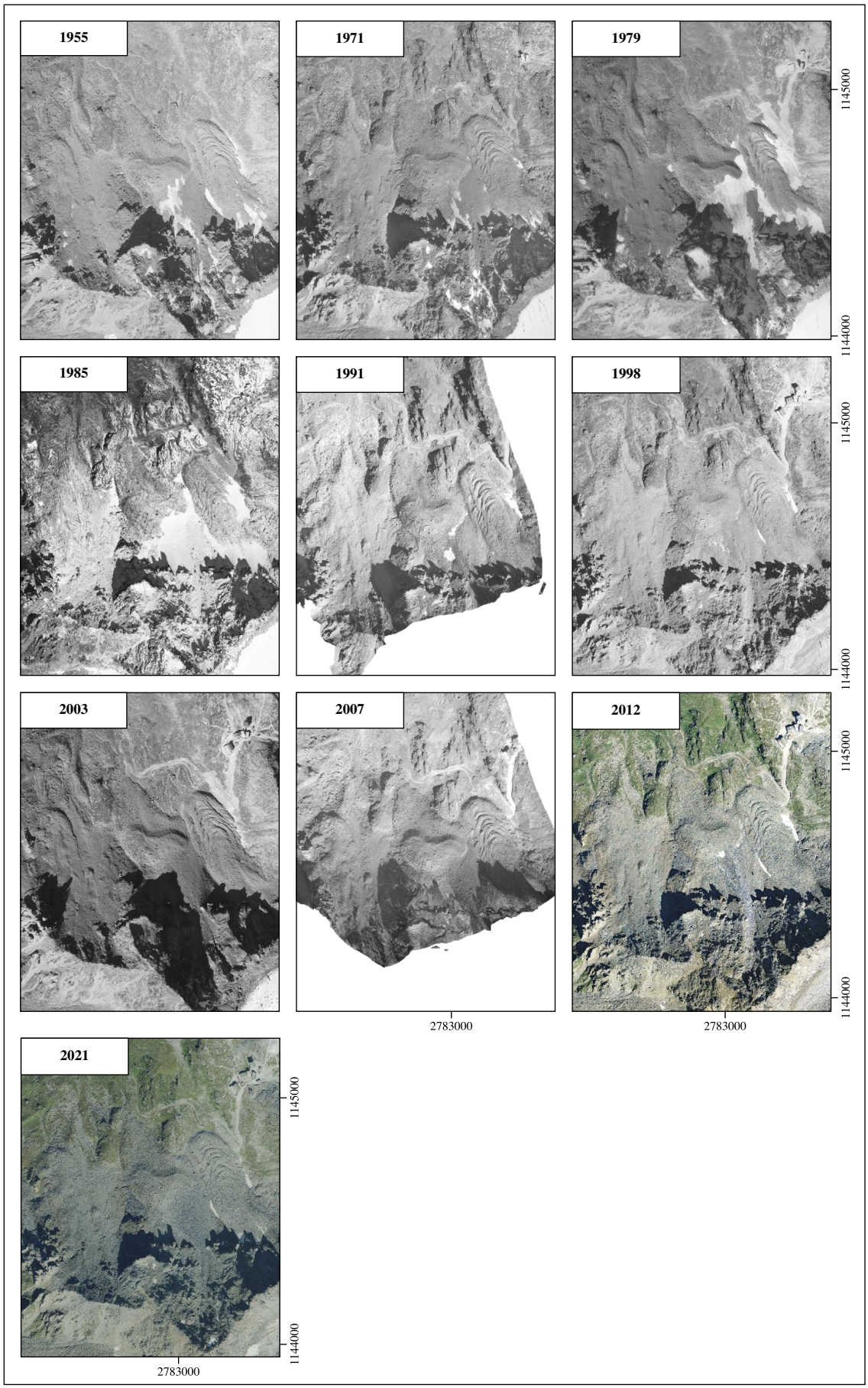

Figure 4-4: The orthophotos between 1955 and 2021 (Swisstopo, 2021).

4.5 Measurement of horizontal velocities

4.5.1 CIAS

Horizontal surface velocities are derived from digital orthoimages using the software CIAS developed at the University of Zurich by Vollmer (1999). CIAS is written in IDL (Interactive Data Language). In this work, the version of 2013 (May 23) is used. Multi-temporal digital orthophoto comparison is performed with the identification of respective image-blocks to obtain horizontal surface movements. As input for CIAS, two co-registered orthophotos (Chapter 4.3.2.2) are required in geotiff or tiff-world format. Both images need to have matching resolutions and they must be in the same channel (Heid & Kääb, 2012; Kääb & Vollmer, 2000; Vollmer, 1999).

To measure an individual horizontal displacement vector, two steps are considered. A reference block (RB) with sufficient optical contrast is selected from the orthophoto of time 1. The coordinates of the pixel in its center must be known. Then, in the so-called test area or search area (SA), the corresponding test block is searched for in the orthophoto of time 2. The differences in the coordinates of the central pixel result in the horizontal displacement between time 1 and time 2 (Kääb & Vollmer, 2000; Vollmer, 1999). A double cross-correlation function is used to calculate the similarity between the reference and test blocks and it is depending on grey values of the orthoimages. It is applied to identify corresponding image blocks in two or more orthoimages and is calculated as following (Vollmer, 1999, p. 21):

$$\phi(i,k)= \frac{\sum_j \sum_l s((i+j, k+l) - (\frac{T_{test}}{N_{test}})) * m((j,l) - (\frac{T_{ref}}{N_{ref}}))}{\sqrt{\sum_j \sum_l s^2 ((i+j, k+l) - (\frac{T_{test}}{N_{test}})) * \sum_j \sum_l m^2 ((j,l) - (\frac{T_{ref}}{N_{ref}}))}}$$

The formula consists of the parameters in Table 4-5:

Table 4-5: Explanation of the parameters of the cross-correlation formula (Vollmer, 1999).

Parameter	Explanation	Reference / test block
ϕ	Double cross-correlation function	
(i, k)	Coordinates	Test block
(j, l)	Coordinates	Reference block
s	Spatial grey-value function	Test block
s(i, k)	Grey value at the location (i, k)	Test block
m	Spatial grey-value function	Reference block
m(j, l)	Grey value at the location (j, l)	Reference block
T_{test}	Sum of grey values	Test block
T_{ref}	Sum of grey values	Reference block
N_{test}	Number of pixels	Test block
N_{ref}	Number of pixels	Reference block

The horizontal distance between the pixel coordinates in the center of the reference and test block is then calculated for the reference block with the largest cross-correlation function. The horizontal displacement in the direction of x and y (dx and dy), the length of the total displacement, the direction of the displacement, the x and y coordinates of the grid, and the maximum as well as the average correlation coefficient are returned as the result (Heid & Kääb, 2012; Kääb & Vollmer, 2000). The schema of measuring surface movements using block-correlation is displayed in Figure 4-5.

The double cross-correlation function ranges between -1 and +1. Total equivalence between the reference and test block is given with a value of +1. To normalize the grey values of the test and reference blocks, the equation contains the terms T / N, to make sure that the differences in the total grey values do not impact the correlation result. A uniform modification in the brightness of a block, for example the test block becoming brighter than the reference block, has therefore no influence on the correlation result. The computational effort is strongly dependent on the size of the test area (Kääb & Vollmer, 2000; Vollmer, 1999).

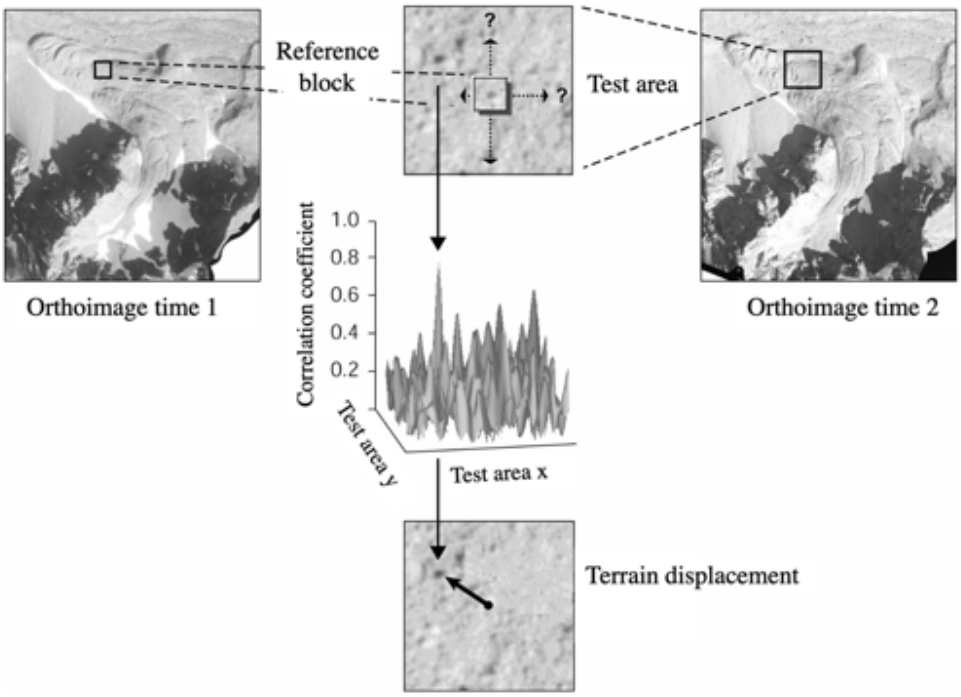

Figure 4-5: Measurement of terrain displacement from repeated orthoimages with block-correlation (from Kääb & Vollmer, 2000, p. 319).

Problems with the measurement of surface movements can occur if, for example, a block is kipt between the two points in time and can therefore no longer be recognized in the test area. The following factors may play a role in the identification of a reference block: changes on the earth's surface, position of the sun, shadows, block sizes, snow left lying on the ground or human interventions. The measurements can be performed in three different approaches. The first option is the area grid measurement, which involves creating a polygon in which measurement points are generated in a predefined grid. Second, the single point measurement, where single measurement points are selected. This measurement method is also called supervised measurement. The third approach is the control file measurement, in which a text file is used to represent the coordinates of the measurement points. This technique is called unsupervised measurement. Small blocks in large test areas should be avoided with this technique (Vollmer, 1999).

4.5.2 Data preprocessing

To determine the horizontal displacement in CIAS, the orthophotos underwent preprocessing steps in QGIS. This involved ensuring that the orthophotos were in the same channel, with consistent coordinate systems and pixel sizes. These properties were edited prior to the analysis in CIAS. All the orthophotos were already in the same coordinate system (CH1903+ / LV95), eliminating the need for any coordinate system adjustments. The year 2021 consists of

several individual orthophotos, which were merged into one single orthophoto. The orthophotos of 2012 and 2021 are the only years that are RGB images and were therefore converted to grayscale images. As the orthophoto from 2021 has a pixel size of 0.1 x 0.1 m, which differs from the pixel size of 0.25 x 0.25 m in the other orthophotos, its resolution was adjusted in QGIS to match the pixel size of the orthophotos from the other years.

4.5.3 Parameter selection in CIAS

To find the test block as the reference block in the search area, the size of the area is selected in accordance to the expected maximum displacement of the block. The rule of thumb for determining the size of the search area is calculated including the time difference between the orthoimages and the maximal velocity. The factor two represents the square propagation of the search area from the block center (Vollmer, 1999). In this study, the size of the search area was determined based on the average time difference between the orthoimages, which corresponds to 7.3 years. The maximum velocity was used from the Marmugnun rockglacier, where maximum horizontal displacements of 2.1 m/a were measured (Gärtner-Roer, 2023, unpublished). The resulting size of the search area was determined to be 30 m. Smaller (20 m), and larger (40 m) search areas were also tested to complement the analysis. The grid distance is maintained at 25 m over the whole analysis.

The size of the test and reference blocks is chosen according to the textural characteristics of the rockglacier surface and has to be adapted to image resolution. If the block sizes are selected too small, the cross-correlation function ϕ has no clear maximum. However, if the block sizes are chosen too large, the computing time increases. In CIAS, the sizes of the search area and the test and reference blocks are inserted based on the number of pixels (Kääb, 2005; Kääb & Vollmer, 2000; Vollmer, 1999). The observed maximum block sizes ranged from 9 m on the Chastelets, 13 m on the Murtèl to 14 m on the Marmugnun rockglacier. However, the majority of the blocks were smaller, measuring approximately less than 7 m. Therefore, two reference block (RB) sizes, 7.5 m and 15 m, were tested.

Figure 4-6 illustrates the density function of annual horizontal movements between 1955 and 1971, aiming to assess the influence of the selected parameters. Six different combinations of reference block sizes and search area sizes were tested. The sizes of these parameters needed to be entered in CIAS in terms of pixels (RB: 7.5 m = 30 pixels, 15 m = 60 pixels; SA: 20 m = 80 pixels, 30 m = 120 pixels, 40 m = 160 pixels). Utilizing a larger reference block (15 m), the density function exhibits a more distinct maximum compared to the less discernible max-

imum using a smaller reference block (7.5 m). With a smaller reference block, the cross-correlation function within CIAS does not display a clear maximum. Furthermore, maintaining a constant reference block size while increasing the size of the search area leads to higher maximum horizontal velocities. Conversely, if the search area remains unchanged, a larger reference block size yields a clearer maximum in the density function, although the maximum horizontal displacement is smaller in magnitude.

The spatial distribution of annual horizontal displacements over the active landforms in the study area, using the same six combinations of reference block and search area sizes as in Figure 4-6, is shown in Figure 4-7. Smooth gradients between the annual horizontal displacements are achieved when using a small search area of 20 m and a large reference block size of 15 m. However, this small search area fails to detect larger displacements. On the other hand, adopting a large search area of 40 m results in punctual values with steep gradients, including some exceptionally high values. Consequently, the use of a large search area is not suitable as well. Thus, a search area of 30 m, representing an intermediate value, is utilized in this study. To ensure the inclusion of the largest blocks in CIAS, a reference block size of 15 m is used.

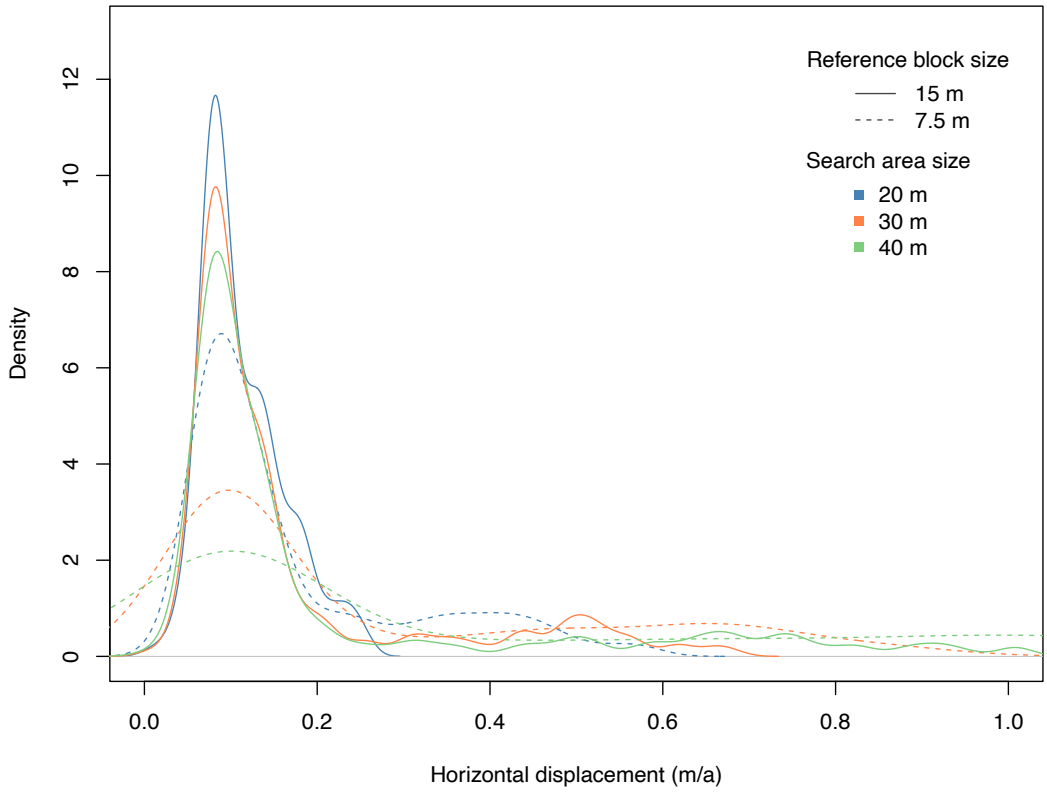

Figure 4-6: Density function of the annual horizontal displacements between 1955 and 1971 for different combinations of reference block sizes (7.5m and 15m) and search area sizes (20m, 30m and 40m).

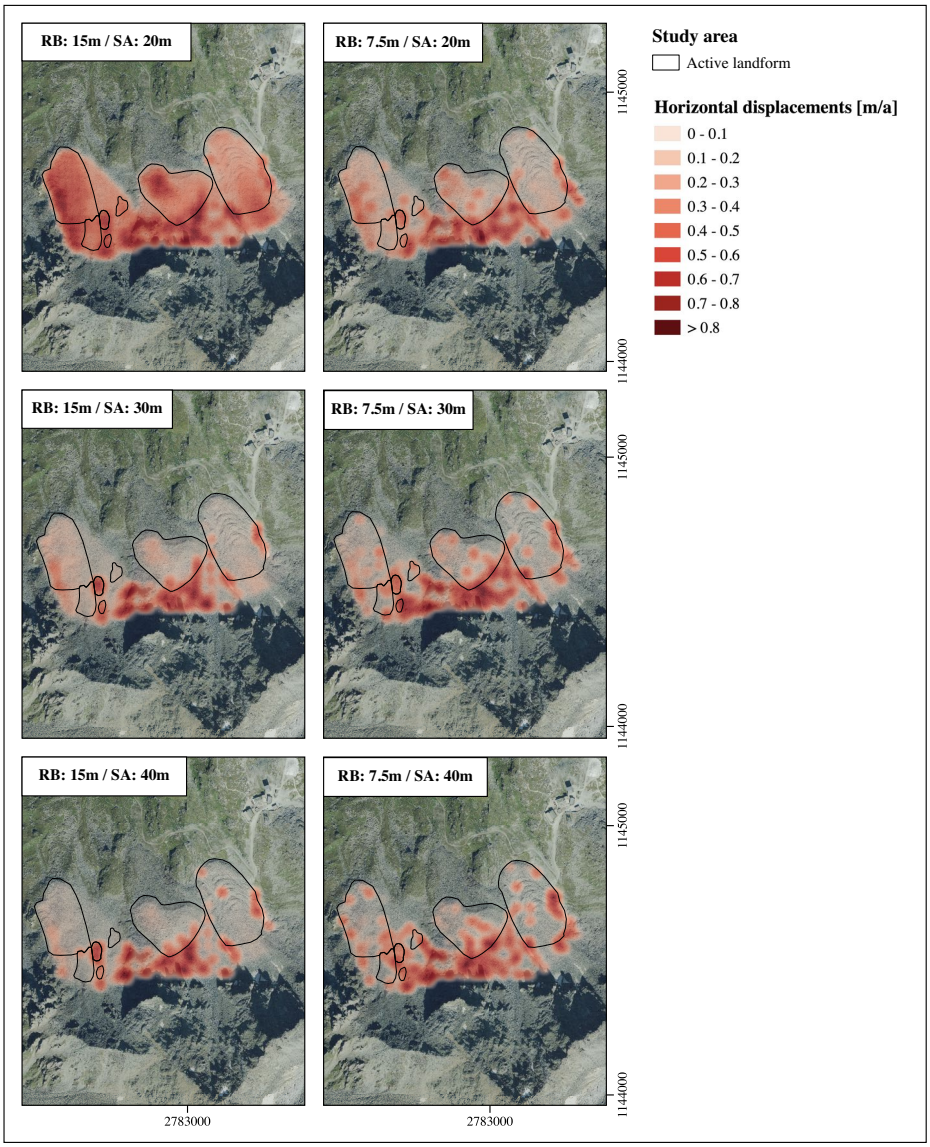

Figure 4-7: Annual horizontal displacements between 1955 and 1971 for different combinations of reference block (RB) sizes (7.5m and 15m) and search area (SA) sizes (20m, 30m and 40m). The orthophoto of 2021 is displayed as background (Swisstopo, 2021).

4.5.4 Accuracy of horizontal displacements

The determination of horizontal displacements involves several sources of uncertainties. Within the DEM's and orthophotos, these include variations in data processing for each year. The remaining errors within the DEM's after the co-registration are listed in Table 4-3. This results in an accuracy of the horizontal displacements of 0.04 m/a – 0.12 m/a.

Limitations in measuring horizontal displacements arise from factors such as shadows and snow patches. Additionally, steep slopes and sharp edges contribute to the overall error. The most prominent and limiting factor is the variable nature of most high-alpine terrain forms and their rapidly changing topography (Kääb, 2005; Kääb & Vollmer, 2000). The selection of the search area and reference block sizes in CIAS introduces potential variations in the re-

sults. According to Kääb & Vollmer (2000), the estimated error of digitally-derived horizontal displacements in CIAS ranges from 10 – 15 %. False correlations in CIAS were addressed by considering the maximum correlation coefficient. Values with low maximum correlation coefficients (lower than the 20 % quantile) were excluded from further analysis. Figure 4-8 illustrates the spatial distribution of points that were excluded from the analysis due to their poor correlation performance. If a point is excluded nine times from the analysis, it indicates a persistently poor correlation throughout all nine investigated time steps. Specific regions can be identified where consistently poor correlation was observed, mainly occurring in shadowed terrain or in places that are often covered with snow (Figure 4-4). Particularly in the talus slope above the Marmugnun rockglacier, consistently low correlation occurred. This can be attributed to the high variability in this area, where the surface topography changes rapidly, primarily due to gravitational mass movements. Consequently, the surface undergoes changes during each event, leading to discrepancies in the presence of blocks utilized for correlation in later time steps. In contrast, flatter areas display fewer distinct patterns of low maximum correlation coefficients compared to the region above the Marmugnun rockglacier. Appendix 11.3 presents the points with low maximum correlation coefficients individually for each time step, further highlighting their individual patterns.

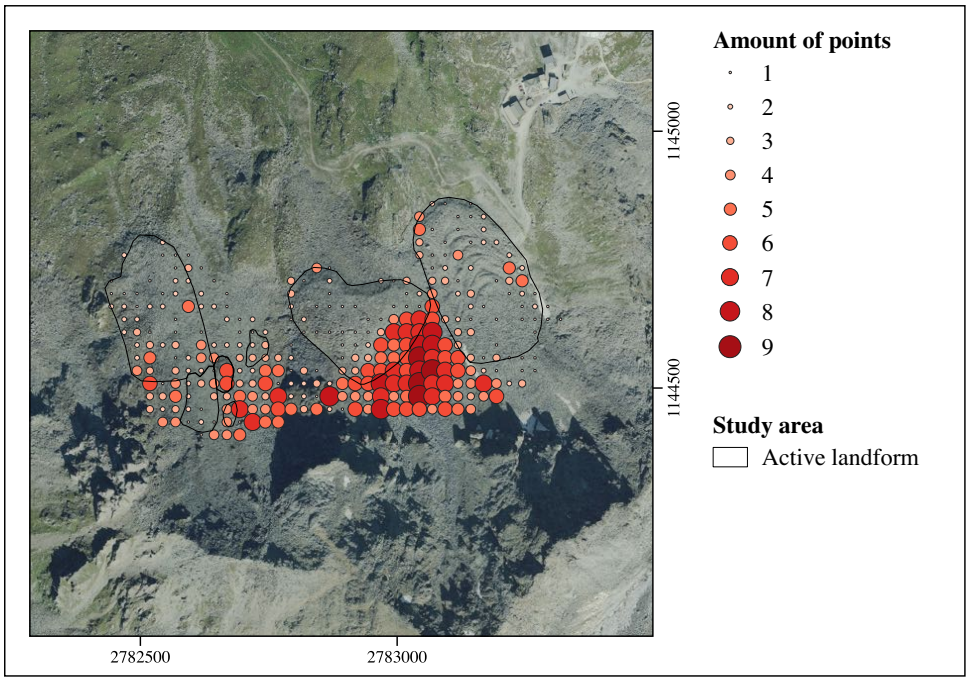

Figure 4-8: Number of points with a maximum correlation coefficient below the 20% quantile. The orthophoto of 2021 is displayed as background (Swisstopo, 2021).

4.6 Measurement of thickness changes

4.6.1 DEM-differencing

Changes in elevation were determined by calculating the differences between the DEM's using QGIS (Raster Calculator). First, the DEM's were shifted in x, y and z directions based on the results of the co-registration (Chapter 4.3.2.2) in relation to the DEM of 2021. The disparities between two DEM's provide a quantitative representation of the vertical changes between the corresponding points in time (Kääb, 2005).

4.6.2 Accuracy of vertical changes

According to Wheaton et al. (2009), assessing uncertainties related to DEM differencing includes quantifying the uncertainties in each individual DEM as well as the propagation of such uncertainties into the DEM of difference (James et al., 2012). The accuracy assessment of surface elevation changes revealed comparable levels of accuracy for both vertical and horizontal changes (Kääb & Vollmer, 2000). The accuracy achieved for vertical changes amounts therefore to 0.04 m/a – 0.12 m/a.

Systematic errors, such as elevation changes due to snow, influence DEM differencing outcomes. Lying snow can distort the height information of the DEM and the resulting DEM-difference. If a measurement of snow height is available, the resulting elevation difference can be corrected accordingly. In the absence of a current snow height measurement, the evolution of snow, such as compaction or melting, and the resulting changes in snow height must be considered (Joerg et al., 2012). In this study, no correction for snow was applied in any year, as only snow patches were observed and no large-scale snow, uniformly distributed over all landforms was present.

4.7 Surface topography

Surface topography changes of the rockglaciers and solifluction lobes were assessed using longitudinal profiles. Depending on the surface variability and observed changes on the orthophotos and from DEM-differencing, one or two profiles were generated for each landform. These profiles provide insights into possible alterations in elevation and downslope movements over time. The locations of the profiles are indicated in Figure 4-9.

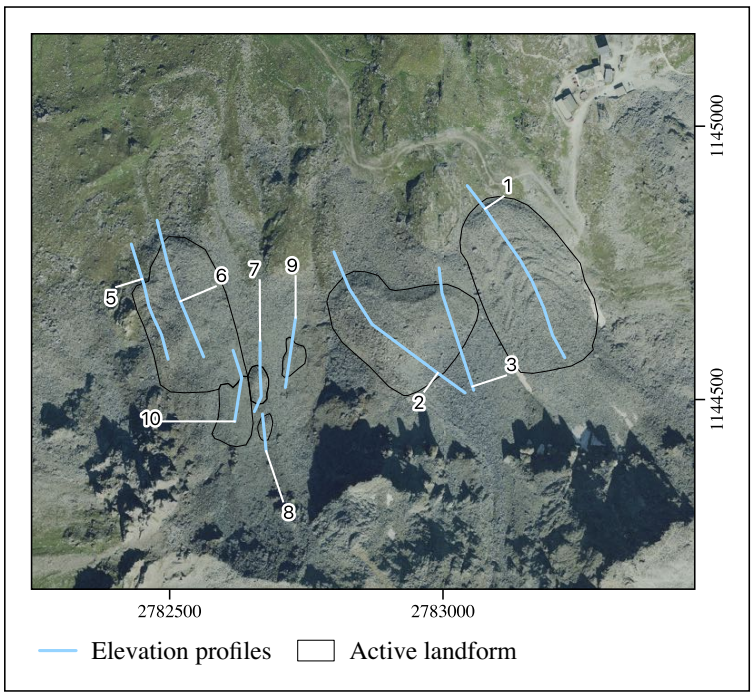

Figure 4-9: Elevation profiles covering the different landforms. The orthophoto of 2021 is displayed as background (Swisstopo, 2021).

4.8 Snow cover

The impact of snow on the movement of the landforms is analyzed, as the timing, thickness and duration of snow cover have a significant impact on permafrost (Kellerer-Pirklbauer & Kaufmann, 2012; PERMOS, 2016; Staub & Delaloye, 2017) (Chapter 2.1.3). To see the varying amount of snow on each landform, the areas covered with snow were digitized manually. Perennial snow patches and remnants from avalanches on the rockglaciers and solifluction lobes were recorded in the existing ten orthophotos. Perennial snow patches are those that persist throughout the year at the base of slopes, indicating the presence of permafrost beneath the surface (Chapter 2.1.5). Especially in 1985, there was fresh snow over a large area. For the purposes of this study, fresh snow is considered part of the perennial snow cover. Snow cover is identified as avalanche snow if the snow patch contains debris that was transported and accumulated during an avalanche event. Conversely, a snow patch that appears white and free of debris is classified as perennial snow. The size of the area covered by snow was then compared with the horizontal displacements. While these changes represent the change within a time period, the amount of snow for the first year of each period is considered for the comparison.

4.9 Rockfall

The Murtèl cirque is surrounded by rockwalls that contribute material to the underlying talus slopes and further down to the rockglaciers. On average, the peak of rockfall activity occurs about 10 days after thawing of the cirque wall after winter (Matsuoka & Sakai, 1999). The annual erosion rate of the headwall below Piz Corvatsch is estimated to be 2 mm (Matsuoka, 2008). Müller et al. (2014) calculated the sediment storage and transport rates for both Murtèl and Marmugnun rockglaciers between 1996 and 2007. Using terrestrial laser scanning (TLS), the released and mobilized material was quantified in terms of geomorphic work (GW), which includes erosion and transport processes within a geomorphic system (Caine, 1976; Müller et al., 2014).

In this study, the same subsystems as described in Müller et al. (2014) were analyzed: the rockwalls, talus slopes, and rockglaciers. The main processes within the rockwalls are rockfalls, while the talus slope is subject to snow avalanches and permafrost creep. The rockglacier exhibits the phenomenon of permafrost creep. In addition to the Murtèl and Marmugnun systems, this study also investigates the Chastelets rockglacier system.

For each time step from 1955 to 2021, elevation changes within each subsystem were calculated by comparing differences in DEM's. The variations between these landforms were calculated and compared to the results of Müller et al. (2014). A decrease in elevation within the subsystems is interpreted as an indication of mobilized material and released energy. However, unlike Müller et al. (2014), this study did not conduct separate analysis of intermediate storages inside the rockwalls, which represents the accumulation of materials in the rockwalls and talus slopes.

5. RESULTS

5.1 Geomorphological Mapping

The rockglaciers and solifluction lobes below the Piz Corvatsch were analyzed by interpretation of orthophotos and direct mapping in the field, resulting in the geomorphologic map (Figure 5-1). The main focus of the mapping was the periglacial environment. Among the prominent rockglaciers, the Murtèl, Marmugnun and Chastelets rockglaciers show clear signs of being in an active state (Chapter 2.2.3.1). The Murtèl rockglacier has a steep front, no vegetation and well-defined creep structures such as furrows and ridges, indicating ongoing deformation. The Marmugnun rockglacier shares similar characteristics with the Murtèl rockglacier, including a steep front, lack of vegetation and distinct creep structures. The Chastelets rockglacier is featured by a steep front, some vegetation and limited furrow and ridge structures, suggesting potential variations in rockglacier movement. Each of these three rockglaciers is connected to a talus slope, which facilitates the transfer of material from the rockwall above to the rockglacier below. Therefore, these active rockglaciers act as rockfall debris traps and are classified as talus rockglaciers based on their occurrence (Chapter 2.2.3.2). Another distinction can be made on the basis of their shape. The Murtèl rockglacier can be de-

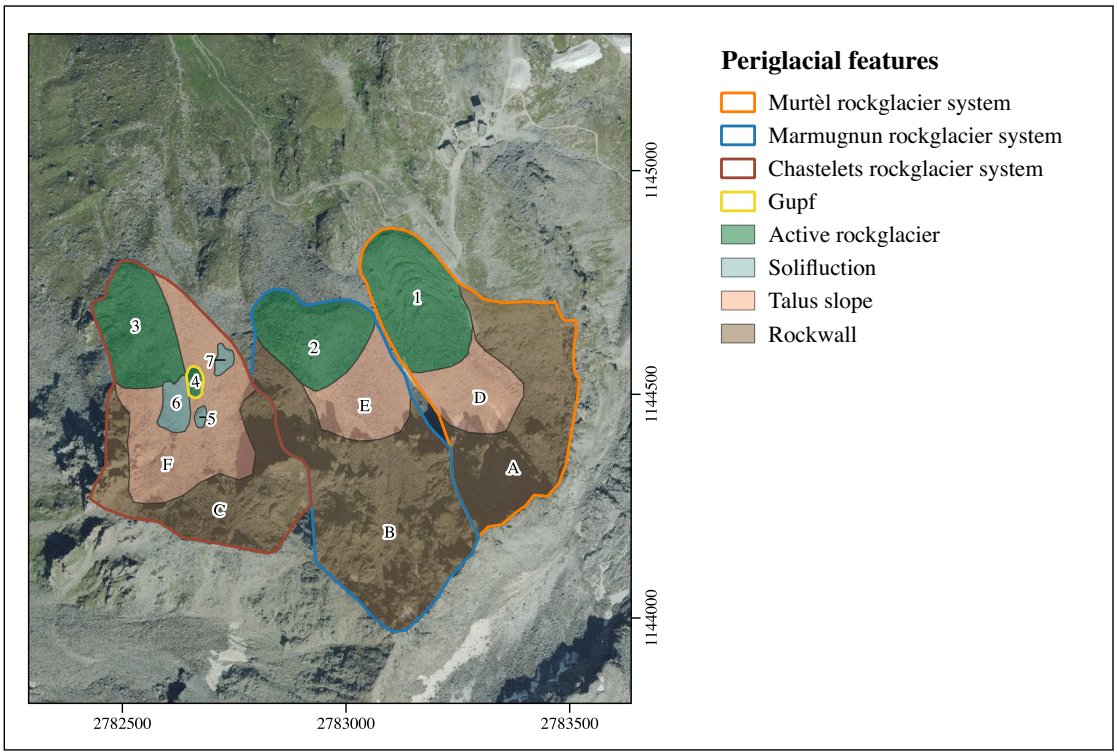

Figure 5-1: Geomorphological map of the periglacial environment at Murtèl cirque. The labels are corresponding to Table 5-1 and Table 5-2. The orthophoto of 2021 is displayed in the background (Swisstopo, 2021).

scribed as a tongue-shaped rockglacier, since its length is greater than its width. The Marmugnun rockglacier, on the other hand, has the opposite ratio and is therefore classified as a lobate rockglacier. The Chastelets rockglacier can be considered either as a tongue-shaped rockglacier, because its length is larger than its width, or as a complex rockglacier, because of the different behavior of the eastern and western parts of the rockglacier (Chapter 2.2.3.3). The Gupf, located within the talus slope of the Chastelets rockglacier, is also considered as an active rockglacier that is developing rapidly. The small rockglacier Gupf displays a steep front, no vegetation, an absence of creep structures and is also classified as a talus rockglacier. Further classifications of the Gupf are not made, because the rockglacier is still small and continuously evolving, making more detailed categorization difficult. Adjacent to the Gupf, within the talus slope of the Chastelets rockglacier, three solifluction lobes can be observed. Because they are not covered by vegetation, they are called free solifluction (Chapter 2.3.2). Their front slope, as well as the slope over the entire lobes, is flatter in all three features compared to the active rockglaciers. The solifluction processes can be narrowed down to gelifluction or plug-like flow, assuming they are influenced by permafrost. A more precise classification would require measurement of MAAT at the locations of the solifluction lobes (Chapter 2.3.1). According to Benedict (1970), these solifluction lobes can be classified as stone-banked lobes, as they are accumulations of stones and boulders and show lobate, steep and rocky fronts (Chapter 2.3.2). In addition, fossil rockglaciers were observed in the forefield of the active rockglaciers. These fossil features are highly vegetated and show distinct characteristics indicative of being in a fossil state of activity (Chapter 2.2.3.1). However, as this study primarily focuses on the active landforms within the study area, further analysis of the fossil structures is not explored in depth. The geomorphometric data for the active periglacial features are presented in Table 5-1, while the data for the talus slopes and rockwalls, indicated as the periglacial environment, are listed in Table 5-2. Depending on how the boundaries between the rockglaciers and talus slopes are defined, the calculated parameters may differ.

Table 5-1: Geomorphological inventory of the periglacial features. The labels are displayed in Figure 5-1.

General information			Geomorphometric data										
label	name	landform	min altitude [m a.s.l.]	max altitude [m a.s.l.]	elevation range [m]	aspect	area [m²]	area [km²]	length [m]	width [m]	mean slope [°]	min / max slope [°]	front slope [°]
1	Murtèl	active rockglacier	2629	2727	98	NNW	54715	0.054715	343	189	19.7	0 to 54	41 to 52
2	Marmugnun	active rockglacier	2612	2699	87	NW	40941	0.040941	245	260	21.7	0 to 57	40 to 50
3	Chastelets	active rockglacier	2543	2684	141	NNW	40370	0.04037	292	160	25.7	0 to 64	45 to 53
4	Gupf	active rockglacier	2667	2712	45	N	2294	0.002294	81	31	29.8	11 to 52	38 to 46
5		solifluction	2718	2754	36	NNE	1263	0.001263	67	25	29.8	16 to 45	28 to 36
6		solifluction	2675	2743	68	N	6466	0.006466	123	60	29.9	17 to 42	28 to 31
7		solifluction	2644	2689	45	NNE	2843	0.002843	77	42	30	20 to 42	32 to 38

Table 5-2: Geomorphological inventory of the periglacial environment. The labels are displayed in Figure 5-1.

General information			Geomorphometric data									
label	location	feature	min altitude [m a.s.l.]	max altitude [m a.s.l.]	elevation range [m]	aspect	area [m²]	area [km²]	length [m]	width [m]	mean slope [°]	min / max slope [°]
A	above Murtèl	rockwall	2662	3073	411	NW	94663	0.094663	163	510	41	1 to 80
B	above Marmugnun	rockwall	2639	3165	526	NNE	146062	0.146062	430	318	42	2 to 82
C	above Chastelets	rockwall	2726	3004	278	N	75707	0.075707	200	520	41	0 to 82
D	above Murtèl	talus slope	2688	2825	137	NW	31318	0.031318	189	182	29	10 to 75
E	above Marmugnun	talus slope	2662	2798	136	NNW	34305	0.034305	168	223	32	5 to 82
F	above Chastelets	talus slope	2563	2853	290	N	88023	0.088023	231	260	31	1 to 77

5.2 Horizontal displacements

The horizontal displacements for nine time periods were computed using CIAS (Chapter 4.5) and are shown in Figure 5-2. The calculated annual values and flow directions for both rock-glaciers and solifluction lobes illustrate the spatial distribution of the horizontal changes on their active parts. Certain time steps clearly indicate a direction of movement (e.g., 1955 – 1971), while in other time steps, no distinct displacement direction could be determined (e.g., 1979 – 1985). The mean annual horizontal surface displacement per landform and time step is displayed in Figure 5-3. The solifluction lobes are labelled according to Figure 5-1. The values of horizontal displacements per landform and time step are listed in Appendix 11.4. The rates of horizontal movements vary between the different landforms as well as across the time steps. The average values range from a few cm/a to individual values exceeding 1 m/a. More detailed information regarding the spatial and temporal variability are given in Chapters 5.2.1 and 5.2.2.

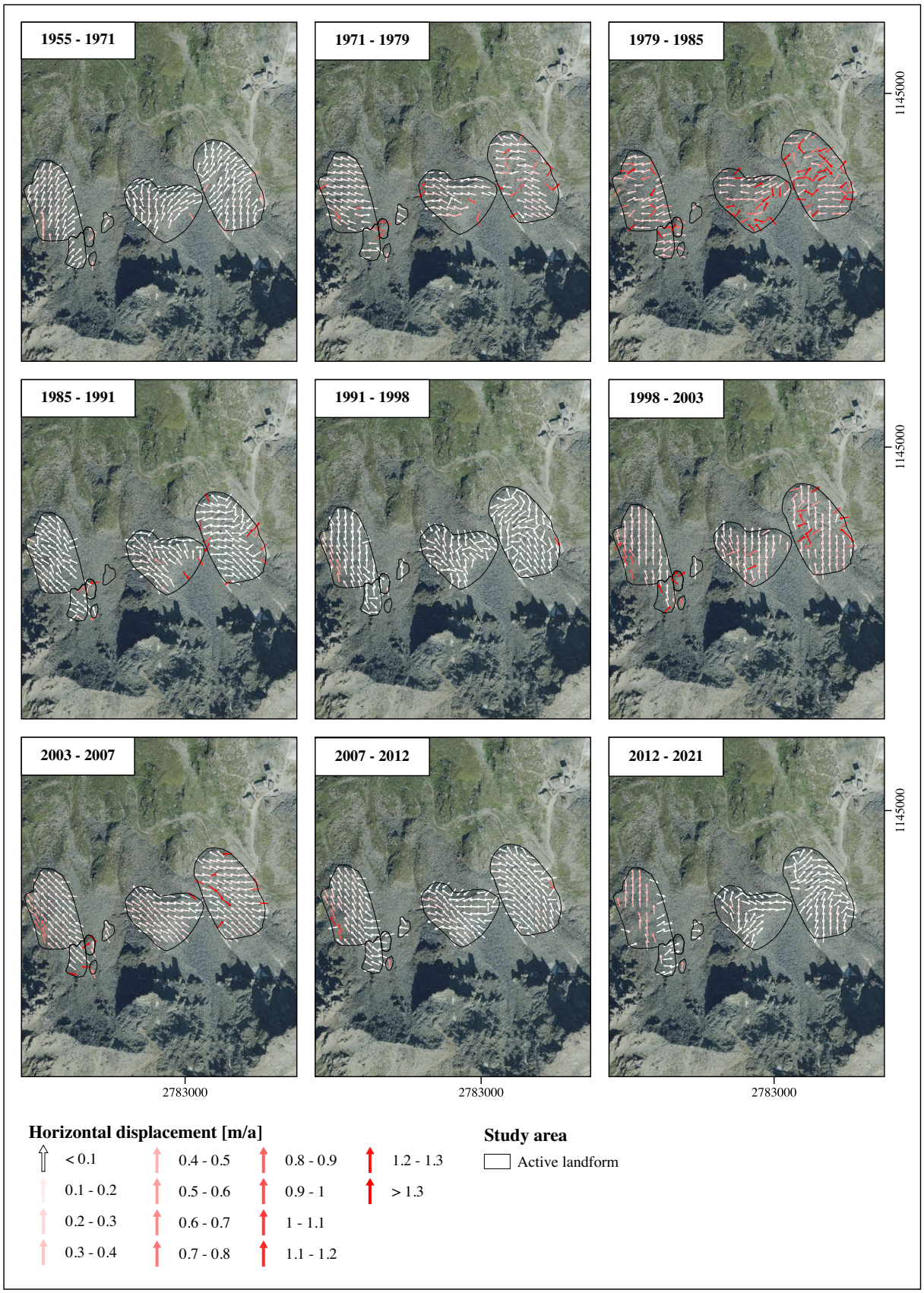

Figure 5-2: Horizontal displacements during different time steps. The orthophoto from 2021 is used as background (Swisstopo, 2021).

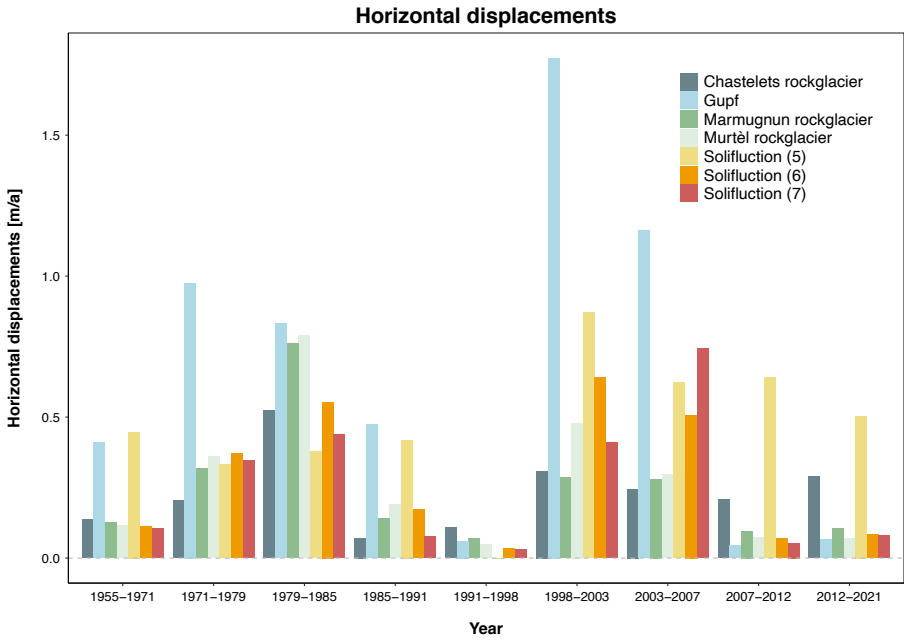

Figure 5-3: Mean annual horizontal surface displacement at different landforms between 1955 and 2021.

5.2.1 Temporal development of horizontal velocities

The temporal development of horizontal displacements per landform is shown in the boxplots of Figure 5-4. During the third period (1979 - 1985), all the landforms show a large interquartile range compared to the other periods. This variation is particularly evident at the Chastelets, Marmugnun and Murtèl rockglaciers. Outliers with higher values (e.g., at the Marmugnun or Murtèl rockglaciers) or large maximum values (e.g. the solifluction lobe number 7) are often observed in the seventh period analyzed (2003 - 2007). For the solifluction lobe (number 5), the analysis is based on a very limited number of data points. As a result, meaningful results can only be derived for the two periods 1979 – 1985 and 1985 – 1991 for this landform. From 1955 to 1985, a general increase in horizontal movement can be observed for the remaining landforms, followed by a decrease until 1998. Remarkably low values can be observed for all landforms during the period from 1991 to 1998. From 1998 onwards, a slight increase can be observed. However, the Gupf and the solifluction lobe (number 6) are exceptions as they show stronger increases compared to the other landforms. Between 2007 and 2021, horizontal movements are generally low again, except for the Chastelets rockglacier, which shows an increase in movement during these years.

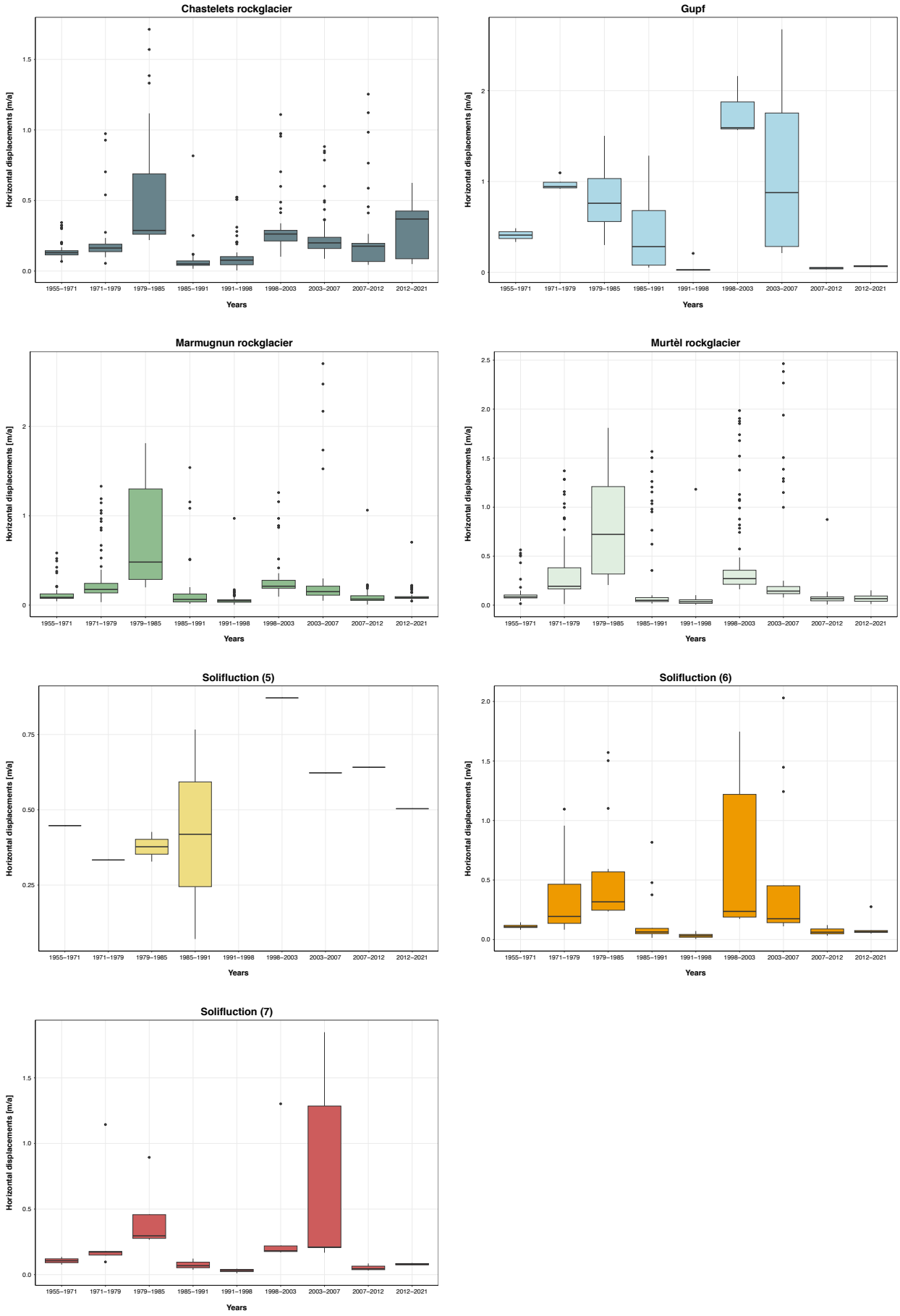

Figure 5-4: Temporal development of horizontal displacements between 1955 and 2021. Note the varying scaling of the y-axis.

5.2.2 Spatial development of horizontal velocities

The spatial variation of the horizontal displacements is shown in the boxplots of Figure 5-5. The data for the solifluction lobe (number 5) are considered only for the years with multiple data points, as mentioned in Chapter 5.2.1 (1979 – 1985 and 1985 – 1991). From 1955 - 1971 and from 1971 – 1979, the Gupf shows the highest values with about 0.4 m/a and nearly 1 m/a, respectively. The remaining landforms show horizontal movements of less than 0.2 m/a (1955 – 1971) or less than 0.5 m/a (1971 – 1979). Several outliers of the Marmugnun and Murtèl rockglaciers show even higher values than those observed on the Gupf. Between 1979 and 1985, all landforms, especially the four rockglaciers, show high horizontal movements, reaching up to 1.3 m/a. The solifluction lobes show values around 0.5 m/a. In the subsequent period of 1985 - 1991, the Gupf again shows the largest horizontal displacements, while the other landforms show smaller movements of approximately 0.1 - 0.2 m/a. The interquartile range of the Murtèl rockglacier is narrow (around 0.1 m/a), while the observed outliers exceed 1.5 m/a. Between 1991 and 1998, as observed in Figure 5-3, all landforms show uniformly small movements. The number of outliers for all landforms, especially for the Murtèl rockglacier, is much smaller than in the other periods. However, the Gupf shows remarkably high horizontal movements between 1998 and 2003 of about 1.8 m/a. The solifluction lobe (number 6) also shows high values during this period, while the other landforms display much smaller movements. Between 2003 and 2007, the Gupf and the solifluction lobe (number 7) show a wide range of values. From 2007 onwards, a slight decrease in horizontal movement is observed for all landforms. In the final period from 2012 - 2021, the Chastelets rockglacier displays an increase in horizontal movement, while the other landforms remain at displacements of approximately 0.1 m/a.

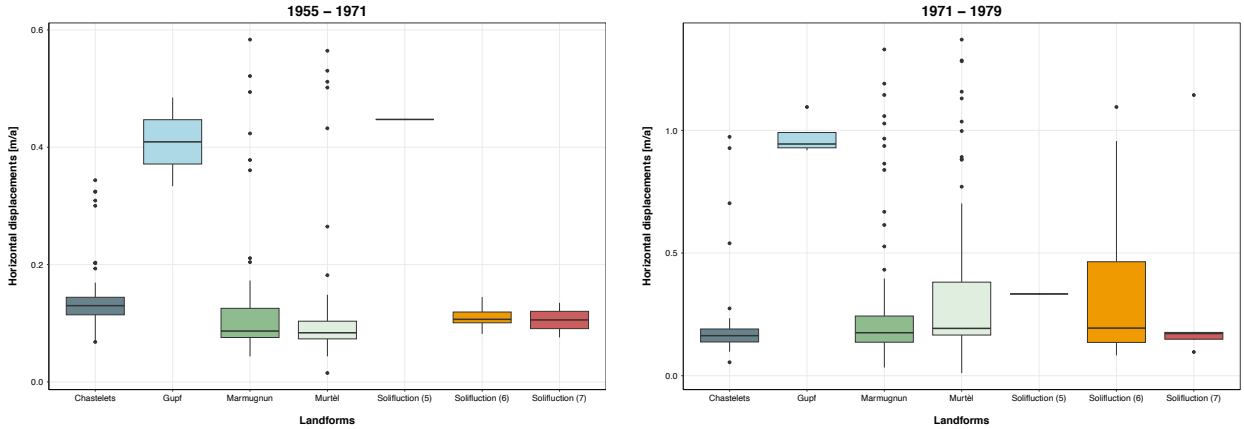

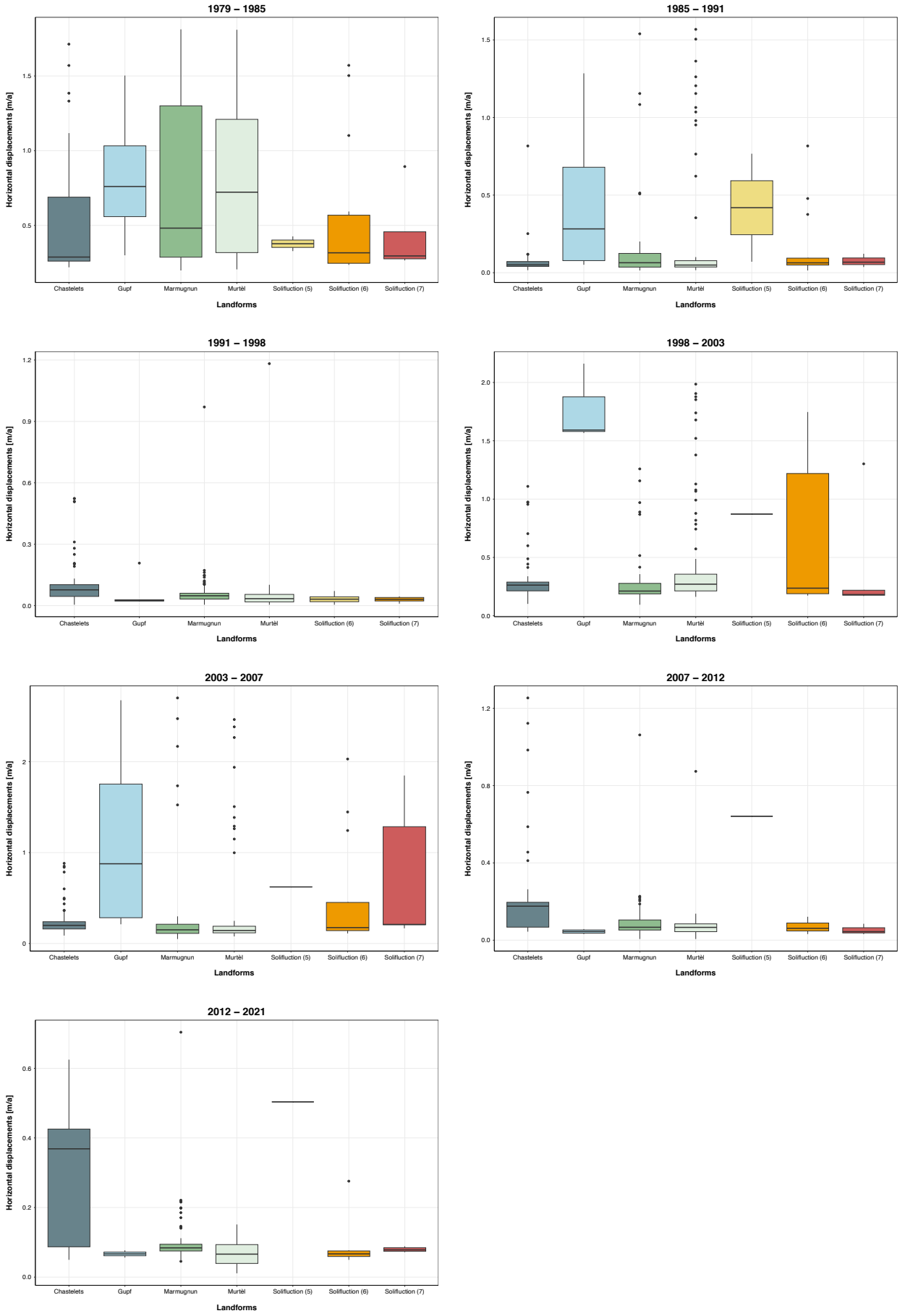

Figure 5-5: Spatial development of horizontal displacements between 1955 and 2021. Note the varying scaling of the y-axis.

5.3 Elevation changes

5.3.1 DEM-differencing

Elevation changes over a time period are evaluated by the difference between two DEM's. The difference between older and more recent DEM's result in positive values if the landscape is higher in the newer DEM compared to the earlier time point, while negative values indicate that the landscape was higher at the time of the earlier DEM. Figure 5-6 shows the DEM differences for all nine time steps.

During the first time step, which shows the difference between the years 1955 and 1971, anthropogenic structures such as buildings and paths are visible in the northwestern part of the image of difference. However, no major differences are observed within the landforms of interest. The negative area on the western side of the Murtèl rockglacier can be attributed to snow accumulation in 1955, while the furrow and ridge structure on its surface are weakly visible, suggesting slight movement. The Chastelets rockglacier shows values close to zero, while the Gupf exhibits positive values in its lower part, indicating downward movement. Moving on to the difference between 1971 and 1979, the image of difference clearly shows the substantial snow cover still present in 1979. Large amounts of snow are observed on the upper side of the Marmugnun and on both sides of the Murtèl rockglacier, resulting in significantly positive values in the image of difference. The Gupf shows positive values in its lower part, and the other three rockglaciers show slightly positive values at their front, indicating forward movement. The comparison between the DEM's of 1979 and 1985 is less clear due to significant snow cover in both years, which introduces uncertainty in the interpretation of the image of difference. On the western side of the Marmugnun rockglacier front, which was free of snow in both years, the positive values indicate a leftward downslope movement. In the fourth time step from 1985 to 1991, the image of difference again reflects the presence of significant snow cover in 1985. From 1991 to 1998, the sides of the rockglaciers have little snow. The landforms studied only show minimal changes in elevation. Between 1998 and 2003, the image of difference mostly shows minimal negative changes. However, the formation of multiple ridges can be seen on the western side of the Chastelets rockglacier front. These ridges are also visible between 2003 and 2007. The Marmugnun rockglacier shows a slight, widespread subsidence, while the Murtèl rockglacier displays almost no changes. In the time step from 2007 to 2012, the ridges on the western side of the Chastelets rockglacier are well visible, and the slight movement of the Gupf is evident from the positive values in its lower part. The latest time step from 2012 to 2021 clearly displays the recently evolved ridges

of the Chastelets rockglacier. Negative values are observed at its higher elevated areas, while positive values are visible in the lower parts, indicating downslope displacement of material. The Gupf and solifluction lobe (number 5) also show negative values at their higher elevated areas and positive values in their lower parts. The Marmugnun rockglacier displays a consistent subsidence over its entire surface. The characteristic furrow and ridges structure of the Murtèl rockglacier is consistently visible in all the images of difference, indicating at least some subtle changes in each time step.

Throughout the years, certain images of difference contain horizontal or vertical lines that are already present in the corresponding orthophotos. For instance, between 1991 and 1998, a horizontal line is visible in the middle of the image. The 2003 orthophoto appears to have two vertical lines, likely because the images were stitched together from multiple individual images, causing such boundaries to be visible at the transitions and resulting in sudden changes in elevation. It is important to be cautions when interpreting the height changes of the rockwalls above the studied landforms, as steep slopes can introduce significant errors in the image of difference. In addition, the rockwalls at the edge of some orthophotos may reflect possible distortions.

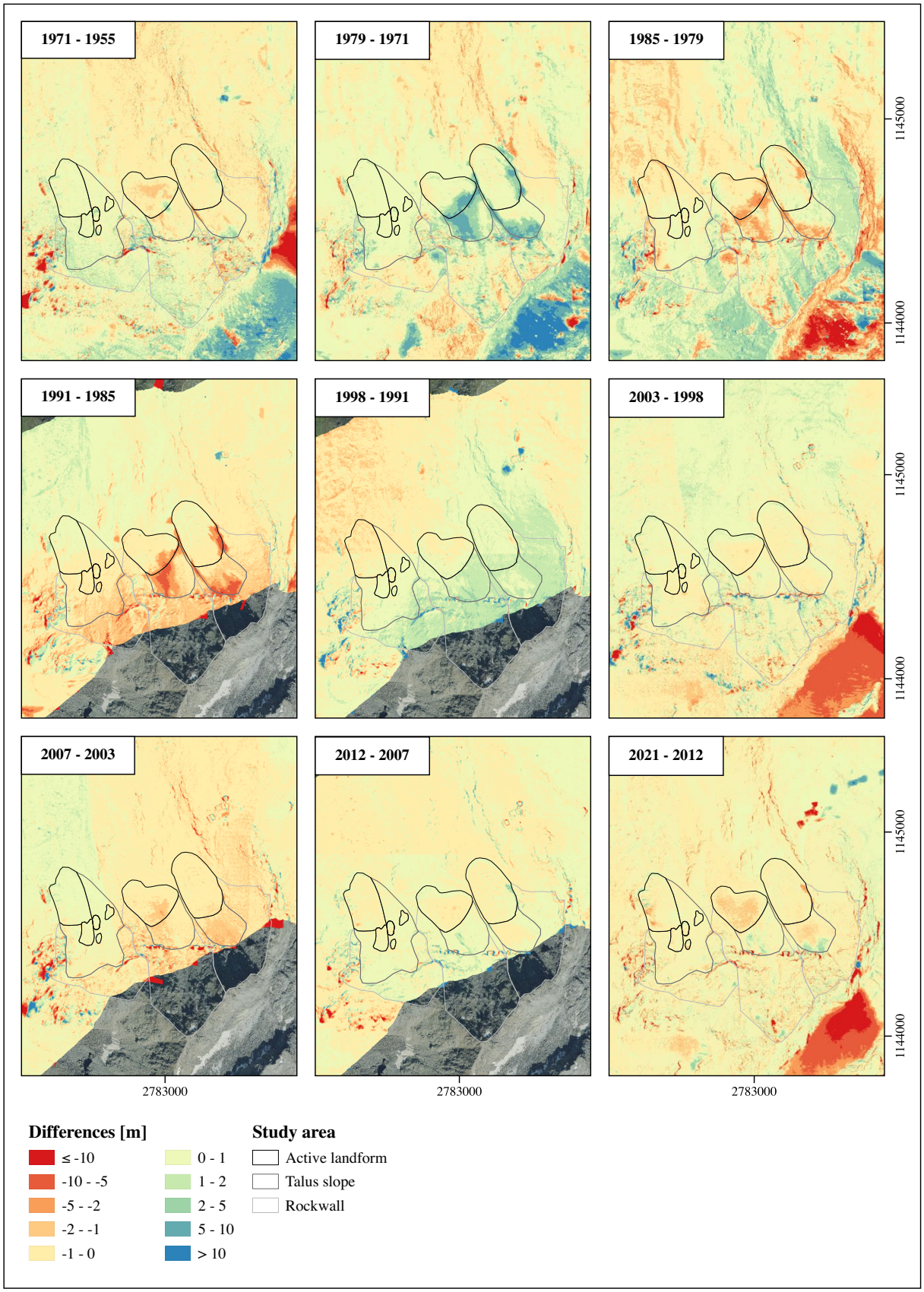

Figure 5-6: Elevation differences for each time step between 1955 and 2021 (Swisstopo, 2021).

The difference in elevation between 1955 and 2021 shows the total change in the topography of the landforms (Figure 5-7). The orthophoto of 1955 shows extensive snow cover on both sides of the Murtèl rockglacier and on its talus slope (Figure 4-4). In addition, snow was present at the lower end of the talus slope above the Marmugnun rockglacier, while small patches of snow are observed around the Chastelets rockglacier and in the area of the solifluction lobes and Gupf. In 2021, the orthophoto shows reduced snow cover, with only limited snow on the sides of the Murtèl rockglacier and minimal snow on its talus slope. In particular, anthropogenic changes in the form of the ski slope next to the Murtèl rockglacier and the ski jumps on the north-eastern edge of the map are visible. The movement patterns of the rockglaciers and solifluction lobes are evident from the elevation changes observed over time. The Murtèl rockglacier shows a pronounced forward movement, with its characteristic surface topography including furrow and ridges, shifting downslope over time. The rockglacier front also shows some forward movement, as indicated by positive values at the front. The talus slope above the Murtèl rockglacier shows negative values of height difference, partly due to the presence of snow in 1955. The sides of the Murtèl rockglacier show negative values as well, since there was more snow cover in 1955 than in 2021. The Marmugnun rockglacier has experienced subsidence of up to six meters during the observed period, and its front also shows a slight forward movement, especially on its western side. Strong forward movement at the left side of the front is observed on the Chastelets rockglacier. The central part of the rockglacier front shows some smaller forward movement. The individual ridges on the left side of the rockglacier show a clear development and downslope movement. Above these

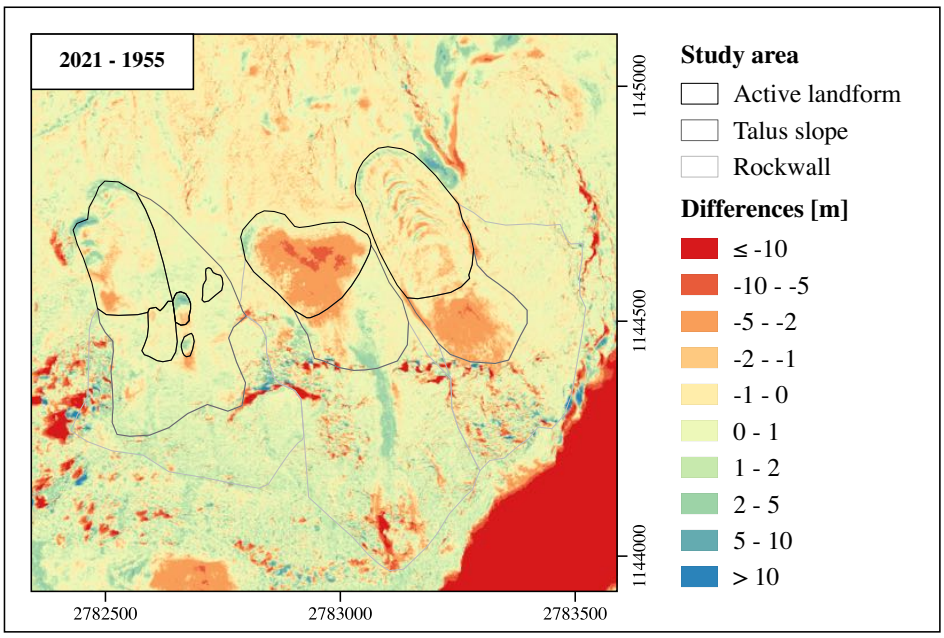

Figure 5-7: Total elevation changes between 1955 and 2021 (Swisstopo, 2021).

ridges, negative values are present. Similar patterns are evident at the Gupf, where clear development and movement are observed. Negative values are also observed above the Gupf. The solifluction lobe above the Gupf (number 5) shows some downslope movement. This lobe appears to have formed relatively recently and has continuously increased in height. On the other hand, the other solifluction lobes (number 6 and 7) show no clear changes or movement during the analyzed 66 years.

5.3.1.1 Vertical changes

Figure 5-8 displays the average annual vertical changes for each landform and time step. The high values during the period 1971 – 1979, especially on the Marmugnun and Murtèl rockglacier, are strongly influenced by the snow cover in 1979. The low values between 1985 and 1991 should as well be treated with caution, due to the large amount of snow in 1985 compared to 1991. Despite being located right next to each other, the three solifluction lobes and the Gupf display distinct behaviors during certain time periods. For example, between 1998 and 2003, the solifluction lobe (number 7) shows twice as much annual change as the Gupf, while the solifluction lobes (number 5 and 6) only show minimal negative changes. Annual vertical changes and mean values per landform and time step are listed in Appendix 11.5. Additional information on the spatial and temporal variability of the vertical changes can be found in the Chapters 5.3.2 and 5.3.3.

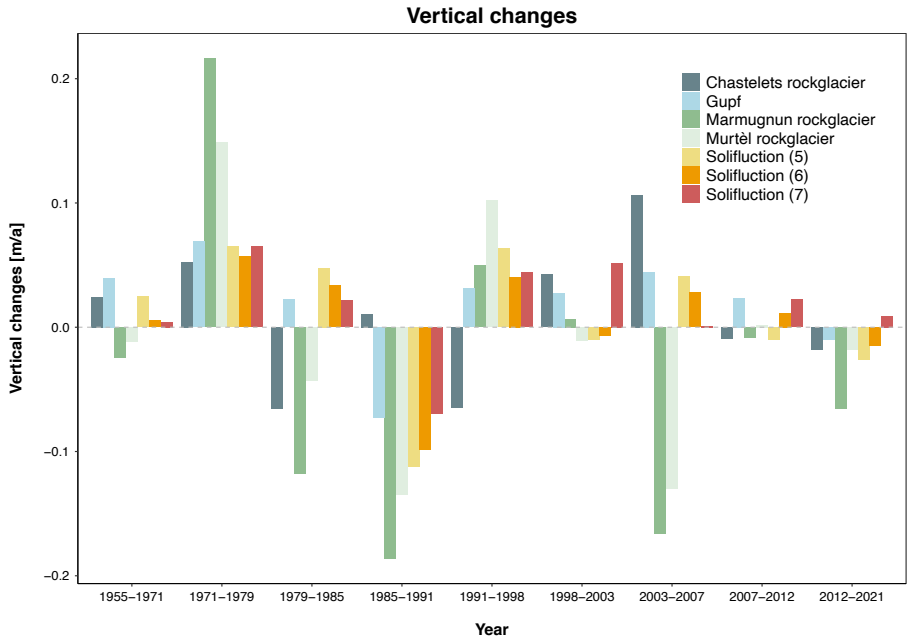

Figure 5-8: Mean annual vertical changes at different landforms between 1955 and 2021.

5.3.1.2 Cumulative vertical changes

Figure 5-9 shows the cumulative vertical changes for each landform from 1955 to 2021. The subsidence at Marmugnun rockglacier exhibits the most negative total values among all the landforms of approximately -1.5 m. This local subsidence is clearly visible in the images of difference in Figure 5-6 and Figure 5-7. The other landforms show changes ranging from around zero at the Murtèl rockglacier to positive values up to 1.5 m at the Gupf. Positive cumulative changes indicate that more material is being accumulated than removed, resulting in a gain of material on the active landforms. Especially for the Gupf and the solifluction lobe (number 5), this accumulation of material within the boundary of the active landforms is also visible in the images of DEM-differences. However, these values represent the average over each landform and do not account for spatial variability within the different parts of the landforms.

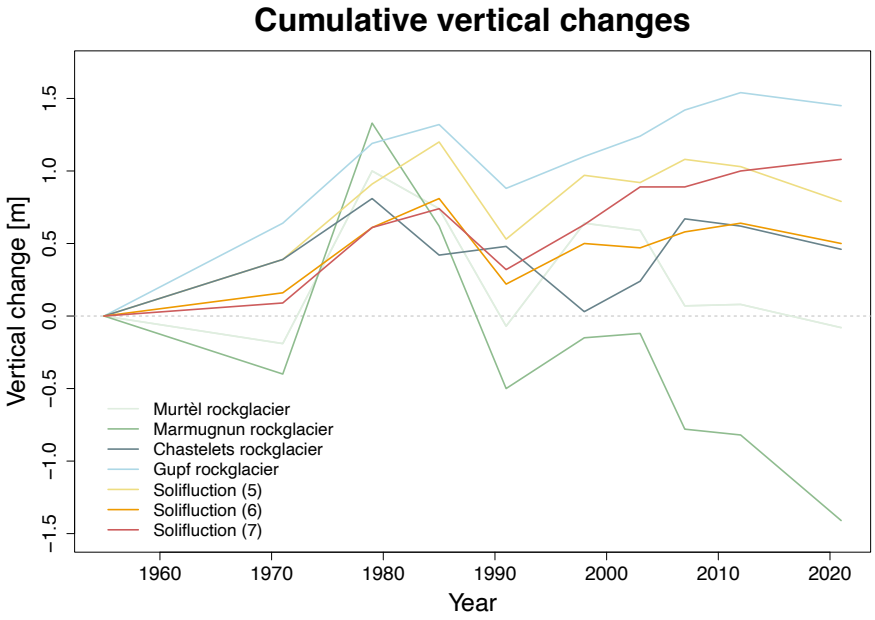

Figure 5-9: Cumulative vertical changes from 1955 to 2021.

5.3.2 Temporal development of vertical changes

The temporal development of the annual vertical changes is shown in the boxplots in Figure 5-10. The Chastelets rockglacier shows a relatively stable median between -0.1 m/a and +0.1 m/a over all time periods, with the highest value recorded between 2003 and 2007. The lowest values were observed between 1979 and 1985. In the most recent period between 2012 and 2021, the Chastelets rockglacier shows no clear changes in elevation. Similarly, the Gupf shows a comparable pattern with values close to those of the Chastelets rockglacier, with a

maximum also between 2003 and 2007. The lowest values at Gupf were recorded between 1985 and 1991. During the latest period, values slightly below zero were observed at the Gupf. Higher values were observed on the Marmugnun rockglacier, especially during the period from 1971 to 1979. This period is influenced by a lot of snow cover and should be treated with care. The outliers at the Marmugnun rockglacier were much higher, with values between -3 m/a and +2 m/a. Negative vertical changes slightly below zero were recorded for the period between 2012 and 2021. A similar pattern is observed for the Murtèl rockglacier, where the most positive vertical changes were recorded between 1971 and 1979, with an average value of about +0.15 m/a. The most negative value is around -0.15 m/a, with a tight range around zero. The most recent period shows average values around zero. For the three analyzed solifluction lobes there is a clear minimum between 1985 and 1991, while during the other time periods similar patterns with comparable values are observed.

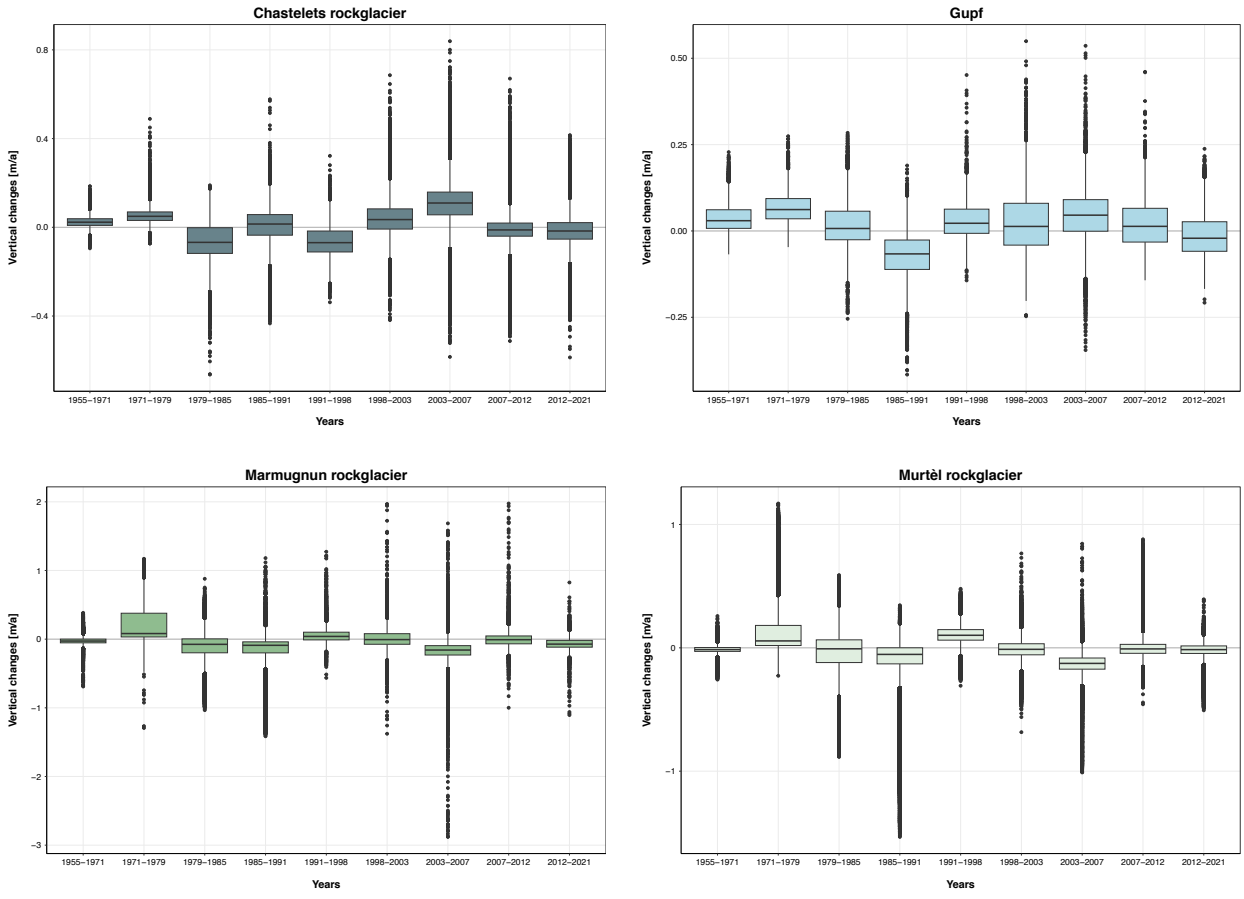

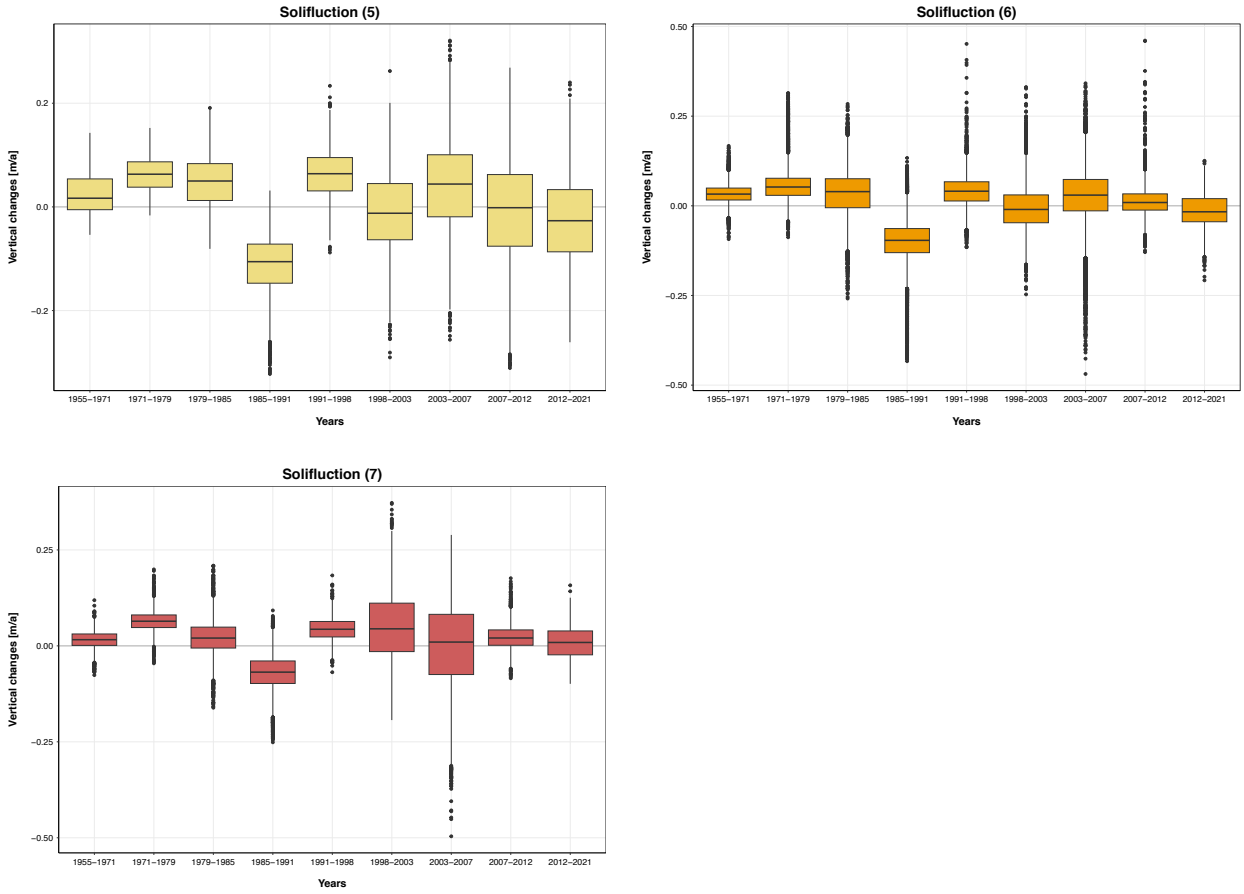

Figure 5-10: Temporal development of vertical changes between 1955 and 2021. Note the varying scaling of the y-axis.

5.3.3 Spatial development of vertical changes

Figure 5-11 illustrates the spatial variability of annual vertical changes. Throughout all time periods, the Marmugnun rockglacier consistently exhibits the largest interquartile range, especially during periods of large snow cover, such as in 1971 – 1979 and 1979 – 1985. It also has the largest range of positive and negative outliers among all landforms for each time period. The three solifluction lobes mostly show similar values.

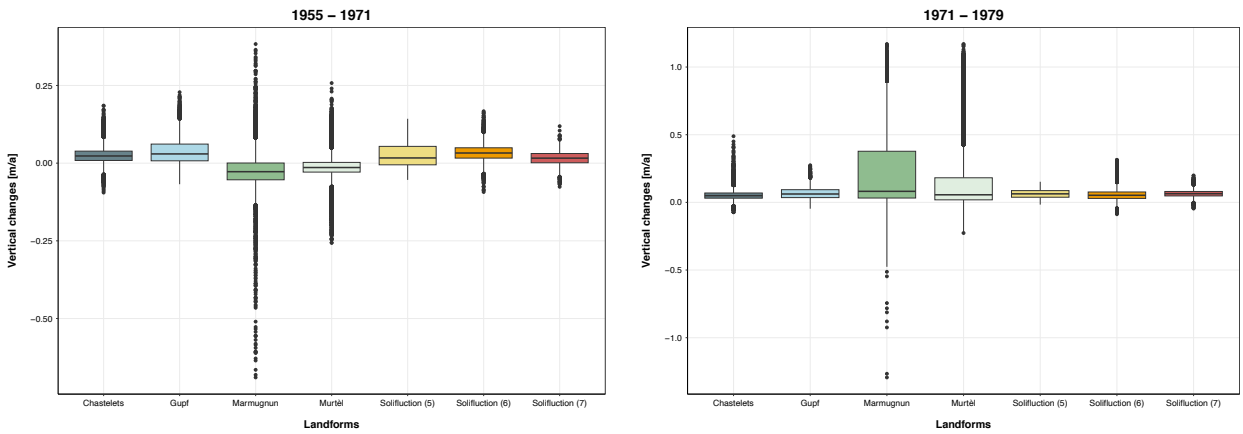

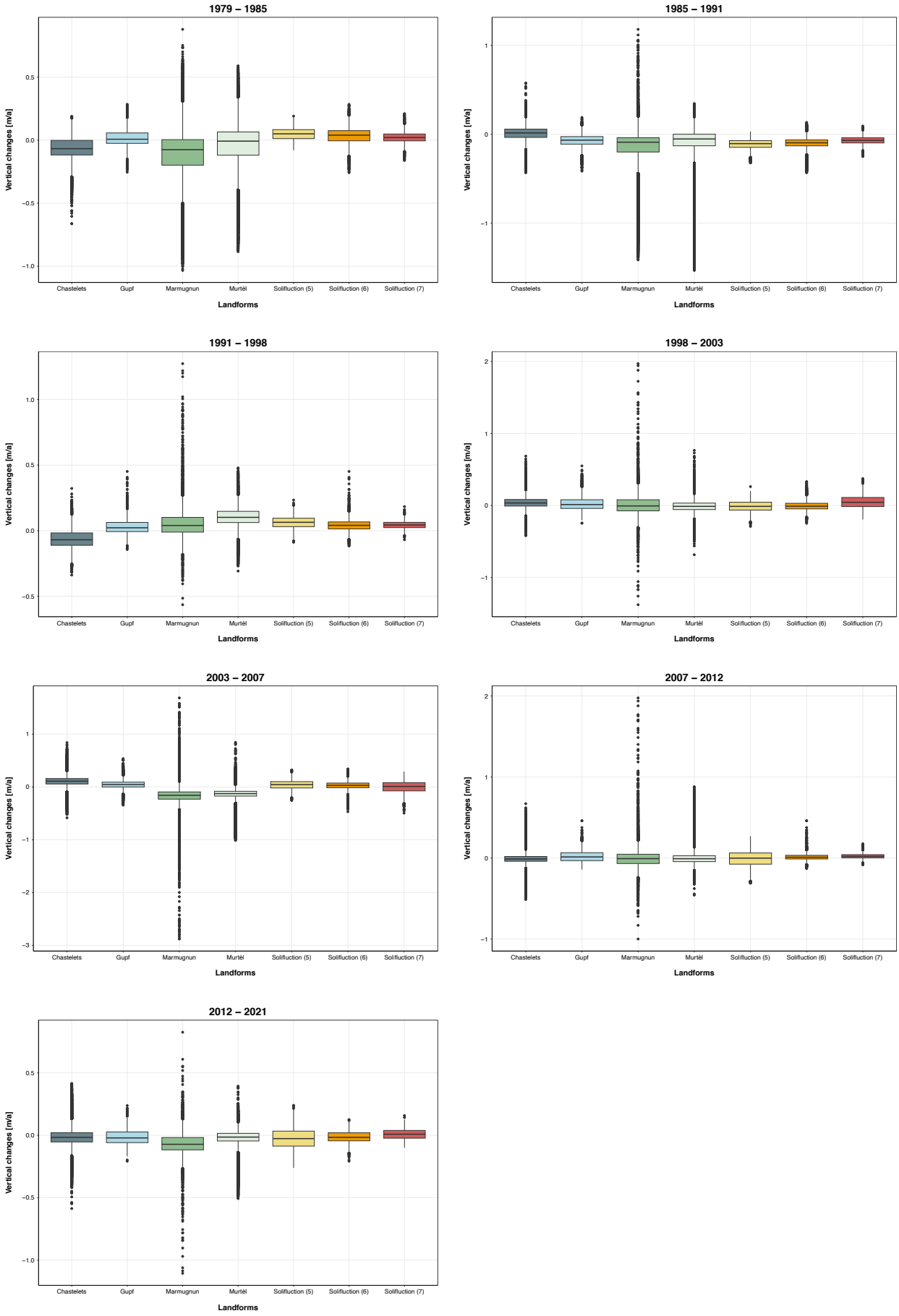

Figure 5-11: Spatial development of vertical changes between 1955 and 2021. Note the varying scaling of the y-axis.

5.4 Changes in surface topography

To analyze the changes in surface topography, longitudinal profiles were computed over the landforms. These profiles are shown in Figure 5-12, and their corresponding locations are illustrated in Figure 4-9. The changes in surface topography of the Murtèl rockglacier (profile 1) are clearly visible. The downslope movement of the furrow and ridge structure and their increasing height as well as depth, especially in the lower and flatter part of the rockglacier, are visible. Since 1955, a new ridge has developed at the top of the rockglacier front. The front only shows a slight downslope movement, compared to the higher movement of the surface. On the other hand, the talus slope of the Murtèl rockglacier shows no clear changes in elevation over time. On the western part of the Marmugnun rockglacier (profile 2), a continuous subsidence of the entire rockglacier body can be observed. Downward movement of a large boulder, located at about 2680 m a.s.l., is also evident. The talus slope of the Marmugnun rockglacier shows a decrease in elevation, while the profiles of 1979 and 1985 display the lying snow during these years. Profile 3, located on the eastern part of the Marmugnun rockglacier, clearly shows the distinct snow height of 1979 as well as the thinner snow cover of 1985. This part of the Marmugnun rockglacier also shows a clear vertical decrease, similar to the western side of the rockglacier. On the Chastelets rockglacier (profile 5), there is a clear recent development of furrow and ridges and their downslope movements on the western side of the rockglacier. Since 2007, continuous changes in surface topography and downward movement of the rockglacier front can be observed. On the eastern part of the Chastelets rockglacier (profile 6), only a small forward movement of the rockglacier front can be observed, indicating a difference in behavior and development between the two sides of the Chastelets rockglacier. Profile 7, representing the Gupf, shows a decrease in elevation in the upper part and an increase in the lower part, revealing downslope movement and continuous steepening of the landform. Similar patterns are observed in profile 8, which represents the solifluction lobe (number 5). It shows a loss of elevation in the upper part and an increase in the lower part. Profiles 9 and 10, representing the other solifluction lobes (numbers 6 and 7), do not show clear changes in surface topography between 1955 and 2021 with the use of longitudinal profiles.

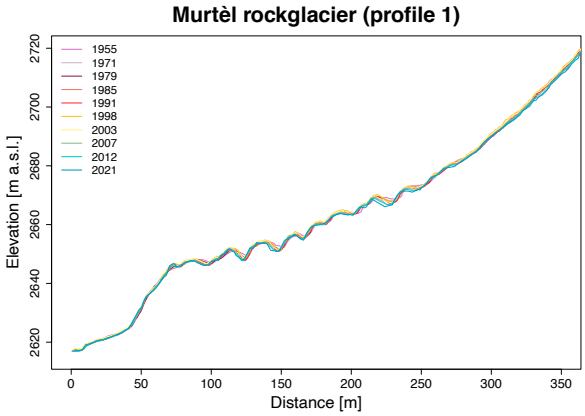
Murtèl rockglacier (profile 1)
Elevation [m a.s.l.]
Distance [m]
1955
1971
1979
1985
1991
1998
2003
2007
2012
2021

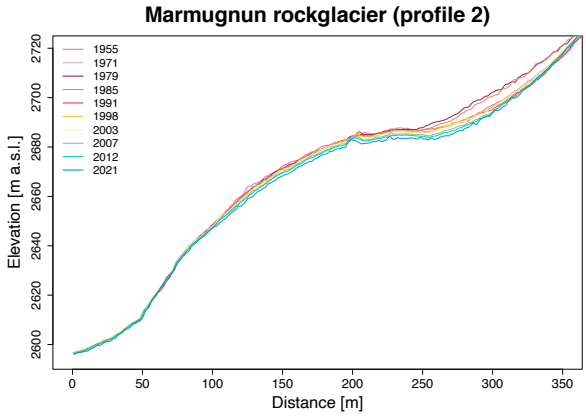
Marmugnun rockglacier (profile 2)
Elevation [m a.s.l.]
Distance [m]
1955
1971
1979
1985
1991
1998
2003
2007
2012
2021

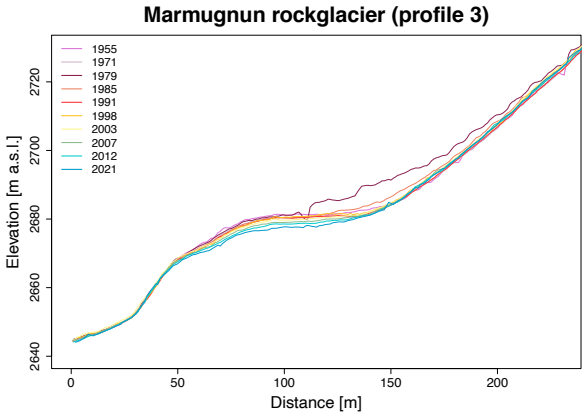
Marmugnun rockglacier (profile 3)
Elevation [m a.s.l.]
Distance [m]
1955
1971
1979
1985
1991
1998
2003
2007
2012
2021

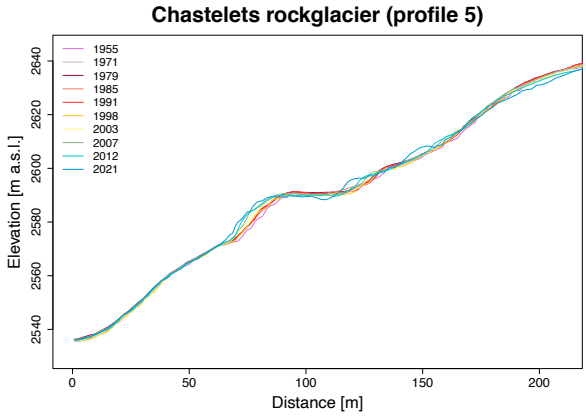
Chastelets rockglacier (profile 5)
Elevation [m a.s.l.]
Distance [m]
1955
1971
1979
1985
1991
1998
2003
2007
2012
2021

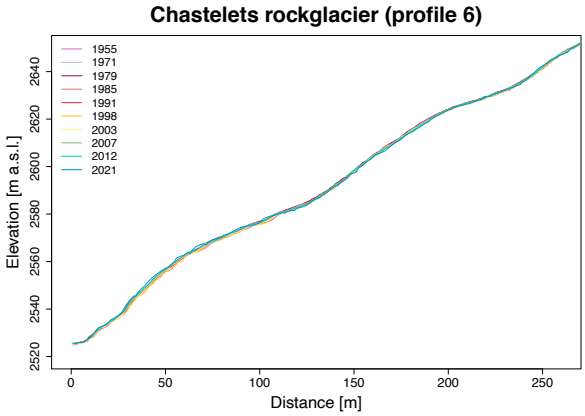
Chastelets rockglacier (profile 6)
Elevation [m a.s.l.]
Distance [m]
1955
1971
1979
1985
1991
1998
2003
2007
2012
2021

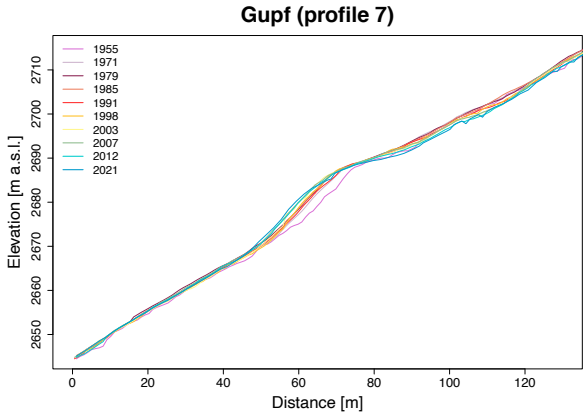
Gupf (profile 7)
Elevation [m a.s.l.]
Distance [m]
1955
1971
1979
1985
1991
1998
2003
2007
2012
2021

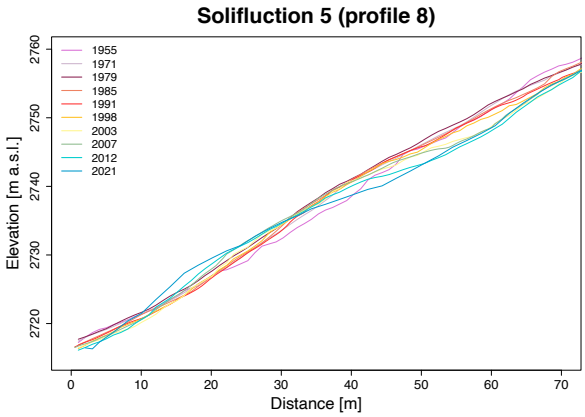
Solifluction 5 (profile 8)
Elevation [m a.s.l.]
Distance [m]
1955
1971
1979
1985
1991
1998
2003
2007
2012
2021

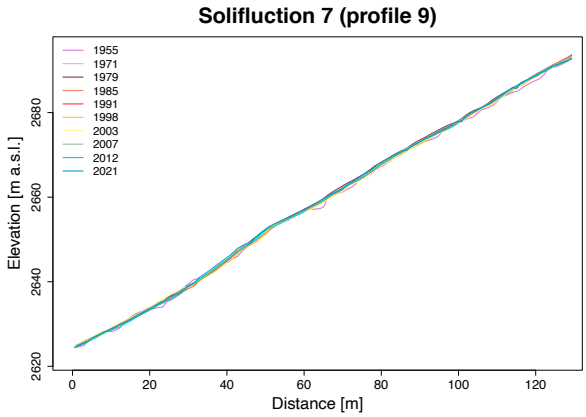
Solifluction 7 (profile 9)
Elevation [m a.s.l.]
Distance [m]
1955
1971
1979
1985
1991
1998
2003
2007
2012
2021

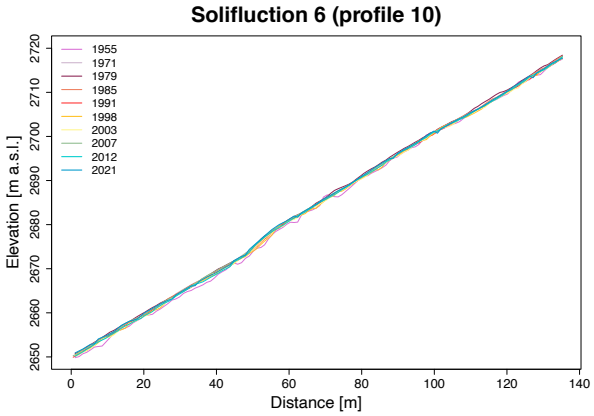

Figure 5-12: Surface topography changes for the different landforms between 1955 and 2021. The profile numbers are displayed in Figure 4-9. Note the varying scaling of the x- and y-axis.

5.5 Snow cover

The spatial variation of snow cover inside the active landforms and talus slopes is shown in Figure 5-13. The type of snow cover is divided into avalanche snow and perennial snow patches. There was no snow in the aerial image of 2007, this year is therefore not included in the analysis. No snow was detected on the solifluction lobe (number 7) in any of the aerial images, so this landform is not included in the analysis as well.

Focusing on the remnants of avalanches, this type of snow cover is observed exclusively on the Marmugnun and Murtèl rockglaciers and their talus slopes (Figure 5-14). Since 1985, aerial photographs show only minimal to negligible amounts of accumulated avalanche snow. This suggests a decrease in avalanche snow cover on both the Murtèl and Marmugnun systems. In particular, these two systems show more avalanche snow accumulation on their talus slopes than on their rockglacier bodies. In particular, the Marmugnun talus slope has consistently more snow cover than the Murtèl talus slope. In addition, the Marmugnun rockglacier itself accumulates more avalanche snow than the Murtèl rockglacier. In contrast, the other rockglaciers and solifluction lobes show no avalanche snow cover. Regarding the temporal evolution of perennial snow, the Marmugnun talus slope often has the highest amount of perennial snow cover, followed closely by the Murtèl talus slope (Figure 5-15). The Marmugnun and Murtèl rockglaciers show similar values of perennial snow. For all landforms, there is a consistent trend of lower values of snow-covered area until 1979, followed by a significant increase and then a return to lower values since 1991. There is no discernible pattern, except for the increased snow accumulation in 1979 and 1985.

The correlations (expressed by r-values) between avalanche, perennial and total snow cover and horizontal displacements are shown in Table 5-3. Avalanche snow on the Murtèl rock-glacier body and its talus slope shows a statistically significant correlation with the horizontal velocities. On the Marmugnun rockglacier and its talus slope, avalanche snow also has a statistically significant effect on horizontal velocities. These correlations are stronger in the Marmugnun than in the Murtèl system. On the Chastelets rockglacier and talus slope, only perennial snow was detected, no avalanche snow. The Chastelets rockglacier, the Gupf and the solifluction lobes (numbers 5 and 6) don't show meaningful correlations between snow cover and horizontal displacements. The statistically significant correlations are all positive, indicating higher horizontal displacements when a larger area is covered by snow.

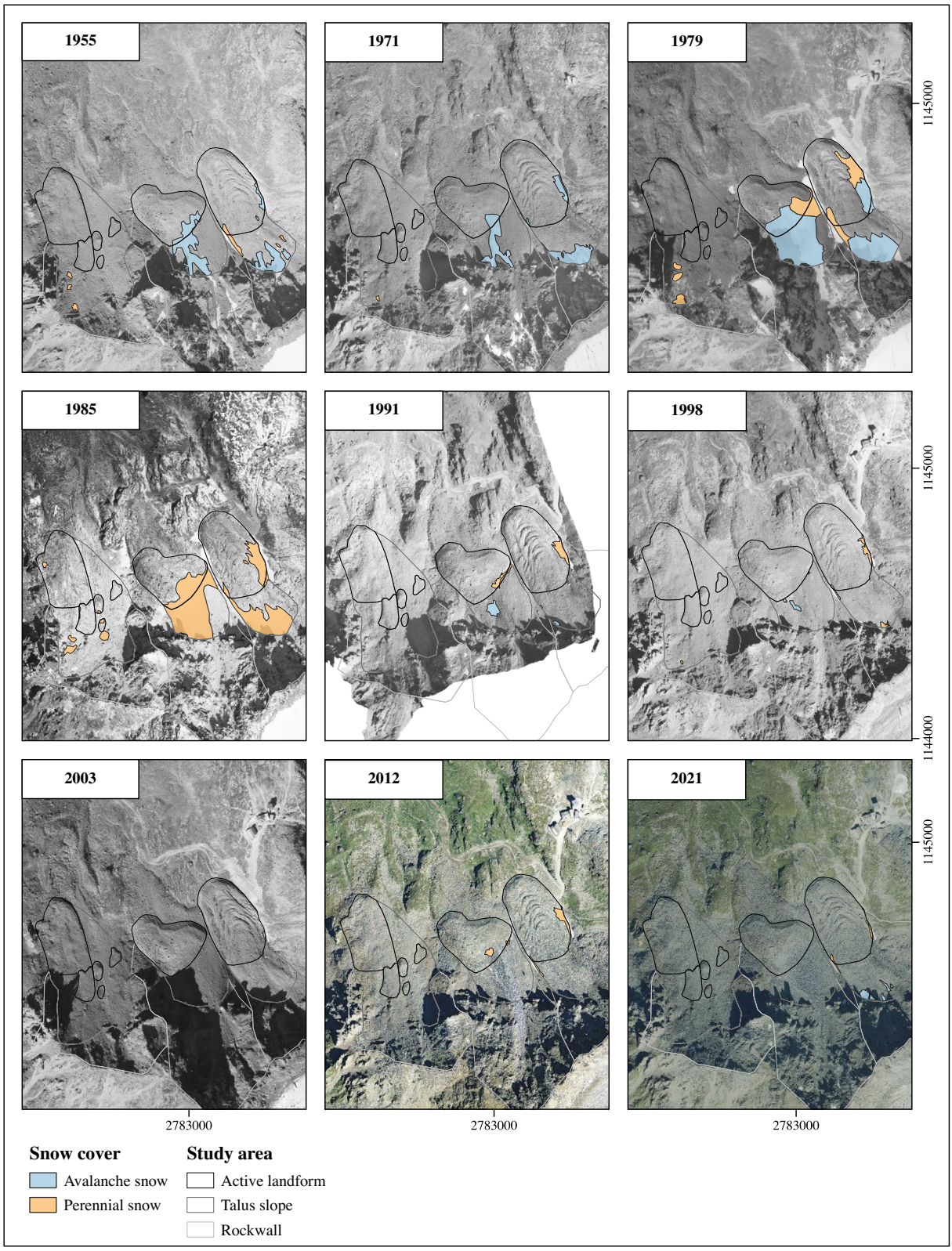

Figure 5-13: Evolution of avalanche and perennial snow cover between 1955 and 2021. On the orthophoto of 2007 no snow was lying and therefore the map of this year is not displayed. For each year, the corresponding orthophoto is displayed (Swisstopo, 2021).

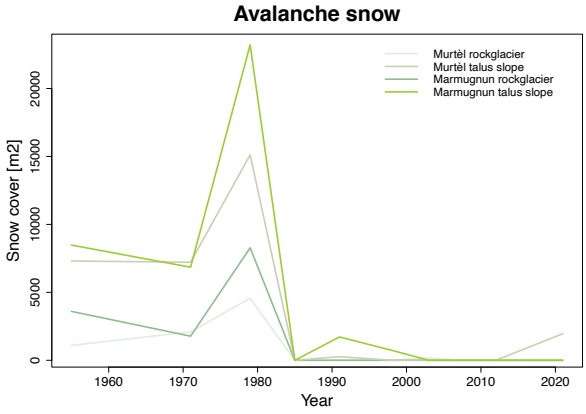

Figure 5-14: Temporal evolution of remaining avalanche snow on the rockglaciers and talus slopes.

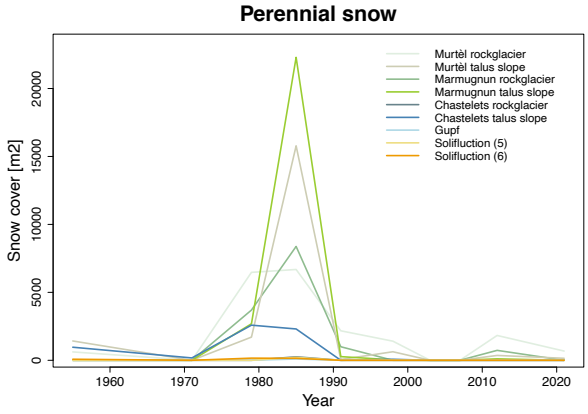

Figure 5-15: Temporal evolution of perennial snow patches on the active landforms and talus slopes.

Table 5-3: Correlations between the type of snow cover and horizontal displacements. The green colored r-values show a statistically significant correlation. The solifluction lobe (number 7) was never covered with snow.

		snow cover	r-value
Murtèl	rockglacier	avalanche	0.79
		perennial	0.42
		total	0.66
	talus slope	avalanche	0.69
		perennial	-0.05
		total	0.50
Marmugnun	rockglacier	avalanche	0.82
		perennial	0.16
		total	0.65
	talus slope	avalanche	0.85
		perennial	-0.07
		total	0.60
Chastelets	rockglacier	perennial	-0.45
	talus slope	perennial	0.26
Gupf		perennial	-0.11
Solifluction (5)		perennial	-0.08
Solifluction (6)		perennial	0.11

5.6 Rockfall

To quantify rockfall, the cumulative elevation changes over all time intervals from 1955 to 2021 have been calculated. The three subsystems rockwall, talus slope, and rockglacier within the Murtèl, Marmugnun, and Chastelets rockglacier systems were analyzed (Figure 5-16). The temporal progression shows a comparable trend in both the Marmugnun and Chastelets rock-walls and talus slopes. These subsystems show slightly positive values (approximately +1 m since 1955). However, the Marmugnun rockglacier shows much more pronounced negative

elevation changes compared to the Chastelets rockglacier, which shows slight elevation increases between 1955 and 2021. Conversely, the Murtèl rockglacier shows a distinctive pattern when compared to the other two landforms analyzed. While its rockwall shows positive cumulative elevation changes, the talus slope displays negative values (-1 m), and the elevation change of the rockglacier is slightly below zero. Further analysis base on these elevation change values.

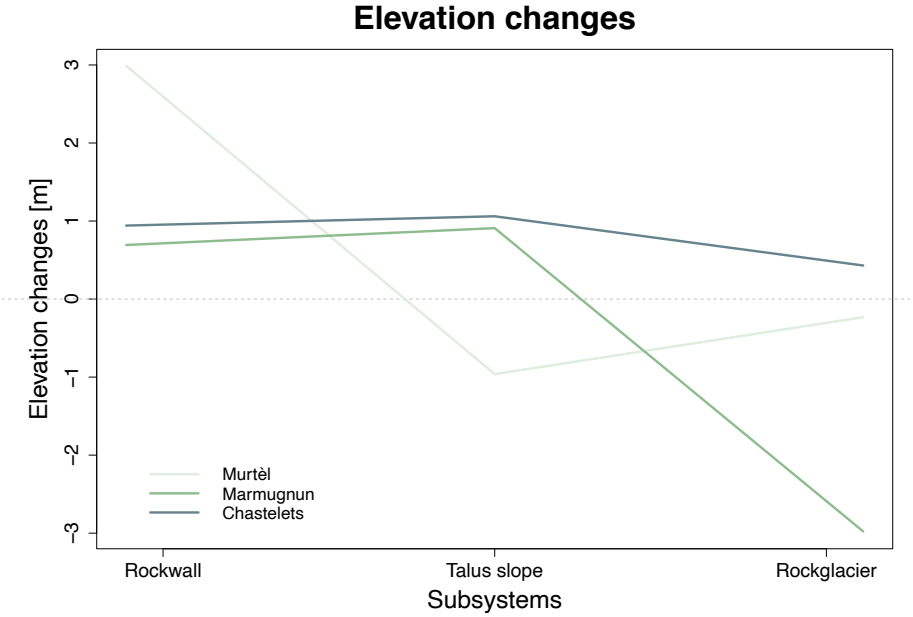

Figure 5-16: Total elevation changes between 1955 and 2021 inside the subsystems of the of the Murtèl, Marmugnun and Chastelets.

In Table 5-4, the correlations of the elevation changes (represented by r-values) between the subsystems of the Murtèl, Marmugnun and Chastelets for all covered time intervals between 1955 and 2021 are illustrated. A positive and statistically significant correlation between the talus slope and the corresponding rockglacier occurs in the Murtèl system. Similarly, the Marmugnun system shows a statistically significant correlation between its talus slope and rockglacier. Conversely, a significant correlation is observed between the rockwall and the talus slope above the Chastelets rockglacier. Notably, the other relationships lack statistical significance. The correlations between the elevation changes of each subsystem and the horizontal displacements between 1955 and 2021 are all small and not statistically significant.

Table 5-4: Correlations of the elevation changes between the subsystems. The green colored values are statistically significant.

			r-value
Murtèl	rockwall	talus slope	0.34
	talus slope	rockglacier	0.94
Marmugnun	rockwall	talus slope	0.59
	talus slope	rockglacier	0.88
Chastelets	rockwall	talus slope	0.85
	talus slope	rockglacier	0.18

The Marmugnun rockwall has 4.3 times more mass loss than the Murtèl rockwall, which is less than that obtained by Müller et al. (2014) (6 times more mass loss). The Marmugnun rockwall shows more mass loss than the Chastelets rockwall as well (1.3 times). In contrast to the study by Müller et al. (2014), the Marmugnun talus slope transports relatively less material on its rockglacier than the Murtèl system.

6. DISCUSSION

6.1 Data quality assessment

6.1.1 Assessment of the DEM-quality for a high alpine study area

After the co-registration process, there was generally a slight improvement in the σ values, indicating generally a high level of accuracy in the DEM's (Table 4-3). However, the years 1985 and 1998 stood out as outliers. The improvement in σ values for these two years after applying corrections only in the z-direction was significantly higher. Distinct natural and anthropogenic structures outside the studied landforms are clearly distinguishable in the difference images with well-defined boundaries (Figure 5-6 and Figure 5-7). This serves as evidence of the high quality and precision of both the data and the co-registration process, resulting in close alignment of the DEM's. These patterns outside the studied landforms are used to visually assess the accuracy of the data.

In this work, co-registration emerges as a key process. Figure 6-1 shows the elevation profile across the Murtèl rockglacier, showing both the co-registered and original DEM's. This profile illustrates both the vertical and horizontal accuracy of the DEM's. The improvement in DEM accuracy after co-registration is effectively illustrated by these longitudinal profiles, highlighting the importance of the correction process. Such high-quality data alignment is critical for studies in high mountain terrain, where detection of movements of permafrost landforms of just a few centimeters is essential. Since these data align very precisely after this shift, their high quality makes them suitable for such a study.

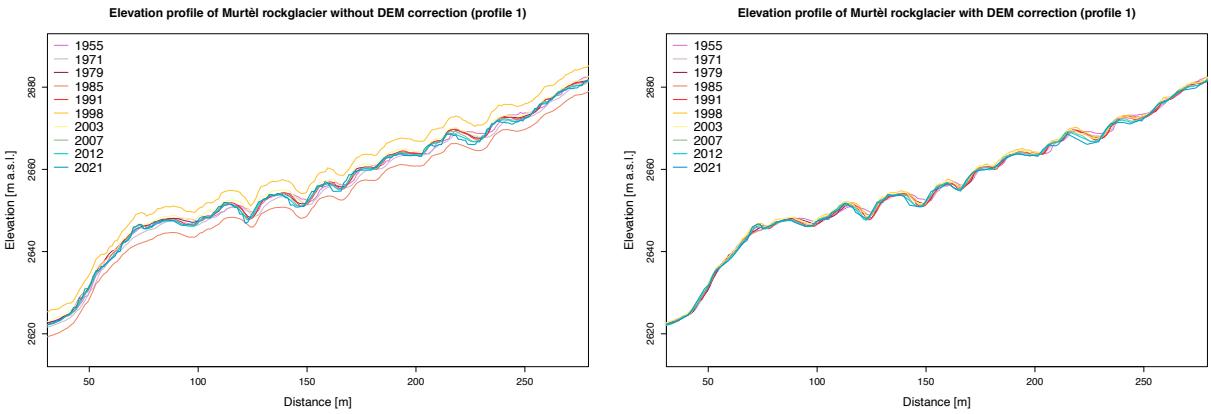

Figure 6-1: Elevation profile of the Murtèl rockglacier without (left) and with (right) co-registrated DEM's. The location of the profile 1 is illustrated in Figure 4-9.

6.1.2 Comparison with LuBis data

The low flown LuBis data from 1996, 2002 and 2007 is used as validation dataset in this study. The comparison of the LuBis data, the co-registered DEM's and the original DEM's is illustrated by the longitudinal profile of the Murtèl rockglacier (Figure 6-2). The years used for the comparison are 1998, 2003 and 2007, which are as close as possible to the years of the LuBis data available. The co-registered data agree very well with the LuBis data. The original, non-registered DEM's differ significantly from these two datasets. Within the LuBis dataset, the changes over time are smaller than in the other two datasets. The downslope movement of furrows and ridges of the Murtèl rockglacier is evident in all datasets. However, within the LuBis dataset, the changes are less pronounced. The comparisons at Marmugnun rockglacier and at the Gupf show the same pattern, the LuBis data agree well with the co-registered data, and the uncorrected original data shows clear differences. The range within the LuBis data is also smaller for these two landforms than for the other two datasets. Despite the different processing of the LuBis and co-registered data, the data match very well. This shows the high accuracy and quality of these two datasets. However, it should be noted that not all of the datasets compared are from the same years, which implies a small uncertainty.

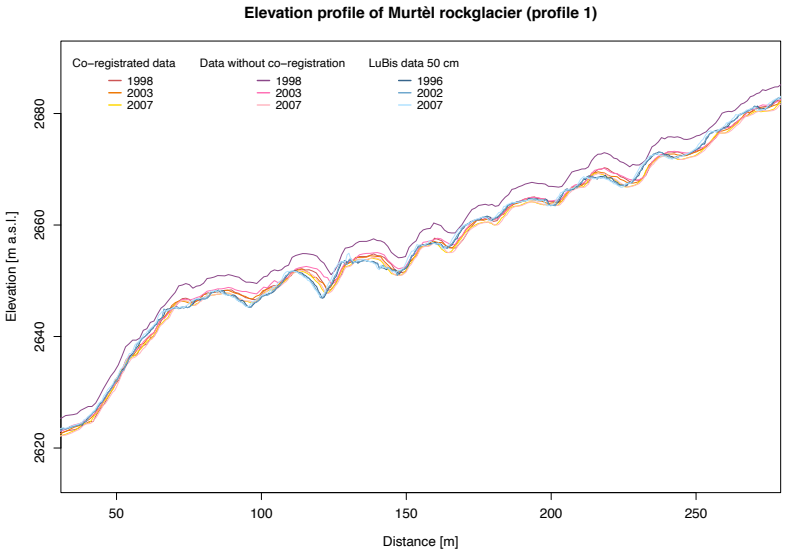

Figure 6-2: Comparison of data with and without co-registration and LuBis data (50 cm) at the elevation profile of the Murtèl rockglacier (profile 1 in Figure 4-9).

6.2 Applied methods

In this study, different methods were used to quantify the horizontal and vertical changes of rockglaciers and solifluction lobes. The different quantitative as well as qualitative methods confirm each other by giving consistent results, which allows the validation of each method. For example, the geomorphologic mapping is based on the field observations as well as on the results of the movements, which in turn were used as a basis for the spatial analysis of the active landforms. Increased horizontal displacement, for example on the western side of the Chastelets rockglaciers, is reflected in the results from CIAS (Figure 5-2) as well as in the DEM-differencing images (Figure 5-6) and the longitudinal profiles (Figure 5-12). In addition, the features resulting from this higher movement are evident in the field. All applied methods were performed with the same datasets (DEM's and orthophotos), allowing a comparison of the findings.

6.3 Horizontal and vertical changes

For the analysis and embedding of the horizontal and vertical movements in the following chapters, the results of CIAS (Chapter 5.2), DEM-differencing (Chapter 5.3.1), longitudinal profiles (Chapter 5.4) and field observations are used. Annual horizontal and vertical displacement rates are calculated for the active landforms as defined in Figure 5-1. These average values do not show the spatial variability within the active landforms. The resulting flowlines from CIAS and DEM-differencing allow spatial analysis at a smaller scale, highlighting the formation and development of smaller subsystems within the active landforms. Longitudinal profiles show the evolution of the landforms and highlight even the smallest changes. However, they only show the landform movement limited to the location of the profile, and the processes away from the profile can't be observed. When interpreting the results, the uncertainty range of both horizontal and vertical changes of 0.04 m/a – 0.12 m/a must be considered. Movements smaller than this range should at least be treated with caution or excluded from further analysis. In particular, the mean vertical changes are often in this range.

6.3.1 Horizontal displacements

In this study, the rockglaciers analyzed generally show low (Murtèl, Marmugnun and Chastelets rockglaciers) to average (Gupf) mean annual horizontal displacement rates (Figure 5-3, Appendix 11.4) compared to other rockglaciers in Switzerland (Chapter 2.2.5). The hori-

zontal displacement values in this study reflect the average displacement over the whole part of each active landform. If individual parts of the active landform move at different rates, this is not reflected in the average displacement values. To see the spatial variability within the active parts, the results from CIAS (Figure 5-2) and DEM-differencing (Figure 5-6 and Figure 5-7) are valuable. In particular, the Chastelets and Marmugnun rockglaciers, as well as the Gupf, show clear spatial variability. In the time steps, where the snow-covered images of 1979 and 1985 are included, all landforms have rather high rates of horizontal movement, which can be partially explained by measurement uncertainties in CIAS due to the snow.

The values of horizontal displacements measured in this study can be compared with values from previous studies (Table 3-2) and from the validation dataset from geodetic surveys (Chapter 4.4.2). The high rates of the Murtèl rockglacier in this study are particularly noteworthy when compared to the horizontal velocities of the studies previously conducted in this study area. Until 2007, significantly higher values (on average about 0.3 m/a) are measured than in the other studies (on average about 0.08 m/a). From 2007 to 2021, movements of 0.07 m/a are measured, which is in line with other studies and the measurements from the geodetic survey. The horizontal movement during the time step between 1979 and 1985 is particularly high for the Murtèl rockglacier (0.79 m/a), which clearly biases the average displacement value. If this value is excluded from the analysis, the average horizontal movement for the Murtèl rockglacier is 0.2 m/a, which is still rather high compared to the other studies. This would correspond to the lowest horizontal movement of all landforms. Altough the resulting values for the Murtèl rockglacier are small and sometimes overlap with the uncertainty range, these small values are plausible when compared to the literature. The horizontal movements of the Murtèl rockglacier during the 1979 - 1985 time step resulting from CIAS don't seem to be accurate (Figure 5-2). The arrows show neither reasonable directions nor clear flow patterns. The resulting displacement values are also not plausible, as they are much higher than in the literature (Table 3-2, Figure 5-3). Therefore, it is assumed that the displacement in this time step was calculated incorrectly in CIAS. The large snow cover in these two years could be a reason for the difference. The displacement in this time step is therefore manually verified in CIAS by examining the displacement of 10 boulders in the snow-free area of the rockglacier. This manual examination minimizes the distorting influence of snow or shadow. The resulting mean movement between 1979 and 1985 on the Murtèl rockglacier is 0.15 m/a. This value is still at the upper limit of observed values from the literature, but it is more plausible than the previously automatically calculated value of 0.79 m/a. Replacing this value of 0.79 m/a with 0.15 m/a for 1979 – 1985 gives the smallest mean horizontal move-

ment for the Murtèl rockglacier over all time steps compared to the other landforms. This is in agreement with the available literature values for all landforms. Gärtner-Roer (2012) studied the horizontal movement along a profile line over the Murtèl rockglacier between 1996 and 2010, which revealed the spatial variability of the surface displacement. Movements between 0.11 m/a (2009-2010) and 0.17 m/a (2002-2007) were observed at the root zone, while at the front values between 0.06 m/a (2009-2010) and 0.18 m/a (2002-2007) were measured. Directly behind the front, the lowest values of 0.05 m/a (2009-2010) and 0.09 m/a (2002-2007) were measured. These values highlight and confirm the spatial variability within the rockglacier, as observed in this study.

The horizontal movements of the Marmugnun rockglacier measured in this study are rather low, but comparable to the values measured in other studies (about 0.2-0.3 m/a). The Marmugnun rockglacier is moving faster on its western side than on the eastern part. The higher velocities in some parts are only slightly reflected in the resulting average horizontal velocities. The geodetic survey has obtained values of up to 2.1 m/a at the Marmugnun rockglacier, which was not reached in this study. On the more active western side, maximum values of 0.5 m/a were measured. The values measured for the Chastelets rockglacier also tend to be lower than those measured in the geodetic survey. This may be related to the spatial variability, which is particularly pronounced for this rockglacier. The western part of the rockglacier moves much faster, as can be seen from the spatial results of CIAS (Figure 5-2) and the longitudinal profiles of both sides of the rockglacier (Figure 5-12). Horizontal displacements of about 0.7-1 m/a since 1998 are consistent with the geodetic survey, which would also roughly correspond to average values for active rockglaciers nationwide. The horizontal displacement values for the Gupf in this study are significantly lower than in the geodetic survey because they are averaged over the entire landform. On the other hand, if only the fast-moving part of the Gupf is considered (Figure 5-2), movement rates of about 1 m/a are observed, which is consistent with the values of the geodetic survey. There are no comparative values for the solifluction lobes in the study area, only theoretical values (Matsuoka, 2001). The solifluction lobes (numbers 6 and 7) show medium (about 0.1-0.4 m/a), while the solifluction lobe (number 5) shows rather high (about 0.3-0.8 m/a) surface velocities. The slower moving solifluction lobes (numbers 6 and 7) also show a different behavior visible in the longitudinal profiles than the faster moving solifluction lobe (number 5) (Figure 5-12). Regarding the longitudinal profiles, the landforms exhibit higher horizontal displacements than front advances, which is consistent with the literature (Gärtner-Roer, 2023; Kääb et al., 1997; Roer, 2005).

A uniform set of parameters was used in CIAS for all time steps and landforms to allow comparison of the resulting horizontal displacements. The parameters could have been adjusted individually for each landform and its properties (block size and displacement rate). The resulting flowlines would have been more accurate for each landform, but the comparability would have been limited. In this work, the decision was therefore made to use uniform parameters. This explains why the flow lines resulting from CIAS do not always agree between the different time steps. Other limitations are shadows or snow, which complicate the recognition and are another reason for the chaotic flowlines. If the surface changes are very small, the arrows at the same points in different time intervals point in opposite directions. Chaotic flowlines should therefore be considered with caution. In such error-prone areas, the DEM-differencing image or, depending on the position, longitudinal profiles provide more reliable results.

6.3.2 Vertical changes

Vertical change is assessed from both the DEM-differencing images and the longitudinal profiles (Figure 5-8, Appendix 11.5). There is no consistent pattern of vertical change among the landforms studied. Vertical changes are complex because they can be influenced by several factors, such as debris supply, climate forcing or the formation of ice (Chapter 2.2.5). A prominent change is the subsidence of the Marmugnun rockglacier, which could be explained by melting of internal ice. This could suggest that the rockglacier is on its way to inactivity. Currently, the rockglacier is still moving slightly forward, indicating that it is still active. The horizontal movement is also represented within the vertical changes on the image of difference. The Chastelets rockglacier has developed three new lobes on its western side, leaving negative values where material has left and positive vertical changes where material has accumulated. Comparative values for vertical changes are only available for the Murtèl rockglacier (Table 3-2). It is not possible to make a clear comparison between the values from this study and those from previous studies, because the time periods were chosen very differently, and the snow in certain years in this study has a strong influence on the vertical changes. However, the values are very similar and differ by only a few millimeters. A more detailed interpretation of the vertical changes is challenging by the small values that result, as the uncertainties are often larger.

6.3.3 Correlation between horizontal and vertical changes

In the case of horizontal displacements, downslope movements occur, which is also reflected in vertical changes. Therefore, the relation between horizontal and vertical changes was investigated. However, no correlation was observed. This can partly be explained by the disturbance of vertical changes caused by snow cover. On the other hand, during horizontal changes, material is transported downslope. This results in a decrease in height in the upper part, while further down, an increase is measured caused by deposition of material. These values of accumulation and transport of material probably balance each other out. Although material from the talus slope regularly reaches the rockglaciers, material is also lost at the front and laterally at the tongue of the rockglaciers. Correlations between horizontal and vertical movements are expected, when high horizontal movements occur and result in vertical compression (thinning). However, as the horizontal movements in this study are rather low, no thinning of the landforms was observed as a result.

6.3.4 Spatial and temporal variability

6.3.4.1 Spatial variations

Using the results from CIAS and DEM-differencing, the spatial variations within the landforms can be identified. The numerical values of the horizontal and vertical changes represent the average value of each whole active landform (Appendices 11.4 and 11.5.). According to Haeberli (1985), the horizontal movements are greatest in the central flow line of the rockglacier and decrease toward the sides. In this study, this is not always the case, since for the Chastelets and Marmugnun rockglacier the western sides move the fastest. In the case of the Murtèl rockglacier, the largest movement is in the center and only little to no change laterally. On the much smaller landform Gupf, there is an even distribution of movement over the entire landform. Forward movements are generally smaller on landforms with a pronounced furrow and ridge surface due to horizontal compression. The small horizontal movements of the Murtèl rockglacier can be explained by such a surface topography, which is strongly present on this rockglacier. Landforms moving over steeper slopes generally show faster movements at the front (Haeberli, 1985). Possible effects of terrain characteristics are investigated in Chapter 6.5.4. Despite their close proximity, comparing the landforms reveals very different developments. Such differences in development highlight the spatial variability and unique responses of each landform to environmental factors over time.

6.3.4.2 Temporal variations

No general temporal trend of neither horizontal nor vertical changes can be observed. As far as horizontal displacements are considered, the Murtèl and Marmugnun rockglaciers behave similarly. All landforms do not show the highest movements in recent periods, opposite to the expected increase in displacements in response to higher temperatures (Arenson et al., 2002). The Chastelets rockglacier is the only landform to show a general increase in horizontal displacements recently. As for vertical changes, the Murtèl and Marmugnun rockglaciers show similar patterns. The Chastelets rockglacier, Gupf, and solifluction lobes are also alike. Since 2003, vertical changes have been declining on all landforms. However, because several complex processes influence vertical changes, no uniform signal was observed. In this study, no seasonal observations were made, allowing only the overall changes to be analyzed and ignoring the temporal variations within the years.

6.4 Geomorphological characteristics

After the analysis of the aerial images and considering the results of the horizontal displacements, all seven landforms were considered to be active. However, some additional characteristics were identified during the surface topography analysis (Figure 5-12). The solifluction lobes (numbers 6 and 7) show minimal to no changes in their longitudinal profiles. In contrast, the solifluction lobe (number 5) shows a changing topography over the years. An evolving trend of increased downslope movement can be observed, resembling to a smaller extent the evolution of the Gupf. It's plausible that these landforms will continue to evolve in a similar manner in the future, with continued downslope movement leading to their enlargement. Since this solifluction lobe (number 5) lies directly above the Gupf, it's possible that these two landforms will merge into a larger unit in the future. Another plausible scenario is that this most active lobe (number 5), treated here as a solifluction feature, may instead be a protalus rampart (Hoelzle et al., 2022b). A protalus rampart is an initiating rockglacier, which is a rockglacier in its early stages that could evolve into a larger rockglacier with further development (Ballantyne & Kirkbride, 1986). In this case, it could again merge with the Gupf to one larger rockglacier.

6.5 Controlling factors

Based on these findings, additional analysis was conducted on potential controlling factors. Factors that could possibly control the development and movement of the landforms include climatic and geomorphologic factors, such as snow cover, rockfall, and local topographic characteristics.

6.5.1 Snow cover

The effect of avalanche and perennial snow cover on the movement of rockglaciers and solifluction lobes was evaluated. However, in this study, detailed conclusions on this issue cannot be drawn because of several limitations. The horizontal and vertical movements of the landforms represent changes within a time period. The snow cover, however, could only be recorded at a single moment in time at the beginning of each period of the available aerial images. Therefore, spatial as well as temporal variations of snow cover within the time periods could therefore not be quantified and included in the analysis. The aerial photographs were taken in early fall and either no or minimal snow cover was present at that time. Therefore, the specific relationship between snow cover and permafrost dynamics of each landform cannot be evaluated in detail in this study. DEM's and the resulting vertical changes were not corrected from lying snow, because the snow was neither over a whole landform area nor uniformly distributed inside the study area. Also, the thickness of the snow cover was not considered in this study. Therefore, the comparison of snow to vertical changes should be considered with caution (Joerg et al., 2012; Schneider et al., 2012). The higher horizontal displacements with more avalanche snow could be explained in two ways. First, during an avalanche, rocky material is transported and deposited on the talus slope as well as on the rockglacier. This additional layer of material could have led to the increase in horizontal movement. On the other hand, the uncertainties of the measured horizontal displacements in CIAS are greatest when a large area is covered by snow (Chapter 4.5.4). These values could be highly uncertain and its potential influence on the movements of the landforms and therefore this correlation should be treated with caution. The decrease in the amount of snow cover over time can be linked to the continuous vertical subsidence of the Marmugnun rockglacier. Lack of snow means less insulation, which may favor the internal melting of the rockglacier and lead to the observed subsidence.

A more precise temporal analysis of snow and snow thickness would be of great interest. Since the exact timing of snowfall in autumn and spring thaw is of great importance for per-

mafrost (Chapter 2.1.3), a more precise temporal analysis would be valuable. Any patterns of changing snow conditions and their consequences due to climate change could be identified in this way. This would require regular aerial surveys of the study area to capture the sometimes rapidly changing snow cover patterns.

6.5.2 Rockfall

In order to quantify rockfall, elevation differences of landforms and their subsystems were recorded. Partially high correlations between neighboring subsystems are observed, which could be explained by high rockfall activity and subsequent sediment transfer. Although smaller sediment transfer rates are expected within subsystems with lower movement rates (Gärtner-Roer, 2012), no correlation between subsystem elevation changes and horizontal movement of rockglaciers could be detected in this study.

The quantification of rockfall based on elevation differences has several limitations. In particular, elevation differences of steep rockwalls should be used with caution, because DEM's in steep terrain are more prone to error. As with the snow cover evaluation (Chapter 4.8 and Chapter 5.5), the rockfall analysis can only be performed at the time of capture of aerial images and therefore represents only a snapshot in time. This analysis explains the elevation changes of subsystems on rockfall and the associated material transfer and deposition. Elevation changes due to, for example, internal ice melt, as it is assumed for the Marmugnun rockglacier (Chapter 6.3.2), are not considered in this part of the analysis, which leads to limitations of the results. To obtain more precise information on rockfall and its correlation with horizontal or vertical movement, regular aerial surveys would be required. To further minimize the limitations, changes could be quantified by volume changes instead of height differences (as in Müller et al., 2014).

6.5.3 Impact of climatic variables

The impact of climatic variables on both horizontal and vertical changes was investigated in relation to air, borehole (9.55 m depth) and GST temperatures and precipitation measurements. The meteorological data (air temperature and precipitation) was obtained from the MeteoSwiss station located on Piz Corvatsch at an altitude of 3297 m a.s.l. (MeteoSwiss, 2023a). The temperature data were adjusted for the Murtèl cirque with a vertical temperature gradient of 0.65 °C / 100 m (Brönnimann, 2018). Borehole (COR_0287) and GST tempera-

tures were obtained from the meteorological station at the Murtèl rockglacier, which is operated by PERMOS (PERMOS, 2023). The meteorological station on the Säntis is used to include a long-term air temperature series and to highlight the trend of increasing warming. This station has been measuring air temperature since 1864 and is the closest mountain station to the Engadin with such a long series of measurements. In comparison, the Corvatsch station has monitored air temperature since 1979. With an altitude of 2501 m a.s.l., the Säntis station is located almost 800 m lower than the station on Piz Corvatsch. However, with its remarkably long series of measurements, the Säntis station shows the steadily increasing air temperature (MeteoSwiss, 2023b). The temperature increase is also evident in the shorter measurement series at Piz Corvatsch (Hoelzle et al., 2022a; MeteoSwiss, 2023a). A comparison of the air (Murtèl and Säntis) and borehole temperatures, GST and horizontal displacements at the Murtèl rockglacier is shown in Figure 6-3. Since the Murtèl rockglacier is the only rockglacier in the study area with meteorological and borehole measurements, this detailed comparison is made only for this landform.

Staub (2015) found a time delay of 10-11 months for the air temperature to reach a depth of 20 m. Since the shear horizon of the Murtèl rockglacier is located at a depth of about 28 m

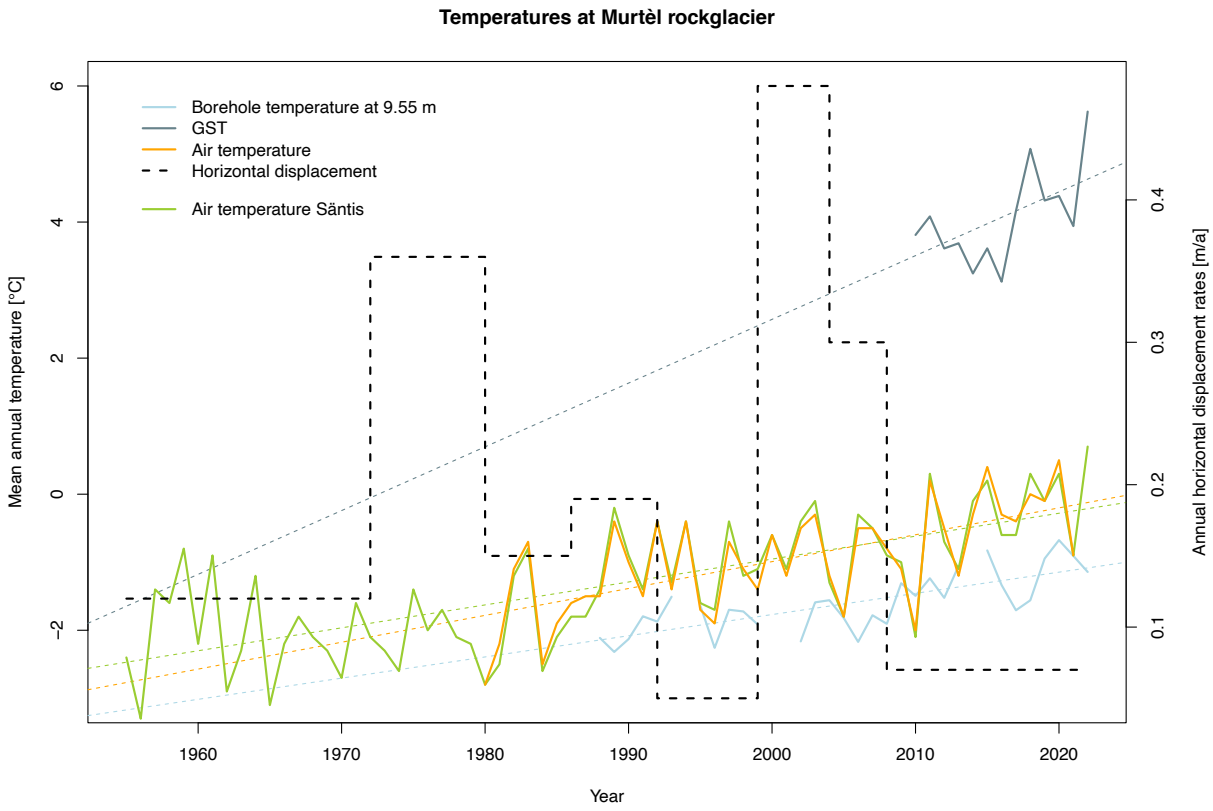

Figure 6-3: Air, borehole (9.55 m depth) and ground surface temperatures in relation to the horizontal displacements at the Murtèl rockglacier. The air temperature measured on top of Säntis is displayed to show the long-term temperature trend (Hoelzle et al., 2022; MeteoSwiss, 2023; PERMOS, 2023).

(Haeberli et al., 1988), a time delay of about 14 months would result. Possible correlations between air temperatures and rockglacier movements are therefore investigated with a time delay of 1 year (Staub, 2015). Regarding the correlation between the air temperature and horizontal displacements, the solifluction lobe (number 5) showed a positive correlation (correlation of 0.38), while all other landforms revealed negative correlations. The most pronounced negative correlations were observed at the Marmugnun (- 0.69) and Murtèl (- 0.67) rockglaciers, suggesting higher horizontal displacements at colder air temperatures. In contrast, the solifluction lobe (number 5) showed small horizontal movements during colder temperatures. The analysis of the correlation between horizontal movement and precipitation revealed that the solifluction lobe (number 7) has the most negative correlation (- 0.56), indicating increased horizontal movement during periods of lower precipitation. Conversely, the solifluction lobe (number 5) showed higher horizontal changes during periods of increased precipitation (0.34). The most positive correlations between vertical changes and temperature were found at the Chastelets (0.37) and Marmugnun (0.29) rockglaciers, implying more positive vertical changes during warmer temperatures. The relation between vertical changes and precipitation showed two main opposite trends. Positive correlations were observed at the Marmugnun (0.52) and Murtèl (0.4) rockglaciers and the solifluction lobe (number 7) (0.27), indicating higher vertical changes during periods of higher precipitation. On the other hand, the solifluction lobe (number 5) (-0.39) and the Chastelets rockglacier (-0.32) have the most negative correlations, indicating more negative vertical changes during periods of increased precipitation. However, none of the observed correlations between climatic variables and surface displacements are statistically significant. No correlation was identified between GST measurements and surface velocities, in contrast to the clear relation observed in other studies (e.g. Bodin et al., 2009; Delaloye et al., 2010; Roer et al., 2005). The only statistically significant correlation was measured between the borehole temperature at 9.55 m depth and horizontal displacements of the Murtèl rockglacier. This confirms one theory that temperature only has effects on rockglacier movement after it has penetrated to depth, since directly at the surface it has no immediate influence, even after a time delay is taken into consideration. Responses can take decades to centuries (Kääb, 1997; Kellerer-Pirklbauer & Kaufmann, 2012; Staub, 2015). While the direct effect of air temperature may be less significant than that of a snow cover, higher air temperatures accelerate snowmelt. This results in a shorter duration of snowpack isolation, which in turn affects permafrost conditions and, consequently, rockglacier movement (Staub, 2015). According to Arenson et al. (2002) or Schneider et al. (2012), direct responses of rockglaciers to temperature changes are expected, while a delay of chang-

es in movement is possible. Rising ground temperatures lead to warming of the ice, which results in higher deformation rates of rockglaciers. Another perspective is presented by Barsch (1996), where increasing temperatures lead to a decrease in horizontal velocities, which may be followed by inactivation of the rockglacier. In this study, no increased rockglacier movement was observed at higher air temperatures. However, a delayed reaction may still occur in the future. In this study, the rockglaciers show a decreasing movement during the last 20 years. This would support the theory of melting of the internal ice as a result of higher temperatures and thus lower rates of movement. On the Marmugnun rockglacier, melting of the internal ice is assumed, which would confirm the connection between higher temperatures and lower rockglacier movements in this specific case. However, several complex factors and interrelationships are interacting with each other, so that no clear effect of rockglacier movement on rising temperatures can be identified at this study site. As the rockglaciers in the study have evolved quite differently despite the same climatic conditions, individual topographic and internal characteristics may have a greater influence on rockglacier movement.

6.5.4 Impact of terrain characteristics

The relation between the mean annual horizontal displacements between 1955 and 2021 and the characteristics of the landforms, such as the area, length and slope (on the landforms and below the rockglacier fronts), was analyzed (Table 6-1). No investigations could be performed regarding the impact of internal characteristics on rockglacier movements, as this information is only available in detail for the Murtèl rockglacier and therefore no comparison between the different landforms could have been done. In terms of the average slope on the landforms, the Murtèl, Marmugnun and Chastelets rockglaciers have low average slopes and small average annual horizontal displacement rates. In contrast, the landforms with steeper

Table 6-1: Correlations between terrain parameters and horizontal and vertical changes. The green colored value is statistically significant.

		r-value
Vertical	area	-0.7
	length	-0.62
	slope (landform)	0.82
	slope (forefield)	-0.26
Horizontal	area	-0.56
	length	-0.57
	slope (landform)	0.48
	slope (forefield)	-0.89

slopes (around 30°), such as the Gupf and the solifluction lobe (number 5), show larger horizontal movements. The solifluction lobes (numbers 6 and 7) also have a slope of approximately 30°, but they show similarly low values of horizontal change as the three large rockglaciers. The correlation between the slope and horizontal displacements is statistically not significant (correlation value of 0.48). Concerning the length of the landforms, shorter landforms such as the solifluction lobe (number 5) and the Gupf have the highest horizontal displacement rates of 0.45 m/a and 0.65 m/a, respectively. The other landforms vary widely in length, but fall within a similar range of horizontal displacements of about 0.2 – 0.3 m/a. A negative correlation of – 0.57 is achieved between the length and horizontal displacements. The area follows a similar pattern to the length, with shorter landforms generally having smaller areas. Both the Gupf and the solifluction lobe (number 5) have the smallest areas (< 2500 m^2), yet they show the largest annual horizontal changes. The other landforms, similar to the length, display comparable horizontal displacements despite significant differences in area size. The correlation between horizontal movements and the area results in a value of – 0.56. There was no statistically significant correlation between the horizontal displacements and the slope below the rockglacier fronts.

The same parameters, slope (on the landforms and below the rockglacier fronts), length and area, were analyzed for mean annual vertical changes. An examination of the mean slope shows a consistent pattern that large slopes correspond to larger vertical changes, while smaller slopes tend to have smaller or even negative vertical changes. A statistically significant correlation value between the average slope and vertical changes of 0.82 was computed. In terms of the area, the smaller landforms such as the Gupf and the three solifluction lobes have positive values for vertical change. Even the much larger Chastelets rockglacier shows minimal positive vertical changes (about 0.01 m/a). However, it is not possible to make a clear statement with such small values. On the other hand, the Murtèl and Marmugnun rockglaciers show negative changes. This results in a negative correlation of – 0.7 between the area and vertical changes. A similar trend emerges when considering the length, given the usually strong correlation between the parameters area and length. Shorter landforms, including the Gupf and the three solifluction lobes, show positive values for vertical changes. A correlation of – 0.62 between the length and vertical changes is resulting. The correlation between the slope in front of the rockglaciers and the vertical changes was not statistically significant.

In summary, the only correlation, which is statistically significant, is observed between the average slope of the landforms and mean annual vertical changes. This positive relation indi-

cates higher vertical displacements when the landform is steeper. The complex composition of vertical displacements must be carefully considered. In addition, it should also be noted that in this study area, the smaller and shorter landforms are located on steeper slopes, while the larger and longer rockglaciers are located in flatter areas. These circumstances affect the analysis because the parameters interact with each other in various ways and have contributed significantly to the current characteristics of the landforms.

7. CONCLUSIONS

Based on the research questions posed (Chapter 1.3), the following conclusions are drawn.

In this study, four rockglaciers and three solifluction lobes have been studied and their movement since 1955 quantified. The studied rockglaciers and solifluction lobes show different rates of movement and trends during the last nearly seven decades. There is no general pattern of movement among the landforms. Although the landforms are in close proximity to each other and their external conditions are very similar, the movements are diverse. The largest horizontal movements were measured at the Gupf, a small, developing rockglacier (up to 1.7 m/a between 1998 and 2003). The largest vertical changes are observed at the Marmugnun rockglacier. Distinct vertical thinning has been observed throughout especially the latter part of the observation period, with maximum values of up to six meters at some points since 1955. The horizontal and vertical movements are subject to uncertainties between 0.04 m/a and 0.12 m/a. No correlation between the movement rates and climatic influencing factors can be recognized, which suggests that individual characteristics and influencing factors play a more prominent role. Likewise, no clear temporal development trend of the movements can be recognized. The differences between and within the landforms are therefore both spatial and temporal, which does not reveal any trend. It is also possible that the landforms are subject to a large time lag and that the response to e.g. rising air temperature has not yet become apparent. One possible response to the rising temperature due to climate change could be the subsidence of the Marmugnun rockglacier, which may be losing internal ice due to melting. Climatic controls do not strongly influence the movements, but some individual topographic characteristics or processes are more decisive for the movements. The influence of such individual factors is subject to many limitations. Deposited avalanche snow shows a statistically significant, positive influence on increasing horizontal movements of some rockglaciers. The obtained values of horizontal and vertical changes were quantified by several methods (block-matching in CIAS, DEM-differencing and longitudinal profiles). The similar to equal results in each case confirm the quality of the individual methods and the accuracy of qualitative methods, such as field observations. All studied landforms show changes and are therefore considered to be active. However, the intensity of change varies both between and within the landforms. Finally, it is an interplay of highly complex systems, process chains, internal processes, delayed responses as well as numerous parameters acting on different temporal and spatial scales.

8. PERSPECTIVES

The evolution of rockglaciers and solifluction lobes in the Murtèl cirque below the Piz Corvatsch has been studied over the last 66 years. For the first time, all permafrost landforms in this study area have been studied and their behavior analyzed. This study has opened new perspectives that can be pursued in the future to increase local and general knowledge about rockglaciers and their evolution, especially in relation to climate change.

Long-term measurements of movements can show the influence of increasing temperature and changing precipitation and snow cover due to climate change. This will help to determine whether the movements of these landforms are in fact decreasing in principle with increasing temperature, or whether a delayed response of increased movement is yet to occur. By recording the internal structures of landforms, important insights into the variability between and within landforms could be gained. A relationship between internal composition and movement rates could be evaluated. It is also proposed to continue monitoring especially the Gupf as well as the solifluction lobe (number 5) to see if they merge into a larger landform. Monitoring the joining or formation of rockglaciers would present an interesting research task. The Marmugnun rockglacier and its vertical thinning should also be observed. In the future, if its surface continues to sink and lose ice, the rockglacier may change its state of activity and probably stop moving and become inactive. The remaining landforms should also be monitored to see if subsidence develops in the future. If the outflow of the rockglaciers were measured, it may be possible to detect increasing ice melt more quickly, or even see a temporal delay in melt.

In the context of natural hazards, it's important to keep a close eye on less stable rockglaciers. As they gradually lose their ice, this process can have several consequences, such as the potential for rock detachment at the front of the rockglacier, which can lead to rockfall events. In addition, this instability can also lead to the formation of debris flows, further emphasizing the need for careful monitoring and assessment of rockglaciers in the future.

9. ACKNOWLEDGEMENTS

First and foremost, I would like to thank my supervisor, Dr. Isabelle Gärtner-Roer. She guided me through this work, provided measurement data and enabled me to gain valuable insights in the field. I would like to thank Prof. Dr. Andreas Vieli, who accompanied my work as faculty representative.

A big thank you goes to Dr. Philip Jörg, Holger Heisig, Cordelia Bucher and Kurt Röthlisberger from the Federal Office of Topography Swisstopo. Philip and Holger prepared the data sets and made them available to me. Within the SwisstopoEDU program they supervised and supported my work and gave me a unique insight into one part of the work of Swisstopo.

I would also like to thank Prof. Dr. Michael Zemp, who helped me with questions about co-registration and Fabienne Maag for providing me with the co-registration worksheet.

And finally, I thank my family and friends for their uncompromising support and care.

10. REFERENCES

Aber, J., Marzloff, I., & Ries, J. (2010). *Small-Format Aerial Photography*. Elsevier. https://doi.org/10.1016/C2009-0-18493-3

Åkerman, H. J. (1993). Solifluction and creep rates 1972–1991, Kapp Linné, west Spitsbergen. *Solifluction and Climatic Variation in the Holocene*, 225–250.

Arenson, L., Hoelzle, M., & Springman, S. (2002). Borehole deformation measurements and internal structure of some rock glaciers in Switzerland. *Permafrost and Periglacial Processes*, *13*(2), 117–135. https://doi.org/10.1002/ppp.414

Ballantyne, C. K. (2017). *Periglacial geomorphology*. John Wiley & Sons.

Ballantyne, C. K., & Harris, C. (1995). *The Periglaciation of Great Britain*. https://www.jstor.org/stable/1552036?origin=crossref

Ballantyne, C. K., & Kirkbride, M. P. (1986). The characteristics and significance of some lateglacial protalus ramparts in upland Britain. *Earth Surface Processes and Landforms*, *11*(6), 659–671. https://doi.org/10.1002/esp.3290110609

Baltsavias, E. P. (1996). Digital ortho-images—A powerful tool for the extraction of spatial- and geo-information. *ISPRS Journal of Photogrammetry and Remote Sensing*, *51*(2), 63–77. https://doi.org/10.1016/0924-2716(95)00014-3

Barrows, T. (2004). Exposure ages for Pleistocene periglacial deposits in Australia. *Quaternary Science Reviews*, *23*(5–6), 697–708. https://doi.org/10.1016/j.quascirev.2003.10.011

Barsch, D. (1973). Refraktionsseismische Bestimmung der Obergrenze des gefrorenen Schuttkörpers in verschiedenen Blockgletschern Graubündens, Schweizer Alpen. Zeitschrift Für Gletscherkunde Und Glazialgeologie, 9, 143–167.

Barsch, D. (1977). Nature and importance of mass-wasting by rock glaciers in alpine permafrost environments. Earth Surface Processes, 2(2–3), 231–245. https://doi.org/10.1002/esp.3290020213

Barsch, D. (1992). Permafrost creep and rockglaciers. Permafrost and Periglacial Processes, 3(3), 175–188. https://doi.org/10.1002/ppp.3430030303

Barsch, D. (1996). Rockglaciers: Indicators for the Present and Former Geoecology in High Mountain Environments (Vol. 16). Springer Berlin Heidelberg.

https://doi.org/10.1007/978-3-642-80093-1

Barsch, D., & Hell, G. (1975). Photogrammetrische Bewegungsmessungen am Blockgletscher Murtèl I, Oberengadin, Schweizer Alpen. *Zeitschrift Für Gletscherkunde Und Glazialgeologie*, *11*(2), 111–142.

Benedict, J. B. (1970). Downslope Soil Movement in a Colorado Alpine Region: Rates, Processes, and Climatic Significance. *Arctic and Alpine Research*, *2*(3), 165–226. https://doi.org/10.1080/00040851.1970.12003576

Bodin, X., Thibert, E., Fabre, D., Ribolini, A., Schoeneich, P., Francou, B., Reynaud, L., & Fort, M. (2009). Two decades of responses (1986-2006) to climate by the Laurichard rock glacier, French Alps: Evolution of the Laurichard Rock Glacier, French Alps (1986-2006). *Permafrost and Periglacial Processes*, *20*(4), 331–344. https://doi.org/10.1002/ppp.665

Brönnimann, S. (2018). *Klimatologie* (1.). utb.

Brown, R. J. E. (1963). Influence of vegetation on permafrost. *Proceedings: Permafrost International Conference*.

Brunner, N. (2020). *Gletscher-Blockgletscher Beziehung beim Grubengletscher, Fletschhorngebiet, Wallis* (p. 93). Universität Zürich.

Burga, C. A., Frauenfelder, R., Ruffet, J., Hoelzle, M., & Kääb, A. (2004). Vegetation on Alpine rock glacier surfaces: A contribution to abundance and dynamics on extreme plant habitats. *Flora - Morphology, Distribution, Functional Ecology of Plants*, *199*(6), 505–515. https://doi.org/10.1078/0367-2530-00179

Caine, N. (1976). A uniform measure of subaerial erosion. *Geological Society of America Bulletin*, *87*, 137–140.

Chaix, A. (1923). Les coulées de blocs du Parc national suisse d'Engadine (Note préliminaire). *Le Globe. Revue genevoise de géographie*, *62*(1), 1–35. https://doi.org/10.3406/globe.1923.5609

Cicoira, A. (2020). *On the Dynamics of Rock Glaciers*. University of Zurich.

Cicoira, A., Marcer, M., Gärtner-Roer, I., Bodin, X., Arenson, L. U., & Vieli, A. (2021). A general theory of rock glacier creep based on in-situ and remote sensing observations. *Permafrost and Periglacial Processes*, *32*(1), 139–153. https://doi.org/10.1002/ppp.2090

Delaloye, R., & Echelard, T. (2022). *Towards standard guidelines for inventorying rock glaciers: Baseline concepts (version 4.2.2).* (p. 13). IPA Action Group Rock glacier inventories and kinematics, University of Fribourg. https://www.unifr.ch/geo/geomorphology/en/research/ipa-action-group-rock-glacier/

Delaloye, R., Echelard, T., Cicoira, A., Jones, N., Vivero, S., & Brardinoni, F. (2022). *Towards standard guidelines for inventorying rock glaciers: Practical concepts (version 2.0).* (p. 10). IPA Action Group Rock glacier inventories and kinematics, University of Fribourg. https://www.unifr.ch/geo/geomorphology/en/research/ipa-action-group-rock-glacier/

Delaloye, R., Lambiel, C., & Gärtner-Roer, I. (2010). Overview of rock glacier kinematics research in the Swiss Alps. *Geographica Helvetica*, *65*, 135–145. https://doi.org/10.5194/gh-65-135-2010

Delaloye, R., Morard, S., Barboux, C., Abbet, D., Gruber, V., Riedo, M., & Gachet, S. (2013). *Rapidly moving rock glaciers in Mattertal*. 21–31.

Delaloye, R., Perruchoud, E., Avian, M., Kaufmann, V., Bodin, X., Hausmann, H., Ikeda, A., Kääb, A., Kellerer-Pirklbauer, A., Krainer, K., Lambiel, C., Mihajlovic, D., Staub, B., Roer, I., & Thibert, E. (2008). *Recent Interannual Variations of Rock Glacier Creep in the European Alps*.

Dramis, F., Guida, D., & Cestari, A. (2011). Nature and Aims of Geomorphological Mapping. In *Developments in Earth Surface Processes* (Vol. 15, pp. 39–73). Elsevier. https://doi.org/10.1016/B978-0-444-53446-0.00003-3

Egels, Y., & Kasser, M. (2001). *Digital Photogrammetry* (0 ed.). CRC Press. https://doi.org/10.4324/9780203305959

Frauenfelder, R., & Kääb, A. (2000). Towards a palaeoclimatic model of rock-glacier formation in the Swiss Alps. *Annals of Glaciology*, *31*, 281–286. https://doi.org/10.3189/172756400781820264

Frauenfelder, R., Laustela, M., & Kääb, A. (2003). Velocities and relative surface ages of selected Alpine rockglaciers [Application/pdf]. *Turbulenzen in der Geomorphologie: Publikation zur Jahrestagung der Schweizerischen Geomorphologischen Gesellschaft*, 239 p. https://doi.org/10.3929/ETHZ-B-000481577

Frehner, M., Ling, A. H. M., & Gärtner-Roer, I. (2015). Furrow-and-Ridge Morphology on Rockglaciers Explained by Gravity-Driven Buckle Folding: A Case Study From the

Murtèl Rockglacier (Switzerland): Rockglacier Furrow-and-Ridge Morphology Explained by Buckle Folding. *Permafrost and Periglacial Processes*, *26*(1), 57–66. https://doi.org/10.1002/ppp.1831

Furrer, G. (1965). Die subnivale Höhenstufe und ihre Untergrenze in den Bündner und Walliser Alpen. *Geographica Helvetica*, *20*(4), 185–192. https://doi.org/10.5194/gh-20-185-1965

Gärtner-Roer, I. (2012). Sediment transfer rates of two active rockglaciers in the Swiss Alps. *Geomorphology*, *167–168*, 45–50. https://doi.org/10.1016/j.geomorph.2012.04.013

Gärtner-Roer, I. (2023). *Geodetic Survey (2009—2023), unpublished*.

Gärtner-Roer, I., Brunner, N., Delaloye, R., Haeberli, W., Kääb, A., & Thee, P. (2022). Glacier–permafrost relations in a high-mountain environment: 5 decades of kinematic monitoring at the Gruben site, Swiss Alps. *The Cryosphere*, *16*(5), 2083–2101. https://doi.org/10.5194/tc-16-2083-2022

Gärtner-Roer, I., & Hoelzle, M. (Eds.). (2021). Rockglaciers of the Engadine. In *Landscapes and Landforms of Switzerland*. Springer International Publishing. https://doi.org/10.1007/978-3-030-43203-4

Gärtner--Roer, I., & Nyenhuis, M. (2009). Volume Estimation, Kinematics and Sediment Transfer Rates of Active Rockglaciers in the Turtmann Valley, Switzerland. In J.-C. Otto & R. Dikau (Eds.), *Landform—Structure, Evolution, Process Control* (Vol. 115, pp. 185–198). Springer Berlin Heidelberg. https://doi.org/10.1007/978-3-540-75761-0_12

Geomorphology Research Group. (2022a, March 29). *Grabengufer (VS)*. Geomorphology Research Group: Grabengufer (VS). https://www.unifr.ch/geo/geomorphology/en/resources/study-sites/grabengufer-rg.html

Geomorphology Research Group. (2022b, March 29). *Tsarmine (VS)*. Geomorphology Research Group: Tsarmine (VS). https://www.unifr.ch/geo/geomorphology/en/resources/study-sites/tsarmine.html

Giardino, J. R., Regmi, N. R., & Vitek, J. D. (1989). Rock Glaciers. *Geological Magazine*, *126*(4), 454–454. https://doi.org/10.1017/S0016756800006828

Gruber, S., & Haeberli, W. (Eds.). (2009). Mountain Permafrost. In *Permafrost Soils* (Vol. 16). Springer Berlin Heidelberg. https://doi.org/10.1007/978-3-540-69371-0

Günzel, F., & Haeberli, W. (2020). *Einfluss der Permafrostdegradation auf Hangstabilität*.

https://doi.org/10.5167/UZH-192417

Haeberli, W. (1975). *Untersuchungen zur Verbreitung von Permafrost zwischen Flüelapass und Piz Grialetsch (Graubünden)* (17; Mitteilungen Der Versuchsanstalt Für Wasserbau, Hydrologie Und Glaziologie). ETH Zürich.

Haeberli, W. (1985). *Creep of Mountain Permafrost: Internal Structure and flow of alpine Rock glaciers* (Nr. 77; Mitteilungen Der Versuchsanstalt Für Wasserbau, Hydrologie Und Glaziologie, p. 142). ETH Zürich.

Haeberli, W., & Beniston, M. (1998). Climate change and Its Impacts on Glaciers and Permafrost in the Alps. *Royal Swedish Academy of Sciences*, *27*(4).

Haeberli, W., Hallet, B., Arenson, L., Elconin, R., Humlum, O., Kääb, A., Kaufmann, V., Ladanyi, B., Matsuoka, N., Springman, S., & Mühll, D. V. (2006). Permafrost creep and rock glacier dynamics. *Permafrost and Periglacial Processes*, *17*(3), 189–214. https://doi.org/10.1002/ppp.561

Haeberli, W., Hoelzle, M., Kääb, A., Keller, F., Mühll, D. V., & Wagner, S. (1998). *Ten years after drilling through the permafrost of the active rock glacier Murtèl, eastern Swiss Alps: Answered questions and new perspectives*. *55*, 403–410.

Haeberli, W., Huder, J., Keusen, H.-R., Pika, J., & Röthlisberger, H. (1988). *Core drilling thorugh rock glacier permafrost*.

Haeberli, W., Kääb, A., Wagner, I. S., Muhll, D. V., Geissler, P., Haas, E. N., & Glatzel-Mattheier, H. (1999). Pollen analysis and 14e age of moss remains in a pertnafrost core recovered frotn the active rock glacier Mur tel-Corvatsch, Swiss Alps: Geotnorphological and glaciological implications. *Journal of Glaciology*, *45*(149).

Haeberli, W., Noetzli, J., Arenson, L., Delaloye, R., Gärtner-Roer, I., Gruber, S., Isaksen, K., Kneisel, C., Krautblatter, M., & Phillips, M. (2010). Mountain permafrost: Development and challenges of a young research field. *Journal of Glaciology*, *56*(200), 1043–1058. https://doi.org/10.3189/002214311796406121

Hanson, S., & Hoelzle, M. (2004). The thermal regime of the active layer at the Murtèl rock glacier based on data from 2002. *Permafrost and Periglacial Processes*, *15*(3), 273–282. https://doi.org/10.1002/ppp.499

Hanson, S., & Hoelzle, M. (2005). Installation of a shallow borehole network and monitoring of the ground thermal regime of a high alpine discontinuous permafrost environment,

Eastern Swiss Alps. *Norsk Geografisk Tidsskrift - Norwegian Journal of Geography*, *59*(2), 84–93. https://doi.org/10.1080/00291950510020664

Harris, C., Arenson, L. U., Christiansen, H. H., Etzelmüller, B., Frauenfelder, R., Gruber, S., Haeberli, W., Hauck, C., Hölzle, M., Humlum, O., Isaksen, K., Kääb, A., Kern-Lütschg, M. A., Lehning, M., Matsuoka, N., Murton, J. B., Nötzli, J., Phillips, M., Ross, N., … Vonder Mühll, D. (2009). Permafrost and climate in Europe: Monitoring and modelling thermal, geomorphological and geotechnical responses. *Earth-Science Reviews*, *92*(3–4), 117–171. https://doi.org/10.1016/j.earscirev.2008.12.002

Harris, C., Davies, M. C. R., & Coutard, J.-P. (1997). Rates and processes of periglacial solifluction: An experimental approach. *Earth Surface Processes and Landforms*, *22*(9), 849–868. https://doi.org/10.1002/(SICI)1096-9837(199709)22:9<849::AID-ESP784>3.0.CO;2-U

Harris, C., Gallop, M., & Coutard, J.-P. (1993). Physical modelling of gelifluction and frost creep: Some results of a large-scale laboratory experiment. *Earth Surface Processes and Landforms*, *18*(5), 383–398. https://doi.org/10.1002/esp.3290180502

Harris, C., Haeberli, W., Vonder Mühll, D., & King, L. (2001). Permafrost monitoring in the high mountains of Europe: The PACE Project in its Global Context. *Permafrost and Periglacial Processes*, *12*(1), 3–11. https://doi.org/10.1002/ppp.377

Heid, T., & Kääb, A. (2012). Evaluation of existing image matching methods for deriving glacier surface displacements globally from optical satellite imagery. *Remote Sensing of Environment*, *118*, 339–355. https://doi.org/10.1016/j.rse.2011.11.024

Heisig, H., & Simmen, J.-L. (2021). Re-engineering the Past: Countrywide Geo-referencing of Archival Aerial Imagery. *PFG – Journal of Photogrammetry, Remote Sensing and Geoinformation Science*, *89*(6), 487–503. https://doi.org/10.1007/s41064-021-00162-z

Higashi, A., & Corte, A. E. (1971). Solifluction: A Model Experiment. *Science*, *171*(3970), 480–482. https://doi.org/10.1126/science.171.3970.480

Hoelzle, M., Hauck, C., Mathys, T., Noetzli, J., Pellet, C., & Scherler, M. (2022a). Long-term energy balance measurements at three different mountain permafrost sites in the Swiss Alps. *Earth System Science Data*, *14*(4), 1531–1547. https://doi.org/10.5194/essd-14-1531-2022

Hoelzle, M., Hauck, C., Mathys, T., Noetzli, J., Pellet, C., & Scherler, M. (2022b). Long-term energy balance measurements at three different mountain permafrost sites in the Swiss

Alps. *Earth System Science Data*, *14*(4), 1531–1547. https://doi.org/10.5194/essd-14-1531-2022

Hoelzle, M., Mühll, D. V., & Haeberli, W. (2002). Thirty years of permafrost research in the Corvatsch-Furtschellas area, Eastern Swiss Alps: A review. *Norsk Geografisk Tidsskrift - Norwegian Journal of Geography*, *56*(2), 137–145. https://doi.org/10.1080/002919502760056468

Humlum, O. (2000). The geomorphic significance of rock glaciers: Estimates of rock glacier debris volumes and headwall recession rates in West Greenland. *Geomorphology*, *35*(1–2), 41–67. https://doi.org/10.1016/S0169-555X(00)00022-2

Humlum, O., Christiansen, H. H., & Juliussen, H. (2007). Avalanche-derived rock glaciers in Svalbard. *Permafrost and Periglacial Processes*, *18*(1), 75–88. https://doi.org/10.1002/ppp.580

Ikeda, A., & Matsuoka, N. (2002). Degradation of talus-derived rock glaciers in the Upper Engadin, Swiss Alps. *Permafrost and Periglacial Processes*, *13*(2), 145–161. https://doi.org/10.1002/ppp.413

Ikeda, A., Matsuoka, N., & Kääb, A. (2003). *A rapidly moving small rock glacier at the lower limit of the mountain permafrost belt in the Swiss Alps*. 455–460.

James, L. A., Hodgson, M. E., Ghoshal, S., & Latiolais, M. M. (2012). Geomorphic change detection using historic maps and DEM differencing: The temporal dimension of geospatial analysis. *Geomorphology*, *137*(1), 181–198. https://doi.org/10.1016/j.geomorph.2010.10.039

Janke, J. R., Regmi, N. R., Giardino, J. R., & Vitek, J. D. (2013). 8.17 Rock Glaciers. In *Treatise on Geomorphology* (pp. 238–273). Elsevier. https://doi.org/10.1016/B978-0-12-374739-6.00211-6

Jiménez-Jiménez, S. I., Ojeda-Bustamante, W., Marcial-Pablo, M., & Enciso, J. (2021). Digital Terrain Models Generated with Low-Cost UAV Photogrammetry: Methodology and Accuracy. *ISPRS International Journal of Geo-Information*, *10*(5), 285. https://doi.org/10.3390/ijgi10050285

Joerg, P. C., Morsdorf, F., & Zemp, M. (2012). Uncertainty assessment of multi-temporal airborne laser scanning data: A case study on an Alpine glacier. *Remote Sensing of Environment*, *127*, 118–129. https://doi.org/10.1016/j.rse.2012.08.012

Kääb, A. (1997). *Oberflächenkinematik ausgewählter Blockgletscher des Oberengadins. Beiträge aus der Gebirgs-Geomorphologie. 158*(Mitteilungen der VAW der ETH-Zürich), 121–140.

Kääb, A. (2005). *Remote sensing of mountain glaciers and permafrost creep*. Geographisches Institut der Universität Zürich.

Kääb, A. (2006). *Photogrammetrische Analyse zur Früherkennung gletscher- und permafrostbedingter Naturgefahren im Hochgebirge* (145; Mitteilungen). Versuchsanstalt für Wasserbau, Hydrologie und Glaziologie der Eidgenössischen Technischen Hochschule Zürich.

Kääb, A. (2007). *Rock Glaciers and Protalus Forms* (pp. 2236–2242). Elsevier. https://doi.org/10.1016/B0-444-52747-8/00114-9

Kääb, A., Frauenfelder, R., & Roer, I. (2007). On the response of rockglacier creep to surface temperature increase. *Global and Planetary Change*, *56*(1–2), 172–187. https://doi.org/10.1016/j.gloplacha.2006.07.005

Kääb, A., Gudmundsson, G. H., & Hoelzle, M. (1998). *Surface deformation of creeping mountain permafrost. Photogrammetric investigations on Murtèl rock glacier, Swiss Alps*. *55*, 531–537.

Kääb, A., Haeberli, W., & Gudmundsson, G. H. (1997). Analysing the creep of mountain permafrost using high precision aerial photogrammetry: 25 years of monitoring Gruben rock glacier, Swiss Alps. *Permafrost and Periglacial Processes*, *8*(4), 409–426. https://doi.org/10.1002/(SICI)1099-1530(199710/12)8:4<409::AID-PPP267>3.0.CO;2-C

Kääb, A., Kaufmann, V., Ladstädter, R., & Eiken, T. (2003). *Rock glacier dynamics: Implications from high-resolution measurements of surface velocity fields*. 501–506.

Kääb, A., & Vollmer, M. (2000). Surface Geometry, Thickness Changes and Flow Fields on Creeping Mountain Permafrost: Automatic Extraction by Digital Image Analysis. *Permafrost and Periglacial Processes*, *11*(4), 315–326. https://doi.org/10.1002/1099-1530(200012)11:4<315::AID-PPP365>3.0.CO;2-J

Kääb, A., & Vollmer, M. (2001). *Digitale Photogrammetrie zur Deformationsanalyse von Massenbewegungen im Hochgebirge* [Text/html,application/pdf,text/html]. https://doi.org/10.5169/SEALS-235808

Kellerer-Pirklbauer, A. (2018). Solifluction rates and environmental controls at local and regional scales in central Austria. *Norsk Geografisk Tidsskrift - Norwegian Journal of Geography*, *72*(1), 37–56. https://doi.org/10.1080/00291951.2017.1399164

Kellerer-Pirklbauer, A., & Kaufmann, V. (2012). About the relationship between rock glacier velocity and climate parameters in central Austria. *Austrian Journal of Earth Sciences*, *105*(2), 94–112.

Kenner, R., Phillips, M., Beutel, J., Hiller, M., Limpach, P., Pointner, E., & Volken, M. (2017). Factors Controlling Velocity Variations at Short-Term, Seasonal and Multiyear Time Scales, Ritigraben Rock Glacier, Western Swiss Alps: Factors driving rock glacier velocity at three time scales. *Permafrost and Periglacial Processes*, *28*(4), 675–684. https://doi.org/10.1002/ppp.1953

Kenner, R., Pruessner, L., Beutel, J., Limpach, P., & Phillips, M. (2020). How rock glacier hydrology, deformation velocities and ground temperatures interact: Examples from the Swiss Alps. *Permafrost and Periglacial Processes*, *31*(1), 3–14. https://doi.org/10.1002/ppp.2023

King, L., Fisch, W., Haeberli, W., & Waechter, H. P. (1987). Comparison of resistivity and radio-echo soundings on rock glacier permafrost. *Zeitschrift Für Gletscherkunde Und Glazialgeologie*, *23*(1), 77–97.

Koblet, T., Gärtner-Roer, I., Zemp, M., Jansson, P., Thee, P., Haeberli, W., & Holmlund, P. (2010). Reanalysis of multi-temporal aerial images of Storglaciären, Sweden (1959–99) – Part 1: Determination of length, area, and volume changes. *The Cryosphere*, *4*(3), 333–343. https://doi.org/10.5194/tc-4-333-2010

Konecny, G., & Lehmann, G. (1984). *Photogrammetrie* (4th ed.). Walter de Gruyter.

Krainer, K. (2015). *Kapitel 1—Blockgletscher: Einführung*. *4*, 9–32.

Krummenacher, B., Budmiger, K., Mihajlovic, D., & Blank, B. (1998). *Periglaziale Prozesse und Formen im Furggentälti, Gemmipass*. *56*, 245.

Kummert, M., Bodin, X., Braillard, L., & Delaloye, R. (2021). Pluri-decadal evolution of rock glaciers surface velocity and its impact on sediment export rates towards high alpine torrents. *Earth Surface Processes and Landforms*, *46*(15), 3213–3227. https://doi.org/10.1002/esp.5231

Lemke, P., Ren, J., Alley, R. B., Allison, I., Carrasco, J., Flato, G., Fujii, Y., Kaser, G., Mote,

P., Thomas, R. H., & Zhang, T. (2007). Observations: Changes in Snow, Ice and Frozen Ground. *Climate Change 2007: The Physical Science Basis. Contribution of Working Group I to the Fourth Assessment Report of the Intergovernmental Panel on Climate Change*.

Luhmann, T. (2018). *Nahbereichsphotogrammetrie* (4.). Wichmann.

Matsuoka, N. (1994). Continuous Recording of Frost Heave and Creep on a Japanese Alpine Slope. *Arctic and Alpine Research*, *26*(3), 245. https://doi.org/10.2307/1551937

Matsuoka, N. (1998). The relationship between frost heave and downslope soil movement: Field measurements in the Japanese Alps. *Permafrost and Periglacial Processes*, *9*(2), 121–133. https://doi.org/10.1002/(SICI)1099-1530(199804/06)9:2<121::AID-PPP281>3.0.CO;2-C

Matsuoka, N. (2001). Solifluction rates, processes and landforms: A global review. *Earth-Science Reviews*, *55*(1–2), 107–134. https://doi.org/10.1016/S0012-8252(01)00057-5

Matsuoka, N. (2008). Frost weathering and rockwall erosion in the southeastern Swiss Alps: Long-term (1994–2006) observations. *Geomorphology*, *99*(1–4), 353–368. https://doi.org/10.1016/j.geomorph.2007.11.013

Matsuoka, N. (2011). Climate and material controls on periglacial soil processes: Toward improving periglacial climate indicators. *Quaternary Research*, *75*(2), 356–365. https://doi.org/10.1016/j.yqres.2010.12.014

Matsuoka, N., Hirakawa, K., Watanabe, T., & Moriwaki, K. (1997). Monitoring of Periglacial Slope Processes in the Swiss Alps: The First Two Years of Frost Shattering, Heave and Creep. *Permafrost and Periglacial Processes*, *8*(2), 155–177. https://doi.org/10.1002/(SICI)1099-1530(199732)8:2<155::AID-PPP248>3.0.CO;2-N

Matsuoka, N., Ikeda, A., & Date, T. (2005). Morphometric analysis of solifluction lobes and rock glaciers in the Swiss Alps. *Permafrost and Periglacial Processes*, *16*(1), 99–113. https://doi.org/10.1002/ppp.517

Matsuoka, N., & Sakai, H. (1999). Rockfall activity from an alpine cliff during thawing periods. *Geomorphology*, *28*(3–4), 309–328. https://doi.org/10.1016/S0169-555X(98)00116-0

Matthews, J. A., Seppälä, M., & Dresser, P. Q. (2005). Holocene solifluction, climate variation and fire in a subarctic landscape at Pippokangas, Finnish Lapland, based on radio-

carbon-dated buried charcoal. *Journal of Quaternary Science*, *20*(6), 533–548. https://doi.org/10.1002/jqs.932

MeteoSwiss. (2023a). *Meteo Station Piz Corvatsch*. Federal Office of Meteorology and Climatology MeteoSwiss. https://www.meteoswiss.admin.ch/services-and-publications/applications/measurement-values-and-measuring-networks.html#param=messnetz-automatisch&lang=en&station=COV&chart=hour

MeteoSwiss. (2023b). *Meteo Station Säntis*. https://www.meteoschweiz.admin.ch/service-und-publikationen/applikationen/messwerte-und-messnetze.html#lang=de&param=messwerte-lufttemperatur-10min&station=SAE&chart=year&table=false&sortColumn=null&sortDirection=null

Müller, J., Gärtner-Roer, I., Kenner, R., Thee, P., & Morche, D. (2014). Sediment storage and transfer on a periglacial mountain slope (Corvatsch, Switzerland). *Geomorphology*, *218*, 35–44. https://doi.org/10.1016/j.geomorph.2013.12.002

Noetzli, J., Arenson, L. U., Bast, A., Beutel, J., Delaloye, R., Farinotti, D., Gruber, S., Gubler, H., Haeberli, W., Hasler, A., Hauck, C., Hiller, M., Hoelzle, M., Lambiel, C., Pellet, C., Springman, S. M., Vonder Muehll, D., & Phillips, M. (2021). Best Practice for Measuring Permafrost Temperature in Boreholes Based on the Experience in the Swiss Alps. *Frontiers in Earth Science*, *9*, 607875. https://doi.org/10.3389/feart.2021.607875

Noetzli, J., Gruber, S., Kohl, T., Salzmann, N., & Haeberli, W. (2007). Three-dimensional distribution and evolution of permafrost temperatures in idealized high-mountain topography. *Journal of Geophysical Research*, *112*(F2), F02S13. https://doi.org/10.1029/2006JF000545

Nötzli, J., & Gruber, S. (2005). Alpiner Permafrost—Ein Überblick. *Jahrbuch Des Vereins Zum Schutz Der Bergwelt (München)*, *70*, 111–122.

Nuth, C., & Kääb, A. (2011). Co-registration and bias corrections of satellite elevation data sets for quantifying glacier thickness change. *The Cryosphere*, *5*(1), 271–290. https://doi.org/10.5194/tc-5-271-2011

Nyenhuis, M. (2005). *Permafrost und Sedimenthaushalt in einem alpinen Geosystem*. Rheinischen Friedrich–Wilhelms–Universität Bonn.

PERMOS. (2016). *Permafrost in Switzerland (2010/2011 to 2013/2014)* (12–15; Glaciological Report (Permafrost)). Swiss Permafrost Monitoring Network (PERMOS).

PERMOS. (2019). *Permafrost in Switzerland (2014/2015 to 2017/2018)* (16–19; Glaciological Report (Permafrost)). Swiss Permafrost Monitoring Network (PERMOS). doi:10.13093/permos-rep-2019-16-19

PERMOS. (2023). *Data Portal: Ground Surface Temperature at the Murtèl-Corvatsch rock-glacier (COR_R002)*. https://www.permos.ch/data-portal/ground-surface-temperature

Pulighe, G., & Fava, F. (2013). DEM extraction from archive aerial photos: Accuracy assessment in areas of complex topography. *European Journal of Remote Sensing*, *46*(1), 363–378. https://doi.org/10.5721/EuJRS20134621

Quarter, A. (2005). *Introduction to Photogrammetry*. The Ohio State University.

Ribi, H. (1975). *In Dufours Diensten im Oberengadin* [Text/html,application/pdf,text/html]. https://doi.org/10.5169/SEALS-550316

Ridefelt, H., Etzelmüller, B., & Boelhouwers, J. (2010). Spatial analysis of solifluction landforms and process rates in the Abisko Mountains, northern Sweden: Spatial Analysis of Solifluction Landforms and Process Rates. *Permafrost and Periglacial Processes*, *21*(3), 241–255. https://doi.org/10.1002/ppp.681

Roer, I. (2005). *Rockglacier Kinematics in a High Mountain Geosystem*. Rheinische Friedrich-Wilhelms-Universität Bonn.

Roer, I., Haeberli, W., Avian, M., Kaufmann, V., Delaloye, R., Lambiel, C., & Kääb, A. (2008). *Observations and considerations on destabilizing active rock glaciers in the European Alps*. https://doi.org/10.5167/UZH-6082

Roer, I., Kääb, A., & Dikau, R. (2005). Rockglacier acceleration in the Turtmann valley (Swiss Alps): Probable controls. *Norsk Geografisk Tidsskrift - Norwegian Journal of Geography*, *59*(2), 157–163. https://doi.org/10.1080/00291950510020655

Roer, I., & Nyenhuis, M. (2007). Rockglacier activity studies on a regional scale: Comparison of geomorphological mapping and photogrammetric monitoring. *Earth Surface Processes and Landforms*, *32*(12), 1747–1758. https://doi.org/10.1002/esp.1496

Romanovsky, V., Gruber, S., Jin, H., Marchenko, S., Smith, S., Trombotto, D., & Walter, K. (2007). *Global Outlook for Ice and Snow: Frozen Ground* (p. 238). United Nations Environment Programme (UNEP). www.unep.org

Schneider, S., Hoelzle, M., & Hauck, C. (2012). Influence of surface and subsurface heterogeneity on observed borehole temperatures at a mountain permafrost site in the Upper

Engadine, Swiss Alps. *The Cryosphere*, *6*(2), 517–531. https://doi.org/10.5194/tc-6-517-2012

Schwarb, M., Frei, C., Schär, C., & Daly, C. (2000). *Mittlere jährliche Niederschlagshöhen im europäischen Alpenraum 1971–1990 (Tafel 2.6)* [Map]. Hydrologischer Atlas der Schweiz.

SLF. (2023). *Permafrost*. Permafrost. https://www.slf.ch/de/permafrost.html

Spillmann, P., & Trommsdorff, V. (2007). *Geologischer Atlas der Schweiz (1:25000). Blatt 1277: Piz Bernina (Atlasblatt 119).* (Swisstopo, Ed.). Federal Office of Topography swisstopo.

Springman, S. M., Arenson, L. U., Yamamoto, Y., Maurer, H., Kos, A., Buchli, T., & Derungs, G. (2012). Multidisciplinary investigations on three rock glaciers in the swiss alps: Legacies and future perspectives. *Geografiska Annaler: Series A, Physical Geography*, *94*(2), 215–243. https://doi.org/10.1111/j.1468-0459.2012.00464.x

Staub, B. (2015). *The evolution of mountain permafrost in the context of climate change – towards a comprehensive analysis of permafrost monitoring data from the Swiss Alps.* University of Fribourg.

Staub, B., & Delaloye, R. (2017). Using Near-Surface Ground Temperature Data to Derive Snow Insulation and Melt Indices for Mountain Permafrost Applications: Snow and Melt Indices Derived from GST Data. *Permafrost and Periglacial Processes*, *28*(1), 237–248. https://doi.org/10.1002/ppp.1890

Steinemann, O., Reitner, J. M., Ivy-Ochs, S., Christl, M., & Synal, H.-A. (2020). Tracking rockglacier evolution in the Eastern Alps from the Lateglacial to the early Holocene. *Quaternary Science Reviews*, *241*, 106424. https://doi.org/10.1016/j.quascirev.2020.106424

Streletskiy, D., Anisimov, O., & Vasiliev, A. (2015). Permafrost Degradation. In *Snow and Ice-Related Hazards, Risks, and Disasters* (pp. 303–344). Elsevier. https://doi.org/10.1016/B978-0-12-394849-6.00010-X

Swisstopo. (1860). *Topographic Map of Switzerland (Dufour Map)* [Map]. https://map.geo.admin.ch/?lang=en&topic=swisstopo&bgLayer=ch.swisstopo.pixelkarte-farbe&layers_timestamp=current,99991231,20071231,2012,18601231&E=2783004.69&N

=1144274.88&zoom=9.266666666666637&layers=ch.swisstopo.swissimage-product,ch.swisstopo.lubis-luftbilder_farbe,ch.swisstopo.lubis-luftbilder_schwarzweiss,ch.swisstopo.lubis-bildstreifen,ch.swisstopo.zeitreihen&layers_visibility=false,false,false,false,true

Swisstopo. (1879). *Topographic Map of Switzerland (Dufour Map)* [Map]. https://map.geo.admin.ch/?lang=en&topic=swisstopo&bgLayer=ch.swisstopo.pixelkarte-farbe&layers_timestamp=current,99991231,20071231,2012,18801231&E=2782336.21&N=1144157.11&zoom=6.928594761553997&layers=ch.swisstopo.swissimage-product,ch.swisstopo.lubis-luftbilder_farbe,ch.swisstopo.lubis-luftbilder_schwarzweiss,ch.swisstopo.lubis-bildstreifen,ch.swisstopo.zeitreihen&layers_visibility=false,false,false,false,true

Swisstopo. (2019). *SWISSIMAGE 10cm* [Map]. Federal Office of Topography swisstopo. https://www.swisstopo.admin.ch/de/geodata/images/ortho/swissimage10.html

Swisstopo. (2021a). *Digital Elevation Models of 1955, 1971, 1979, 1985, 1991, 1998, 2003, 2007, 2012, 2021.* [Map].

Swisstopo. (2021b). *Orthophotos of 1955, 1971, 1979, 1985, 1991, 1998, 2003, 2007, 2012, 2021.* [Map].

Swisstopo. (2023a). *Swiss Map Raster 10* [Map]. https://www.swisstopo.admin.ch/de/geodata/maps/smr/smr10.html

Swisstopo. (2015). *National Map of Switzerland 1:25'000 (NM25)*. Federal Office of Topography Swisstopo. https://map.geo.admin.ch/?lang=de&topic=ech&bgLayer=ch.swisstopo.pixelkarte-farbe&layers=ch.swisstopo.zeitreihen,ch.bfs.gebaeude_wohnungs_register,ch.bav.haltestellen-oev,ch.swisstopo.swisstlm3d-wanderwege,ch.astra.wanderland-sperrungen_umleitungen&layers_opacity=1,1,1,0.8,0.8&layers_visibility=false,false,false,false,false&layers_timestamp=18641231,,,,&E=2781557.84&N=1144800.08&zoom=5.679477143558609

Swisstopo. (2023b). *Swiss Geoportal*. Geo.Admin.Ch.

https://map.geo.admin.ch/?topic=luftbilder&lang=en&bgLayer=ch.swisstopo.pixelkarte-grau&layers=ch.swisstopo.lubis-luftbilder_schwarzweiss,ch.swisstopo.lubis-luftbilder_farbe,ch.swisstopo.lubis-bildstreifen&layers_timestamp=99991231,99991231,&E=2782774.45&N=1144894.04&zoom=7.479477143558602 5&catalogNodes=1179,1180

van Everdingen, R. (2005). *Multi-language glossary of permafrost and related ground-ice terms* (International Permafrost Association, pp. 1–159).

Vollmer, M. (1999). *Kriechen alpinen Permafrostes: Grundlagen zur digitalen photogrammetrischen Bewegungsmessung.* University of Zurich.

Vonder Mühll, D. (1993). *Geophysikalische Untersuchungen im Permafrost des Oberengadins* (p. 222 S.) [ETH Zurich; Application/pdf]. https://doi.org/10.3929/ETHZ-A-000891391

Vonder Mühll, D., & Haeberli, W. (1990). Thermal Characteristics of the Permafrost within an active rock glacier (Murtèl/Corvatsch, Grisons, Swiss Alps). *Journal of Glaciology*, *36*(123), 151–158.

Vonder Mühll, D. S., & Klingelé, E. E. (1994). Gravimetrical investigation of ice-rich permafrost within the rock glacier Murtèl-Corvatsch (upper Engadin, swiss alps). *Permafrost and Periglacial Processes*, *5*(1), 13–24. https://doi.org/10.1002/ppp.3430050103

Wagner, S. (1992). Creep of alpine permafrost, investigated on the murtel rock glacier. *Permafrost and Periglacial Processes*, *3*(2), 157–162. https://doi.org/10.1002/ppp.3430030214

Wahrhaftig, C., & Cox, A. (1959). Rock Glaciers in the Alaska Range. *Geological Society of America Bulletin*, *70*(4), 383. https://doi.org/10.1130/0016-7606(1959)70[383:RGITAR]2.0.CO;2

Wheaton, J. M., Brasington, J., Darby, S. E., & Sear, D. A. (2009). Accounting for uncertainty in DEMs from repeat topographic surveys: Improved sediment budgets. *Earth Surface Processes and Landforms*, n/a-n/a. https://doi.org/10.1002/esp.1886

White, S. E. (1976). Rock Glaciers and Block fields, Review and new data. *Quaternary Research*, *6*(1), 77–97. https://doi.org/10.1016/0033-5894(76)90041-7

Zemp, M., Thibert, E., Huss, M., Stumm, D., Rolstad Denby, C., Nuth, C., Nussbaumer, S. U., Moholdt, G., Mercer, A., Mayer, C., Joerg, P. C., Jansson, P., Hynek, B., Fischer,

A., Escher-Vetter, H., Elvehøy, H., & Andreassen, L. M. (2013). Reanalysing glacier mass balance measurement series. *The Cryosphere*, *7*(4), 1227–1245. https://doi.org/10.5194/tc-7-1227-2013

Zepp, H. (2017). *Geomorphologie: Eine Einführung* (7th ed.). utb.

11. APPENDICES

11.1 Qualitative analysis

Comparison of the DEM's and the national map of 2023 (Swisstopo, 2023). The numbers in the first column are illustrated in Figure 4-2. A positive difference indicates that the test-DEM lies higher than the reference map, while a negative difference signifies that the test-DEM is located lower at this point location [m]. Values labeled as "NA" lie outside the coverage of the DEM for that particular year (in the DEM's of 1991 and 2007), indicating a lack of corresponding values. The mean (MEAN) represents the average difference among all points for each year, while the MEAN* excludes the maximum and minimum values in order to provide a more representative mean value. The root mean square error (RMSE), the standard deviation (STDEV) and the standard error (SE) are other calculations to evaluate the DEM's in comparison with reference points.

point	National Map 2023 [m a.s.l.]	1955	1971	1979	1985	1991	1998	2003	2007	2012	2021
		differences [m]									
1	2888	-4.8	-3.0	-3.4	-7.2	*NA*	-0.8	-0.9	*NA*	-2.6	-3.2
2	3098	-3.5	-3.3	-1.7	-4.7	*NA*	2.7	-0.9	*NA*	-1.3	-0.7
3	3165	-2.9	-3.1	-1.8	-4.4	*NA*	3.3	-0.2	*NA*	-1.1	-1.5
4	2860	-14.2	-10.5	-4.5	-10.3	0.2	1.9	-8.7	0.1	-2.1	-0.2
5	2620	-2.7	-2.2	-0.9	-4.2	-0.1	1.5	-0.6	-0.2	-0.8	-0.3
6	2508	-0.8	-2.6	-0.9	-5.0	-0.2	-0.3	-0.5	-0.3	-0.8	-0.5
7	2408	2.0	0.2	1.0	-2.3	1.2	2.1	1.3	1.0	0.7	0.7
8	2819	-2.7	-2.2	-2.6	-3.8	-0.1	2.8	0.8	-0.3	-1.6	0.0
9	2600	0.4	-0.2	0.2	-3.1	0.2	3.1	1.1	0.0	-0.3	0.2
10	2500	0.4	-0.4	0.1	-3.0	0.2	2.6	1.2	-0.1	-0.4	0.3
11	2500	1.1	-1.0	0.4	-3.3	0.6	2.4	0.0	0.9	0.8	1.1
12	3000	0.9	0.8	2.6	0.5	*NA*	5.9	3.8	*NA*	2.3	2.6
13	2354	0.2	-0.3	-0.2	-3.8	*NA*	2.6	-0.3	*NA*	-0.2	-0.4
14	2600	-2.0	-2.0	-1.1	-4.8	-1.6	0.9	-1.2	-1.9	-2.6	-2.1
15	2560	0.5	0.1	0.5	-2.6	0.8	3.1	1.1	0.7	0.5	0.4
		statistical values [m]									
MEAN		-1.9	-2.0	-0.8	-4.1	0.1	2.2	-0.3	0.0	-0.6	-0.2
MEAN*		-1.2	-1.5	-0.8	-4.0	0.2	2.2	0.1	0.1	-0.7	-0.2
RMSE		7.2	7.6	3.2	16.0	0.3	8.7	1.1	0.0	2.4	0.9
STDEV		3.9	2.7	1.8	2.4	0.8	1.6	2.6	0.8	1.3	1.3
SE		1.0	0.7	0.5	0.6	0.2	0.4	0.7	0.2	0.3	0.3

11.2 Co-registration parameters

Co-registration parameters [m] resulting from the method after Nuth & Kääb (2011).

1955-2021		Original DEM	x and y	z		x, y and z	
Iteration			1	1	2	1	2
Results	x	0.7	-0.2	0.4	0.4	0	0
	y	-0.1	-0.2	0.2	0.1	0.1	0.2
	z	-0.2	-0.1	0.1	0	0.2	-0.1
	σ	2.36	2.35	2.52	2.5	2.6	2.61

1971-2021		Original DEM	x and y			z		x, y and z		
Iteration			1	2	3	1	2	1	2	3
Results	x	-1	3.1	-2.2	4.5	-0.3	-0.4	0.6	-0.5	-0.5
	y	-1.3	-3.2	-2.9	0.4	-1.3	-1.3	-0.5	0	0
	z	-0.8	-2.1	-1	-1.4	0.3	0	0.3	0.2	0
	σ	2.74	7.39	4.78	6.33	2.34	2.26	2.36	2.27	2.24

1979-2021		Original DEM	x and y	z		x, y and z
Iteration			1	1	2	1
Results	x	-0.9	0	-0.5	-0.5	0.4
	y	0.2	0.3	0.5	0.5	0.5
	z	0.2	0.1	-0.1	0	-0.1
	σ	3.14	3.07	3.24	3.24	3.2

1985-2021		Original DEM	x and y			z		x, y and z	
Iteration			1	2	3	1	2	1	2
Results	x	-0.9	-2.3	1.9	0	-1	-1.1	2.6	2.7
	y	-1.3	-2.3	1.1	0.3	0.4	-0.5	-1.4	-0.5
	z	-3.7	-3.5	-3.6	-3.6	0.7	-0.1	0.2	0.3
	σ	5.85	7.09	5.88	5.72	3.09	3.13	4.84	4.77

1991-2021		Original DEM	x and y		z		x, y and z	
Iteration			1	2	1	2	1	2
Results	x	-0.1	0	0	-0.1	-0.1	0	0
	y	-0.3	0.1	0.1	-0.3	-0.3	0.1	0.1
	z	0.2	0.2	0.2	-0.1	0	0	0
	σ	1.08	1.14	1.14	0.97	1.02	1.04	1.04

1998-2021		Original DEM	x and y	z			x, y and z		
Iteration			1	1	2	3	1	2	3
Results	x	0	0	-0.7	-0.7	-0.7	-0.7	0	0
	y	-0.7	0.1	-1	-0.9	-0.9	-0.1	-0.3	-0.4
	z	3.1	3.2	-0.5	0.1	-0.1	-0.5	0.2	-0.1
	σ	4.21	4.29	2.27	2.1	2.11	2.3	2.12	2.15

2003-2021		Original DEM	x and y	z		x, y and z
Iteration			1	1	2	1
Results	x	-0.4	-0.3	-0.8	-0.8	-0.8
	y	-1.3	-0.5	-1.1	-1.1	-0.3
	z	0.5	0.6	-0.1	0	0
	σ	1.79	1.81	1.73	1.73	1.76

2007-2021		Original DEM	x and y	x, y and z
Iteration			1	1
Results	x	0.6	0.1	0.1
	y	-0.4	0	0
	z	0	0	0
	σ	0.94	0.94	0.94

2012-2021		Original DEM	x and y		z	x, y and z		
Iteration			1	2	1	1	2	3
Results	x	0.9	-0.1	-0.1	0.5	0	-0.7	0.2
	y	-0.2	-0.2	-0.2	0.1	0.1	-0.3	-0.3
	z	-0.1	-0.1	-0.1	0	0.1	0	0
	σ	1.13	1.08	1.08	1.26	1.37	1.17	1.11

11.3 Low correlation coefficients in CIAS

Points in CIAS with a maximum correlation coefficient < 20 % quantile for every time step. These measurements were excluded from further analysis. The orthophoto from 2021 is displayed as background (Swisstopo, 2021).

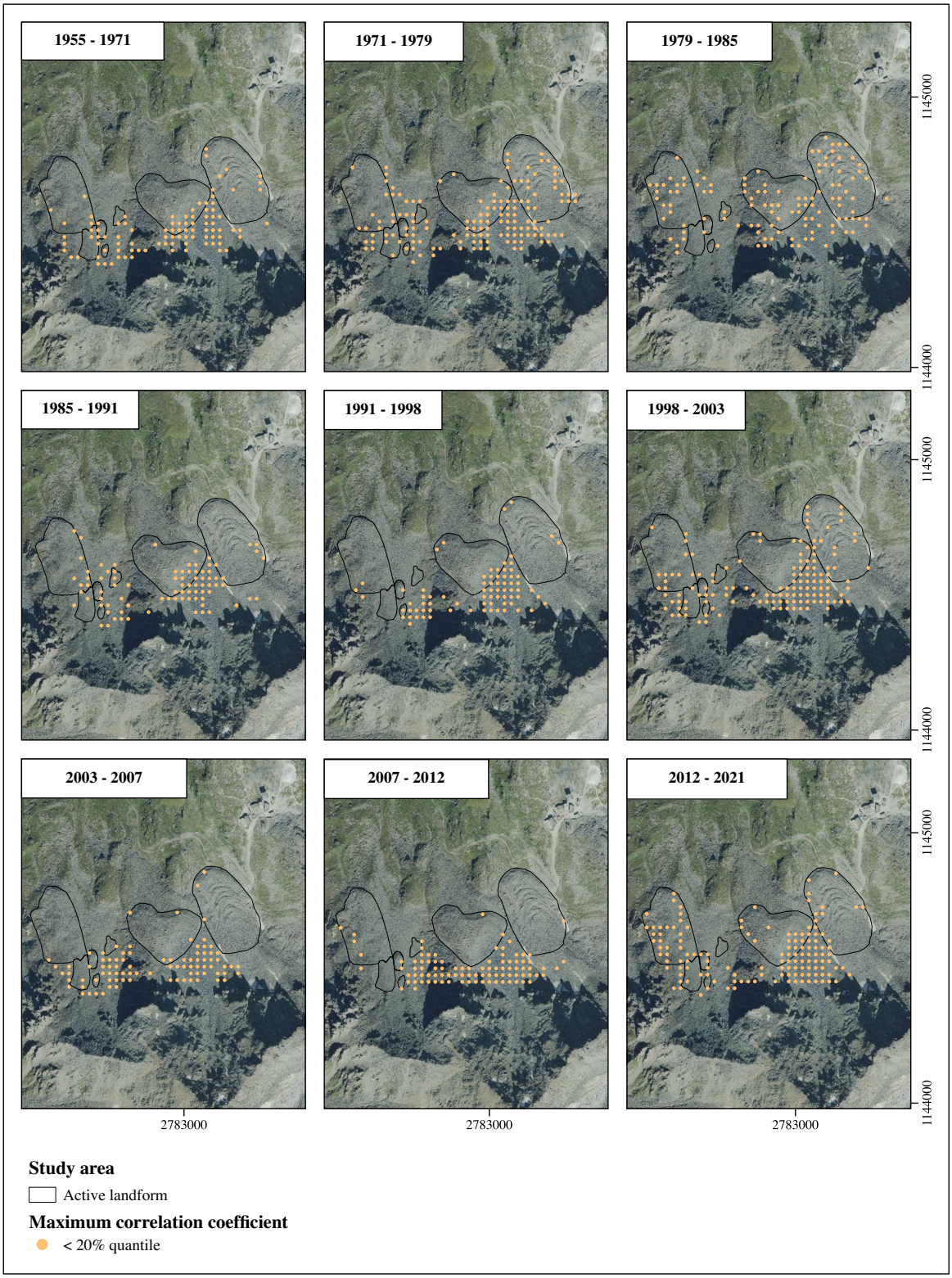

11.4 Annual horizontal displacements

Annual horizontal displacements and mean values per landform and time steps resulting from CIAS.

		Horizontal displacements [m/a]							
		Murtèl	Marmugnun	Chastelets	Gupf	Solifluction (5)	Solifluction (6)	Solifluction (7)	
1955	1971	0.12	0.13	0.14	0.41	0.45	0.11	0.11	0.21
1971	1979	0.36	0.32	0.20	0.98	0.33	0.37	0.35	0.42
1979	1985	0.79	0.76	0.52	0.83	0.38	0.55	0.44	0.61
1985	1991	0.19	0.14	0.07	0.48	0.42	0.17	0.08	0.22
1991	1998	0.05	0.07	0.11	0.06	0.00	0.03	0.03	0.05
1998	2003	0.48	0.29	0.31	1.77	0.87	0.64	0.41	0.68
2003	2007	0.30	0.28	0.25	1.16	0.62	0.51	0.74	0.55
2007	2012	0.07	0.10	0.21	0.04	0.64	0.07	0.05	0.17
2012	2021	0.07	0.11	0.29	0.07	0.50	0.08	0.08	0.17
		0.24	0.22	0.22	0.56	0.44	0.24	0.21	

11.5 Annual vertical changes

Annual vertical displacements and mean values per landform and time steps.

		Vertical changes [m/a]							
		Murtèl	Marmugnun	Chastelets	Gupf	Solifluction (5)	Solifluction (6)	Solifluction (7)	
1955	1971	-0.01	-0.02	0.02	0.04	0.02	0.01	0.00	0.01
1971	1979	0.15	0.22	0.05	0.07	0.06	0.06	0.06	0.10
1979	1985	-0.04	-0.12	-0.07	0.02	0.05	0.03	0.02	-0.01
1985	1991	-0.13	-0.19	0.01	-0.07	-0.11	-0.10	-0.07	-0.09
1991	1998	0.10	0.05	-0.06	0.03	0.06	0.04	0.04	0.04
1998	2003	-0.01	0.01	0.04	0.03	-0.01	-0.01	0.05	0.01
2003	2007	-0.13	-0.17	0.11	0.04	0.04	0.03	0.00	-0.01
2007	2012	0.00	-0.01	-0.01	0.02	-0.01	0.01	0.02	0.00
2012	2021	-0.02	-0.07	-0.02	-0.01	-0.03	-0.02	0.01	-0.02
		0.00	-0.02	0.01	0.02	0.01	0.01	0.02	

12. PERSONAL DECLARATION

I hereby declare that the submitted Thesis is the result of my own, independent work. All external sources are explicitly acknowledged in the Thesis.

Zurich, December 2023

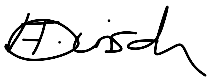

Flurina Durisch